

MECHANISM OF OXYGEN REDUCTION ON PLATINUM IN  
NEUTRAL SALINE AND EFFECTS OF INTERSTITIAL FLUID

---

A Dissertation  
Presented to  
the Faculty of the Graduate School  
University of Missouri

---

In Partial Fulfillment  
of the Requirements for the Degree  
Doctor of Philosophy

---

by  
Jeffrey Bruce Cooper

The undersigned, appointed by the Dean of the Graduate Faculty, have examined a thesis entitled

Mechanism of Oxygen Reduction on Platinum  
in Saline and Effects of Interstitial Fluid

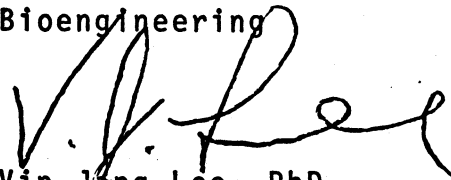
presented by Jeffrey Bruce Cooper

a candidate for the degree of Doctor of Philosophy

and hereby certify that in their opinion it is worthy of acceptance.



Allen W. Hahn, DVM, PhD  
Investigator Space Sciences  
Research Center and Professor  
of Veterinary Medicine and  
Bioengineering



Vin-Jang Lee, PhD  
Associate Professor of  
Chemical Engineering



James W. Johnson, PhD  
Professor of Chemical Engineering  
and Research Associate Space  
Sciences Research Center

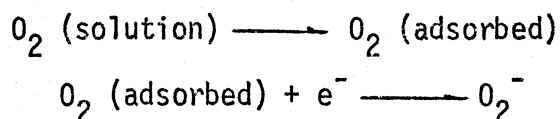
MECHANISM OF OXYGEN REDUCTION ON PLATINUM  
IN NEUTRAL SALINE AND EFFECTS OF INTERSTITIAL FLUID

Jeffrey Bruce Cooper

Allen W. Hahn, D.V.M., Ph.D.      Dissertation Supervisor

ABSTRACT

The mechanism of oxygen reduction on a platinized platinum electrode was studied in a buffered saline solution in the neutral pH region. The Tafel slope was  $135 \pm 18$  mv and the reaction orders 1.1 and 0.19 with respect to oxygen and hydrogen ion respectively. These criteria were interpreted as being consistent with a consecutive adsorption and one electron transfer rate controlling step as follows:



The pH dependency is attributed to a shift in the potential of zero charge with pH in chloride solution.

The factors affecting the performance of platinum activated carbon cathodes in hybrid biogalvanic fuel cells were also examined. It was found that by-products of aluminum and zinc anodes had no

effect on the cathode output voltage. An artificial interstitial fluid either with or without bovine serum albumin shifted the voltage vs. current curve downwards by approximately 100 mv. These tests were performed under aseptic conditions for periods up to five days. The major cause of low in-vivo cathode voltages was attributed to mass transfer limiting conditions which were examined in-vitro in both buffered saline and artificial interstitial fluid.

An automated load switching system for evaluating hybrid fuel cell characteristics is also described. The system utilizes a Linc-8 computer and Calcomp plotter to produce voltage vs. current curves from up to sixteen different anode - cathode pairs. The usefulness and limitations of the system are described.

## ACKNOWLEDGEMENTS

There is no way to adequately express my gratitude to my principle adviser and friend, Dr. Allen W. Hahn for the continuous encouragement and invaluable advice which he has given to me throughout the course of my graduate education. To him, I will always be indebted. I also wish to thank my co-adviser, Dr. Vin-Jang Lee for his helpful counsel and many intriguing and thought provoking discussions.

To Dr. James W. Johnson and Dr. H. Vaidya Nathan, I offer my deepest appreciation for the recommendations and guidance which they have made available to me in preparing this dissertation. Also, I wish to thank Dr. Olen R. Brown for his many helpful suggestions.

A special thank you to the staff of the Space Sciences Research Center for providing a most pleasant atmosphere in which to work. Their congeniality and stimulation have made my task a great deal easier.

Last, and most important, to my wife, Madelaine, I can but offer my love for her unfaltering faith in me. Without her, this may not have been possible.

## TABLE OF CONTENTS

	page
I. Introduction .....	1
The Hybrid Biogalvanic Fuel Cell .....	1
Problems with Hybrid Cells .....	3
Topics to be Investigated .....	6
II. Literature Review .....	9
In-Vitro Cathode Data .....	10
In-Vivo Cathode Performance .....	15
Mechanisms of Oxygen Reduction .....	18
Open Circuit Potentials .....	19
Diagnostic Criteria For Oxygen Reduction .....	21
Suggested Mechanisms .....	24
Influence of Foreign Ions on Oxygen Reduction .....	27
Composition of Interstitial Fluid .....	28
III. Experimental .....	32
Mechanism on Platinized Platinum .....	32
Electrode Material and Preparation .....	32
Equipment .....	34
Electrolyte and Gases .....	40
Procedures .....	43
Pretreatment .....	43
Tafel Slope .....	44
Reaction Orders .....	44
Characteristics of Activated Carbon in Neutral Saline .....	45
Equipment .....	46
Procedures .....	55
Galvanostatic .....	55
Automated Load Switching .....	58
Foreign Ion Effects on Activated Carbon Cathodes .....	58

	page
Addition of By-products From Hybrid Fuel Cell Anodes .....	58
Interstitial Fluid Effects on Activated Carbon Cathodes .....	59
IV. Results .....	62
Platinized Platinum .....	62
Activated Carbon in Neutral Saline .....	73
Galvanostatic .....	73
Constant Load .....	82
Foreign Ion Effects on Activated Carbon .....	87
Effects of By-products Produced at Hybrid Fuel Cell Anodes .....	87
Artificial Interstitial Fluid .....	87
V. Discussion .....	93
Oxygen Reduction on Platinized Platinum .....	93
Activated Carbon Cathode .....	104
Interpretation of In-Vivo Performance From In-Vitro Data .....	104
Analysis of Automated Test System .....	112
VI. Conclusions and Recommendations .....	116
Bibliography .....	119
List of Symbols .....	126
Appendix A	
List of Equipment and Materials .....	128
Appendix B	
Culture Media Composition .....	131
Appendix C	
Limiting Current From Diffusion Layer Theory .....	132

## LIST OF FIGURES

Figure	page
1	Voltage vs. Current Density Teflon Bonded Pt Black Electrodes ..... 12
2	Voltage vs. Time In-Vivo ..... 17
3.	Scanning Electromicrograph of Platinized Pt Electrode ... 35
4	Photograph of Platinized Pt Electrode ..... 36
5	Diagram of Glass "H-Cell" ..... 37
6	Photograph of Glass "H-Cell" ..... 38
7	Photograph of Potentiostatic and Galvanostatic Equipment ..... 41
8	Diagram of Potentiostatic Circuit ..... 42
9	Scanning Electronmicrograph of Activated Carbon Cathode ..... 47
10	Photograph of Activated Carbon Cathode ..... 48
11	Diagram of Galvanostatic Circuit ..... 50
12	Photograph of Cell Bath for Automated Load Switching Tests ..... 52
13	Diagram of Switching Arrangement for Automated Load Switching Tests ..... 53
14	Photograph of Insulated Cell Baths and Switch Box for Automated Load Switching Tests ..... 56
15	Voltage vs. Current Density Platinized Pt Electrode ..... 63
16	Current Response to Voltage Step Change Platinized Pt Electrode ..... 65
17	Voltage vs. Current Density - Platinized Pt Electrode with Variable $PO_2$ ..... 67
18	Voltage vs. Current Density - Platinized Pt Electrode with Variable pH ..... 68
19	Current Density vs. $PO_2$ - Platinized Pt Electrode with Variable pH ..... 70
20	Voltage vs $PO_2$ - Platinized Pt Electrode ..... 71



Figures	page
21 Current vs. pH at Constant Voltage - Platinized Pt Electrode .....	72
22 Voltage response to Current Step Change Activated Carbon Cathode .....	74
23 Voltage vs. Current Density - Activated Carbon Cathode with Variable $PO_2$ .....	75
24 Voltage vs. $PO_2$ - Activated Carbon Cathode .....	76
25 Voltage vs. pH - Activated Carbon Cathode .....	77
26 Voltage vs. Temperature - Activated Carbon Cathode .....	78
27 Voltage vs. Current Density - Activated Carbon Cathode, Stirred and Unstirred Solutions .....	81
28 Voltage vs. Current Density - Activated Carbon Cathode by Automated Load Switching .....	83
29 Voltage vs. Current Density - Activated Carbon Cathode by Automated Load Switching, Variable Switching Interval .....	84
30 Voltage vs. Current Density - Activated Carbon Cathode, Automated Load Switching vs. Galvanostatic .....	86
31 Voltage vs. Current Density - Activated Carbon Cathode in Artificial Interstitial Fluid .....	88
32 Voltage vs. $PO_2$ - Activated Carbon Cathode in Artificial Interstitial Fluid .....	90
33 Voltage vs. Current Density - Activated Carbon Cathode in Artificial Interstitial Fluid plus Protein .....	92
34 Nernst Diffusion Layer Model .....	110
35 Voltage vs. Current Density - Teflon Bonded Pt Black by Automated Load Switching .....	114

## LIST OF TABLES

Table		page
1	Diagnostic Criteria for Teflon Bonded Pt Black from Henry and Fishman (39) .....	14
2	Electrolyte Composition of Interstitial Fluid .....	30
3	Non-electrolyte Composition of Interstitial Fluid .....	30
4	Effect of $Al^{+3}$ and $Zn^{+2}$ on Cathode Voltage ..	87

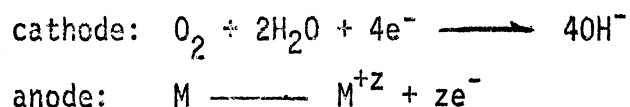
## INTRODUCTION

For many years there has been a concentrated effort to develop an implantable power supply for cardiac pacemakers and related devices which would greatly extend their present two year average life expectancy. A number of methods have been proposed to accomplish this (1,2) including a variety of conventional type battery systems (3), piezoelectric energy converters (4,5,6), a plutonium 238 nuclear source (7), a solid state lithium cell (8), and galvanic cells utilizing interstitial fluid as the electrolyte (9,10,11,12). In addition to the galvanic method of bioenergy production, a fuel cell reducing oxygen at the cathode and oxidizing carbohydrates at the anode has been considered (13-16). A combination of the galvanic and fuel cell approaches, a hybrid biogalvanic fuel cell, has been shown to have great promise by a few investigators but is, as yet, unproven for long term application (17-26). This work is primarily aimed at gaining a deeper understanding of the characteristics and mechanism of oxygen reduction at platinum cathodes under the constraints imposed by the biological system.

### The Hybrid Biogalvanic Fuel Cell

The hybrid biogalvanic fuel cell consists of a catalytic, oxygen reducing cathode and a sacrificial metal anode. The cell is implanted either subcutaneously or intramuscularly and generally has a total volume on the order of twenty-five cubic centimeters. The half cell

reactions are thought to be:



where M represents a particular metal or alloy. Aluminum, zinc, and magnesium (in either pure or alloyed form) have been considered as possible anode materials. There are a number of materials which have been tested for use as cathodes including platinum (10,17-26) palladium (27), ferric phthalocyanine (28), and gold-palladium alloys (29). In theory, the total life expectancy of a power cell is a function of the anode mass. The maximum deliverable power is limited by the surface area of the cathode. It is estimated that an average power of 100 microwatts would be required for driving a cardiac pacemaker and a ten year life expectancy would be acceptable. With these criteria in mind, it has been demonstrated, under in-vitro and in-vivo conditions, that a hybrid cell would be a suitable source of energy (21-26).

The advantages of the hybrid biogalvanic fuel cell have been described elsewhere (30). The most important, of course, is the extended life expectancy from a low volume package, but there is also a distinct advantage in using interstitial fluid as the electrolyte. Conventional battery systems are plagued by either leakage of body fluids into the cell causing short circuiting of the battery or leaking of battery by-products causing short circuiting of electronic components. These problems are negated with the hybrid cell because there is no enclosure.

## Problems with Hybrid Cells

One of the difficulties with hybrid cells has been a degradation in the power output after the first few days of implantation. This is due mainly to a decrease in the cathode voltage. There have been a few hypotheses advanced to explain this phenomenon, the major ones being as follows:

- 1) The oxygen partial pressure in subcutaneous tissue is very low (20-30 mmHg) and is not sufficient to sustain the cathode reaction (27);
- 2) Precipitates from products of the anode reaction (metal hydroxides and oxides) block the cathode surface lowering its active surface area (24);
- 3) The reaction at the cathode is a mixed one involving the oxidation of carbohydrates causing a lower, mixed potential (16,29);
- 4) Proteins and other charged particles present in interstitial fluid "poison" the cathode (15,16,31);
- 5) Catalyst material is worn away from the current collecting screening material due to abrasive movements of surrounding tissue (31).

Many of these conjectures have been crudely tested at one time or another, but to date, there is a great lack of concrete evidence to describe the in-vivo operating characteristics of cathode materials. Even so, possible solutions to the supposed problems have been suggested and attempted. In the case of limiting oxygen concentration, one can increase performance slightly by varying implantation site or by enhancing the growth of vascular tissue in the capsule which forms

around implanted cells. Roy has used a silastic membrane window to increase  $PO_2$  at a platinum cathode (10). However, this is not a very practical approach. In reality, if the partial pressure of oxygen at the cathode surface were the major factor involved in the decrease of the cathode voltage, there is little that can be done from a practical standpoint. Thus, an accurate determination of the oxygen dependency of cathode materials is indispensable in evaluating the maximum capabilities of a hybrid fuel cell.

If the precipitation of insoluble products of the anode reaction or the presence of ions formed at the anode have a detrimental effect on the cathode reaction there are possible alternatives. First, one anode might be preferred over others if it were found to be less harmful in this respect. Secondly, an anion exchange membrane could separate the anode from the cathode preventing the escape of cations. This latter alternative has been suggested by Tseung and King also as a means of preventing toxic side effects of anode materials (24). This approach has one of the same disadvantages as conventional cells; i.e., a leaky membrane would negate the original purpose and thus presents a mode of failure which was hopefully circumvented by the use of a hybrid cell. It should also be mentioned that the topic of toxicity of aluminum and zinc at concentration levels produced by bioenergy sources is controversial (1) and may prove to be of no consequence.

The effects of mixed potentials and poisoning present similar solutions and problems as do the effects of anode by-products. Again, neither effect has actually been shown to be significant, but if this were the case, there are specific steps that could be taken. Modification of catalyst material and/or structure has been suggested (29).

In theory, it should be possible to formulate a catalyst which would be specific for oxygen reduction and not be hampered by local oxidation of carbohydrates. The gold-palladium alloys are said to have such properties, however, the claim of their enhanced capabilities is controversial (26). It is here that a clear understanding of the oxygen reduction process would be most useful. As will be detailed in the next section, the reduction of oxygen has been the center of many investigations over the past twenty years. Typically, the reaction has been studied in either strong acid or basic environments and very little attention has been given to neutral electrolytes.

More information about the mechanistic and adsorptive properties of catalyst materials in near neutral solutions might lead to the design of a more efficient cathode. It is quite possible though, that the mixed potential effect on platinum in biological fluids is not a significant factor in the problem of in-vivo voltage degradation. This point remains to be clarified.

The idea of an oxygen permeable membrane as a cathode enclosure has been mentioned in a number of publications (15,16,24,31). Its primary advantage would be to exclude larger molecules and prevent both the mixed potential effect and poisoning of the cathode, while permitting oxygen to arrive at the catalyst surface unhindered. Many investigators have taken for granted that such a membrane is, in fact, feasible. However, it has been shown that silicone rubber membranes, which perform quite well in simple salt solutions, are not suitable under in-vivo conditions (31). The task of developing a membrane system for a hybrid or pure fuel cell may prove to be formidable. Again the poisoning question has not been clearly defined and awaits intense scrutiny.

In contrast to the previous problems, erosion of the active catalyst surface seems to have been solved. Teflon bonded platinum catalysts, which have found frequent in-vivo usage, are very unsuitable because of their fragile structure. An activated carbon electrode, manufactured by ESB research, has been shown to have superior capabilities in this respect. Partly for this reason and also because of its adequate catalytic properties, the ESB electrode is the primary subject of this investigation.

### Topics to be Investigated

With the previous discussion in mind, the overall scope of this dissertation can be described. It is obvious that even after a number of years of investigation, the in-vivo operating characteristics and reaction mechanism of oxygen reduction on bio-fuel cell cathodes are not clear. The task of clarifying each of the above mentioned aspects of the problem is enormous, and only certain topics will be covered here.

The most difficult venture is the elucidation of the oxygen reduction mechanism. It would be idealistic to expect that the current controversy concerning the mechanism will be settled. However it is hoped that data will be presented which will open the discussion of the mechanism in neutral chloride solutions. Indeed, there have been many problems associated with reproducibility of platinum electrodes in strong acid and basic solutions. It is, then, understandable that this lack of reproducibility would be encountered when neutral solutions are utilized and even more so with the presence of chloride ions (chloride is strongly adsorbed on platinum). However, there has been no attempt to



date to collect steady-state mechanistic data from platinum electrodes in neutral chloride solutions and the research presented in this work is aimed at exploring this area. Thus, steady-state overvoltage curves and oxygen and pH dependencies in the neutral region will be described and their implications examined.

Some mention of the type of electrode to be studied for mechanistic purposes is required here. More detail will be given later. Porous electrodes present great difficulties in the studies of reaction mechanism as there are no accurate means of accounting for concentration gradients inside the porous structure or for distributed voltage drops. In the case of platinum black dispersed in a teflon binder, an attempt has been made to analyze over-voltage characteristics on the basis of a number of structural parameters (32). It was determined that this type of electrode supposedly could be analyzed in a manner analogous to a smooth electrode. Other means have also been used to adapt the porous structure to a form which could be more easily investigated (33,34). However, the activated carbon electrode, which has been found to be so satisfactory for in-vivo hybrid cells, is even much more difficult to study than a simple dispersed platinum-black cathode. Thus, for initial considerations, a lightly platinized platinum electrode has been utilized for the study of the oxygen reduction mechanism. The assumption that the mechanism is the same on the different surfaces may or may not be valid, but at the present state of knowledge, it will be used. Thus, the mechanism will first be investigated on the simplest surface, then, depending on the results, further steps can be taken to study the initial assumptions.

Aside from the mechanistic study, performance data under carefully controlled conditions will be presented. These are divided into a number of areas. First, the performance of the ESB cathode under galvanostatic control in a simple buffered saline solution will be described. Oxygen and pH dependency as well as overvoltage characteristics have been observed although no strict mechanistic analysis is attempted because of the complexity of the electrode structure. The overvoltage data under galvanostatic control can also be compared to performance data collected under less stringent conditions which have been used to compare various cathode materials (35). Thus, the validity of this latter form of data can be tested.

To determine the effects of anode by-products, porous cathodes have been observed for periods of days in solutions saturated with aluminum and zinc ions. Similarly, in the case of interstitial fluid components, tests have been conducted using a simulated interstitial fluid as the electrolyte. In the latter, it is most important that rigid aseptic conditions be maintained to prevent growth of possible interfering organisms. This factor has not been accounted for in other published investigations (29,31) and has limited their testing times to relatively short periods.

With the results of experiments conducted as outlined above, the factors involved in the operation of hybrid fuel cell cathodes can be separated and more clearly understood. Also, some insight will have been gained into the mechanism of oxygen reduction on platinized platinum in neutral chloride solutions. From this point, further decisions can be made as to what courses of action, if any, should be taken to improve cathode performance.

## LITERATURE REVIEW

### Cathodes for Oxygen Reduction in Biological Fluids

The most widely used cathode for both hybrid and pure biological fuel cells has been platinum black dispersed in a binder material. This type of electrode\* typically had a catalyst loading of from 10 mg to 40 mg per  $\text{cm}^2$  of geometrical surface. The catalyst was spread on a current collector screen of tantalum. This structure was rather fragile and catalyst material could easily be removed by rubbing. Other investigations have utilized laboratory manufactured electrodes similar in structure to the above cathode (24,36,39). Quite detailed studies in neutral media on platinum black and other similar cathodes have been carried out by the Monsanto Research Corporation (37). However, in each case mentioned, where mechanisms were proposed they are based on data collected from electrodes with a porous structure. As mentioned previously, mechanistic analyses of this form of platinum electrode have not been proven to be valid.

Cathodes manufactured by ESB Research are more complex and the actual manufacturing techniques are still proprietary. However, the basic sequence in manufacture consists of first precipitating platinum black on carbon. This is then dispersed in a Teflon binder and, in some cases, spread on a Teflon backing. A tantalum screen is

---

\*Types AA-1 and AA-40 obtained from American Cyanamid Corporation.

then pressed into the electrode. Electrodes are also produced without teflon backing in a similar manner. These electrodes have performed quite well in both in-vivo and in-vitro tests and the catalyst material is not easily removed by abrasion(25).

### In-Vitro Cathode Data

There are a great deal of performance type data in the literature which have described the characteristics of platinum black oxygen cathodes under relatively simple conditions. That is, although the electrolyte solutions utilized simulate the pH and salt concentration of biological fluids, neither the protein, amino acid, nor oxygen concentrations are usually duplicated.

Polarization data have been collected by two different means. Usually, cathodes are tested as a part of a particular power cell; i.e., with a sacrificial metal or carbohydrate oxidizing anode. The electrode pair is subjected to different simulated loads in the form of a pure resistance and voltage monitored. A plot of half-cell voltage vs. current is then used to assess the cathode and anode performance. A saturated calomel electrode (SCE) is most often the reference electrode and the electrolyte is either isotonic saline or Ringer's solution. An alternative to load simulation is a galvanostatic technique in which current is controlled with a DC power supply and large series resistance. In this case, either the anodes described above or a platinum counter electrode is used for the other half of the test cell. The data collected by both of these techniques is similar in that the rate of reaction (current) is, for all practical

purposes, the controlled (independent) variable rather than the cathode voltage.

It would be impractical to present data here for all types of cathodes. Moreover, much of the data reported includes only total cell voltage and, in many cases the test conditions were not well controlled or are unsuitable for analysis. However, some knowledge of the characteristics of typical cathodes is necessary and this can be conveyed in the form of a few graphical representations of data collected.

An extensive investigation of materials for hybrid power cells has been carried out by Hahn and Cooper, et al. (40). For their studies, an automated data collection system was developed for gathering voltage versus current data (35). Half-cell voltages were monitored, loads switched at appropriate intervals, current calculated and voltage versus current plotted by a Linc-8 computer and Calcomp plotter. In Figure 1, a typical computer generated polarization curve is shown. The cathode was type AA-1 American Cyanimid platinum black on tantalum screen and the anode was aluminum, both with geometric area =  $4\text{cm}^2$  (2 cm x 2 cm). Superimposed on this graph are data from four different publications in which a similar (Teflon bonded) cathode material has been tested and testing conditions were similar (i.e.  $37^\circ\text{C}$ , atmospheric oxygen and in saline or Ringer's solution). The only difference worthy of mention is that in the investigation by Tseung and King (24) the cathode material was manufactured by the authors.

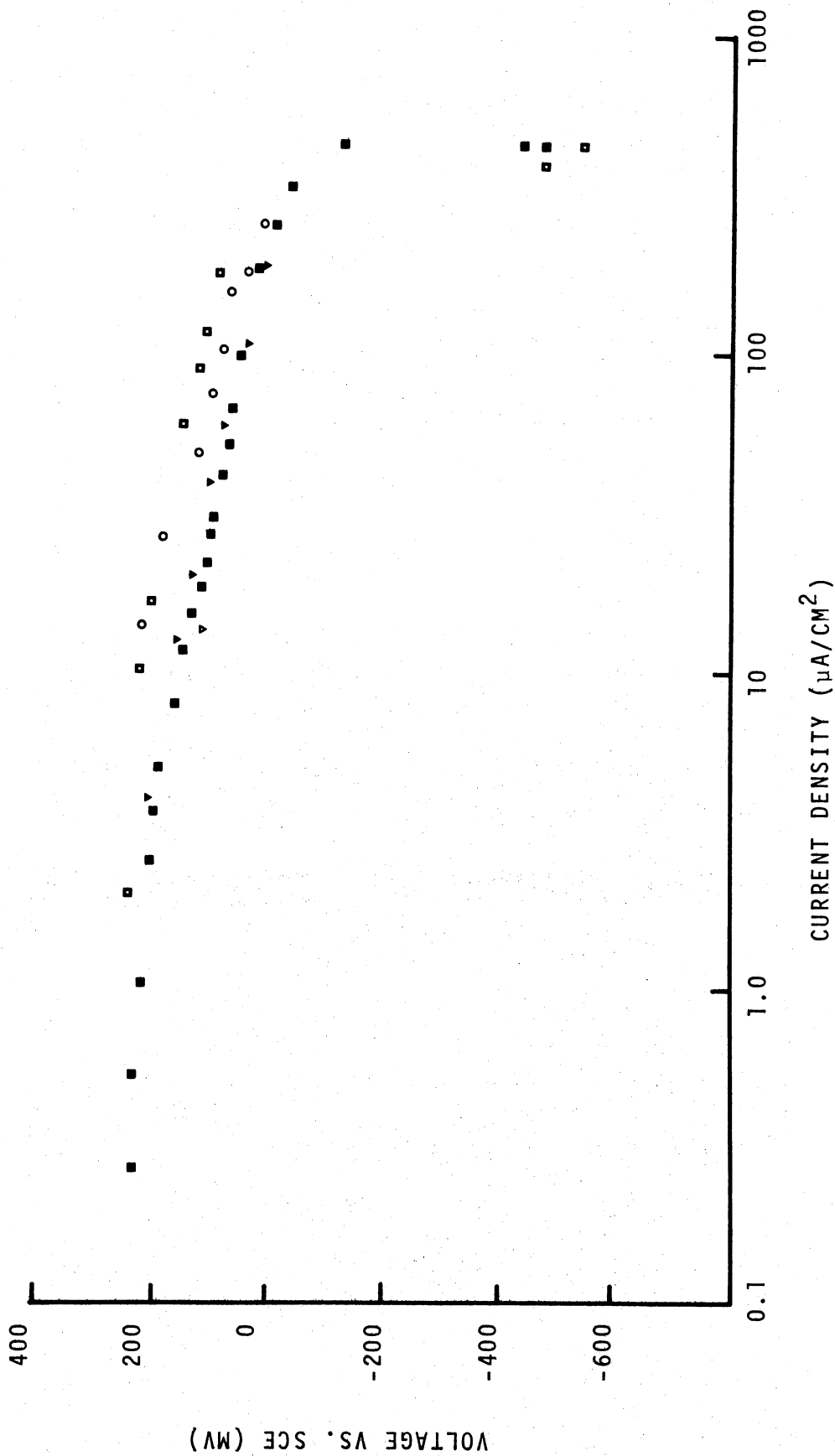
It can be seen that in-vitro data from Teflon bonded cathodes is generally reproducible under simple conditions. In the linear region,

FIGURE 1

VOLTAGE VERSUS CURRENT DENSITY  
TEFLON BONDED PLATINUM BLACK ELECTRODES

- Cooper and Hahn (42)
- ▼ Derosa (36)
- ▲ Planck (18)
- ▣ Sonne (27)
- Tseung and King (24)

FIGURE 1



the slopes of the curves are on the order of 140 millivolts per decade and limiting current about  $450 \mu\text{a}/\text{cm}^2$ \*. The greatest spread in the data is 125 millivolts at  $14 \mu\text{a}/\text{cm}^2$  between the measurements of Plank and Derosa. All of the points plotted, except those of Hahn and Cooper, have been interpolated from graphical data presented in the various publications and are subject to slight error.

Data concerning the oxygen dependency of implantable cells have been reported by Sonne (27). In this case, a constant simulated load ( $20 \text{ K } \Omega$  with  $4 \text{ cm}^2$  cathode) was maintained across a hybrid cell and the voltage monitored at oxygen partial pressures from 0.01 to 0.209 atmospheres. The results of these experiments would indicate that there is a marked decrease in both total cell and cathode voltages at oxygen partial pressures in the physiological range of subcutaneous or intramuscular tissue.

Henry and Fishman (39) have reported briefly on galvanostatic data taken from metal black diffusion electrodes in acid, basic and neutral solutions without chloride ion. Their data is sketchy and methods are not clear; however, it is the only publication in which a full range of parameters was varied. For a platinum black Teflon bonded electrode, a summary was given and is shown in Table 1. (See page 14).

There are a few publications in which attempts have been made to assess the effects of interstitial fluid components on platinum oxygen cathodes. Both constant voltage and constant current (or load) techniques have been employed. The methods usually consist of

---

\*area based on one side only



TABLE 1

pH	Tafel slope (mv)		$\frac{\partial E}{\partial \log PO_2}$	$\frac{\partial \log i}{\partial \log PO_2}$	$\frac{\partial E}{\partial pH}$		$\frac{\partial \log i}{\partial pH}$ O <sub>2</sub> & air
	O <sub>2</sub>	air			O <sub>2</sub>	air	
1-2.5	-60	-60	30	.45- .6	-95	-100	-.9 to 1.4
5-8	-120	-125	60	.2 - .4	-60	-60	-.5
12-14	-60	-60	35	.4 - .5	-30	-30	-.4

adding certain substances to a cell which has a simple salt (Ringer's, Kreb's-Ringer's, or Saline) solution as an electrolyte. The results of these experiments are extremely difficult to interpret quantitatively because of the variation in conditions. Also, in no case has bacterial growth been prevented although in one instance this was unsuccessfully attempted (15).

It appears that oxygen reduction is moderately inhibited in the presence of dextrose (13,25). Fishman and Henry maintain that the reduction in current is at least 50% at 0.80 volts (vs. NHE at same pH, i.e. about 200 mv polarization from initial open circuit) (29). However, there are apparently some contradictions in the data presented (25). Briefly, the current densities reported are extremely high and may be in the limiting current region. Also, catalyst loading is abnormally large (100 mg Pt/cm<sup>2</sup>) and the duration of the test cycle is relatively short (one hour after addition). Wolfson, *et al.*, mention that addition of glucose to a half-cell oxygen cathode caused "an immediate loss of output with partial recovery", but state no actual figures (13).

In one investigation, 10% plasma additions to basic electrolyte solutions were shown to reduce cathode performance (28,38). Only a relatively fast voltage sweep technique (0.25 and 0.10 volts/min.)

was used, making it difficult to predict long-term steady state performance. However, from interpolation of graphical data, there is apparently a decrease in half-cell voltage of approximately 180 mv at about  $40 \mu\text{a}/\text{cm}^2$  on a smooth platinum wire in solution saturated with oxygen (1 atm.)

The effect of protein addition to hybrid fuel cells has been studied (31). Low protein concentrations (0.5 gm%)\* effected an initially drastic decrease in voltage (at constant load) with almost complete recovery. High concentration (2.0 gm%) of protein caused a greater initial drop and less recovery. The tests were only qualitative in conjunction with an attempt to utilize oxygen permeable membrane as a protective covering for implantable cells. Results of these experiments also indicate that membranes may not be effective in preventing voltage degradation in-vivo.

#### In-Vivo Cathode Performance

The majority of investigations into the operation of implantable oxygen reducing cathodes have, been of an in-vitro nature with few, if any, implantation experiments. In cases where in-vivo data are reported, half-cell voltages are often not measured and other experimental variables are unclear. However, investigators do generally agree that in-vivo cathode performance is substantially below that determined in in-vitro testing (10,17,19,23,31). Typically, there is a pattern of voltage deterioration during the early days of

---

\*gm% = grams per 100 ml solution

implant followed by a recovery to levels still below the initial voltage. Examples of this are shown in Figure 2. Curves #1 and #2 represent total voltage data from Hahn, et al., in which activated carbon cathodes and aluminum alloy or zinc anodes were implanted in dogs (41). In the former curve, the load consisted of a functional cardiac pacemaker pulsing at a rate of about 110 pulses/min. (25). Average current drain is about  $2 \mu\text{a}/\text{cm}^2$ , but drawn in a pulsed mode (zinc anode). Voltages in curve #2 were measured by means of an implanted voltage monitoring transmitter powered by the hybrid cell (41). Here the anode was an aluminum alloy and current drain averaged less than  $1 \mu\text{a}/\text{cm}^2$ . Prior to implant, cells are run in-vitro with their respective loads for a number of days and individual half-cell voltage is measured. In-vivo, anode and cathode voltages are monitored by reference to a SCE placed on a wetted area of skin. Although, this is not a highly accurate technique, results indicate that cathode voltage, after stabilization, is about 300-400 mv less than that measured in-vitro. Curve #3 shows similar data taken from Roy and Wehnert (10). This particular cell was a Teflon dispersed Pt black cathode (approximately  $13 \text{ cm}^2$  area) and zinc anode. A constant load of 3,300 ohms across the terminals drew a current of about  $19 \mu\text{a}/\text{cm}^2$ . It is estimated that cathode voltage would be about -200 mv versus SCE since zinc anodes have typically operated near -1000 mv versus SCE in-vivo. (42)

Although it is difficult to accurately quantitate the decrease in cathode performance, it can be seen that in-vitro and in-vivo operating characteristics are not identical. Hopefully, the factors

FIGURE 2

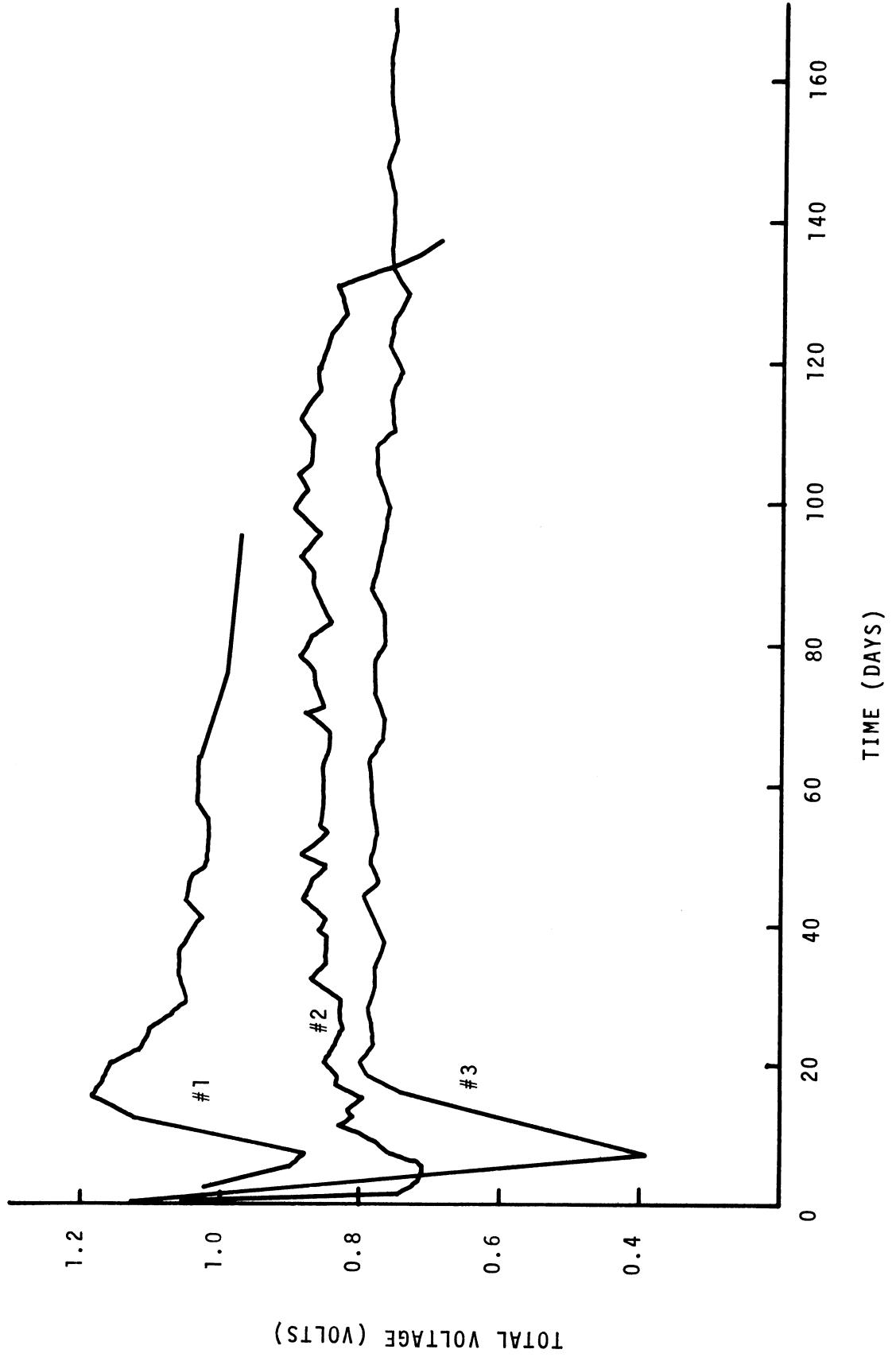
VOLTAGE VERSUS TIME IN-VIVO

#1 - Hahn, et. al. (26)

#2 - Hahn, et. al. (26)

#3 - Roy and Wehnert (10)

FIGURE 2



accounting for this discrepancy will become clear with the presentation of data in sections to follow.

### Mechanisms of Oxygen Reduction

#### Solutions and Surfaces Studied

There are a number of recent reviews in which oxygen reduction on platinum is thoroughly discussed. Three of these deemed most important are those by Bockris and Conway (1969) (43), Hoare (1968) (44), and Vetter (1967) (45). Even with the results of a large number of investigations there appears to be a lack of agreement on the mechanism of this complex reaction. Following will be a concise summary of the major relevant points pertaining to this area of research especially where these points could apply to the reaction in neutral media.

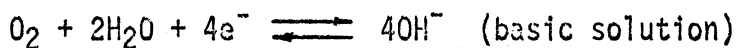
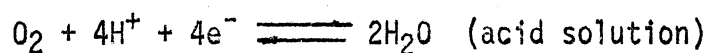
Oxygen reduction has been most frequently studied in acid (pH 1-3) electrolytes although alkaline media (pH 11-14) have received a fair amount of attention. In the former, sulfuric (0.1-2N) and perchloric (1N) acids were most often utilized and in the latter, sodium and potassium hydroxides (1N). There are very few reports of mechanistic studies in neutral media. Delahay determined polarization curves on platinum in KCl solution (pH 6.9) by an indirect technique, but encountered unexplainable variations in current during the course of experiments (46). More recently, Kozawa, et al., used linear sweep voltammetry and a ring-disc electrode in comparing various materials for oxygen reduction in buffered neutral saline (pH = 7.22) (28). Hoar, in a 1933 publication,

gives one voltage-current curve for a phosphate buffer electrolyte (pH 7.0) along with others for acid and basic solutions (47). Steady state polarization data and reaction orders are, however, not generally available for the case of neutral chloride containing solutions.

In studies of reaction mechanism, smooth platinum surfaces were typically used. The pretreatment of the metal surface has been shown to have a pronounced effect on the behavior of the electrode at open circuit and/or under polarization conditions. Bianchi and Mussini treated platinum discs by ten different means and found a wide variation in Tafel slopes; i.e., 60-240 mv/decade (48). Damjanovic and Bockris have shown that a bare platinum surface is a much better oxygen reducing catalyst than an oxide-covered one (49). The question of the oxide vs. adsorbed oxygen surfaces has been discussed (43,44). There seems now to be some agreement that above 1 volt versus the normal hydrogen electrode (NHE), oxygen is present in the form of platinum oxides, whereas below 1 volt, oxygen is an adsorbed species. Thus, at true steady state, oxygen dissolution should occur at an oxide free surface, since oxides will eventually be removed. Interpretation of experimental results from some investigations is difficult because it is not clear as to what type of surface was actually studied. Relatively fast measurements on anodically treated surfaces are probably dealing with an oxide covered platinum while cathodically treated electrodes should be oxide free.

#### Open Circuit Potentials

The overall reaction for the reduction of oxygen is known to be:



The theoretical open circuit potential from thermodynamic considerations is:

$$\phi = \phi_0 + \frac{RT}{4F} \ln P_{\text{O}_2} + \frac{RT}{F} \ln [\text{H}^+] - \frac{RT}{2F} \ln [\text{H}_2\text{O}] \quad (\text{acid})$$

or

$$\phi = \phi_0' + \frac{RT}{4F} \ln P_{\text{O}_2} - \frac{RT}{F} \ln [\text{OH}^-] + \frac{RT}{2F} \ln [\text{H}_2\text{O}] \quad (\text{basic})$$

with

$$\phi_0 = 1.227 \text{ volts} \quad (\text{acid})$$

$$\phi_0' = 0.400 \text{ volts} \quad (\text{basic})$$

at 25°C

Thus, at pH = 0 and  $P_{\text{O}_2} = 1$  atmosphere,  $\phi = 1.227$  volts for the thermodynamically reversible electrode reaction. It is well known that this potential is rarely observed under normal experimental conditions. Bockris and Huq (1956) were the first to observe the 1.23 potential at open circuit (50). Later, Watanabe and Devanathan measured an oxygen partial pressure dependence to be very close to the theoretical 15 mv per tenfold change in pressure. In both instances, the results were obtained under ultrapure conditions after prolonged anodic and cathodic preelectrolyses. Hoare has shown that the reversible potential can be attained with an electrode pretreated in nitric acid (52).

Usually, a potential of about 0.98 volts (pH = 0,  $P_{\text{O}_2} = 1$  atmosphere) is observed on platinum. There have been a number of theories advanced for this deviation from the reversible value.



Wroblowa, et al., have reviewed many of these and concluded that low levels of impurities could well account for this phenomena (53). The exchange current density for the oxygen reaction is about  $10^{-10}$  amp/cm<sup>2</sup> and, it has been shown that residual impurities of  $10^{-11}$  gmole/liter could begin to affect the reversible potential (43). Hoare presented a number of metal-metal oxide equilibrium potentials which could conceivably cause a mixed open circuit voltage of about 1.0 volts, but rejects them because of other evidence, especially the observed oxygen dependency of 60 mv/decade which accompanies the 0.98 potential (44).

#### Diagnostic Criteria for Oxygen Reduction

There are conflicting experimental results with respect to the various diagnostic criteria which are necessary for elucidation of the oxygen reaction mechanisms. Some of the conflict is probably due to variation in surface properties of the platinum studied, but in other instances, there are no readily apparent reasons for inconsistencies in data from different investigations. Also, there is evidence that the reaction mechanism is not the same in both acid and alkaline solution. However, it is often stated that the reaction in neutral solution follows the same path as that in acid solution (45). A summary of past observations should place the present status of knowledge in some perspective.

Generally, voltage versus log current density plots show a linear (Tafel) region from about one to one hundred  $\mu$ amp/cm<sup>2</sup>. At an oxygen pressure of one atmosphere, a diffusion limiting current sets in at

one  $\text{mA}/\text{cm}^2$  and the potential decreases to the region of hydrogen evolution. Both Damjanovic and Brusic (54) and Bianchi and Mussini (48) reported a Tafel slope of about  $-60 \text{ mV}$  for an oxide free platinum surface in acid solution. Hoare indicated that the slope was actually closer to  $-2(2.3)RT/F$  ( $-120 \text{ mV}$ ) for surfaces which would seem to be oxide free; i.e., prolonged cathodic prepolarization (55). In another publication, Damjanovic, et al., measured a cathodic slope of  $-2(2.3)RT/F$  ( $-120 \text{ mV}$ ) for an oxide covered electrode (anodic pretreatment), but they mention difficulty with reproducibility of cathodic data (56). More recently, Damjanovic and Genshaw utilized a rotating disk electrode to remove mass transfer limitations at higher current densities (57). They found that the slope of  $-60 \text{ mV}$  which they determined earlier on oxide free Pt increased to  $-120 \text{ mV}$  above one  $\text{mA}/\text{cm}^2$ .

In alkaline solution, a value of about  $-(2.3)RT/F$  has been reported for the Tafel slope on oxide covered (54,56,57,58) and oxide free surfaces. As in acid solution at higher current densities, a change of slope to  $-2(2.3)RT/F$  was observed (57). In a  $1/15 \text{ M}$  phosphate buffer (pH 7.0), Hoar measured a value of  $118 \text{ mV/decade}$  for  $\partial V/\partial \log i$  on bright Pt (47). However, the curve in neutral solution was shifted far below that in acid solution ( $0.1 \text{ N H}_2\text{SO}_4$ ) or alkaline solution ( $0.1 \text{ N NaOH}$ ) indicating a much lower activity. Winkelmann, at pH 8.6 (phosphate buffer), indicates that at this near neutral condition, the voltage-current curve is very steep and apparently varies somewhat with oxygen concentration (59). However, his curves were taken rather quickly (10 seconds at each point) and are probably far from steady state.

The oxygen and pH dependencies of the oxygen electrode reaction have been determined in both acid and basic solutions. On oxide covered electrodes the values summarized by Bockris (43) are  $\partial V/\partial \text{pH} = 60 \text{mv}$  (acid);  $-90 \text{mv}$  (alkaline) and  $\partial \log i/\partial \log \text{PO}_2 = 0.30$  (acid);  $0.24$  (alkaline). On oxide free electrodes values are given as follows:  $\partial V/\partial \log \text{PO}_2 = 60 \text{mv}$  and  $\partial V/\partial \text{pH} = 100 \text{mv}$ . In contrast, Vetter agrees that the oxygen reduction reaction is first order with respect to oxygen, but asserts that it is independent of hydrogen ion concentration in acids, i.e. zero order with respect to  $[\text{H}^+]$ , and first order in alkaline solution (45).

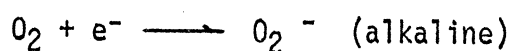
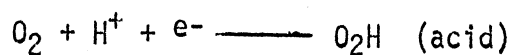
Another very important factor in the elucidation of the oxygen reduction mechanism is the formation of hydrogen peroxide. It has been detected by many investigators during the course of the former reaction on platinum and other metals. The question which has been raised often is whether or not the peroxide formed is an intermediate in the oxygen reaction mechanism or the product of some impurity side reaction. The reviews cited earlier discuss the usual arguments in some detail, but there still exists a distinct lack of agreement. In highly purified solutions it has been shown on a ring disc electrode that hydrogen peroxide is not produced above  $0.15 \text{V}$  versus the hydrogen electrode (60). Thus, in conjunction with results of the studies on the reversible oxygen electrode in ultra-pure solutions, it would seem that solution purity can have a marked affect on mechanistic determinations (51,53).

Tracer studies by Davies, et al., with  $^{18}\text{O}$  on active carbon in  $1 \text{M KOH}$  led to the conclusion that the O-O bond is not broken during the intermediate reduction process of oxygen to hydrogen

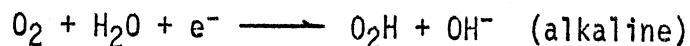
peroxide (61). However, it has been suggested that on oxide-free platinum in oxygen saturated solution the adsorption of  $O_2$  may be accompanied by dissociation (62). No conclusive proof for this has been presented (43). Thus, in proposed mechanisms, either one assumption or the other is usually made at the outset.

### Suggested Mechanisms

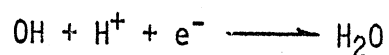
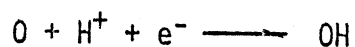
There have been numerous mechanisms proposed for the oxygen electrode reaction. In fact, it has been stated often that the reaction may occur along different paths in the anodic and cathodic directions (44). Damjanovic, Dey, and Bockris have listed fourteen suggested paths and calculated Tafel slopes which would be associated with each step (56). In a latter work, it was suggested that the reaction is different in alkaline and acid solutions and that the first step in each was rate determining and as follows (54):



or



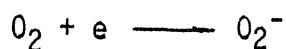
Although steps following the rate controlling step cannot be determined, they are thought to be (43):



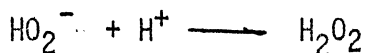
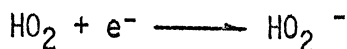
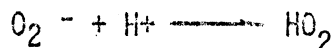
These conclusions were drawn for oxide-free platinum whereas, for

oxide covered Pt, other paths are suggested, again different for acid and alkaline electrolytes. Also, a change in adsorption conditions has been indicated from the shift in Tafel slopes in going from low to high current densities (51).

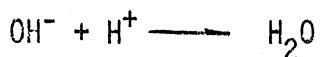
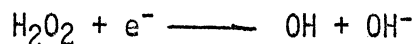
The above paths directly to  $H_2O$  may occur in parallel with peroxide reactions in solutions that are not sufficiently purified; i.e. impurities greater than  $10^{-7}$  gmole/liter, as suggested in the Bockris and Conway review (43). This low level of impurities is difficult to attain and most electrolytes are certainly impure based on such a standard. Thus, the peroxide intermediate is most often considered in kinetic studies. Hoare (44) and Vetter (45) both conclude that the reaction most likely begins with:



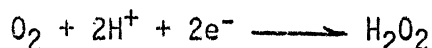
and is followed by:



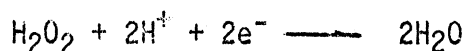
The peroxide formed can be desorbed or react further by:



The two overall cathodic reactions are:



and

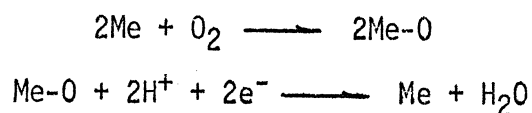


It is also possible that a local cell mechanism is responsible for peroxide decomposition by:

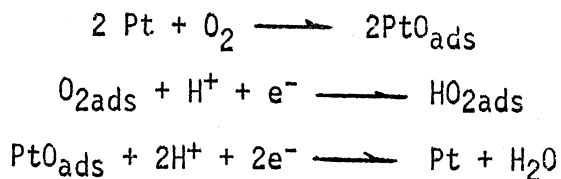


with the  $\text{O}_2$  liberated being reduced by repeating the earlier scheme.

A second class of mechanisms proposes that surface oxides or hydroxides participate in the reduction process. This particular type of mechanism has not been looked upon very favorably in the most recent reviews. However, such a mechanism could take the general form:



Bianchi and Mussini propose that in the potential region of 960 to 680 mv vs NHE the behavior of smooth platinum in acids depends on three parallel reactions (48):



At lower potentials, they contend that  $\text{H}_2\text{O}_2$  formation begins and that below 250mv peroxide reduction sets in.

Vetter has summed up the present state of affairs with regards to the oxygen electrode(45):

"A large number of variants on the mechanisms.... can be found in the literature. Since all these possibilities are discussed on a purely speculative basis, a detailed discussion is not appropriate. The mechanism of the  $\text{O}_2$  electrode is simply not clear at present."

## Influence of Foreign Ions on Oxygen Reduction

As complex as oxygen reduction is in relatively simple solutions, the process becomes even more complicated with the presence of additional substances. In-vivo, the situation is almost inextricable when carbohydrates, amino-acids, proteins, lipids, and a number of salts must be considered. It is well known that a platinum surface will adsorb a great variety of species which can then affect its oxygen reducing capability to great extent. In particular, anion adsorption has been considered on smooth and platinized platinum as to its potential dependence and the degree to which it inhibits oxygen reduction in acid and basic solutions. On the other hand, oxygen reduction in the presence of organics found in the biological system has been given almost no attention.

Kozawa investigated the effects of a variety of anions and cations on both oxygen reduction and evolution (63). He used a relatively fast (2.5 mv/sec) linear sweep technique in sulfuric acid and sodium hydroxide electrolytes. It was found that, among a variety of ions tested, only halides in acid solution and alkaline earth metal ions in alkaline solution had "a marked effect" on the reduction process.

Bianchi and Mussini found that the addition of chloride ion to 0.5M  $H_2SO_4$  substantially lowers the open circuit potential and greatly increases the Tafel slope. (48) Moreover, the slope increased with increasing anion concentration. Specifically, with 0.02M  $Cl^-$  the rest potential was 150 mv less than in  $H_2SO_4$  alone and the Tafel slope rose to 130 mv/decade. At 1.0 M  $Cl^-$  in sulfuric

acid, the Tafel slope was 170 mv/decade.

Studies have been made concerning the adsorption of chloride ion on platinum and its effect on oxygen adsorption. Using a differential capacitance technique, Popat and Hackerman demonstrated that in a 1.0N KCl solution, chloride ion is being desorbed from smooth Pt in the region between 0.8 volts and -0.4 volts versus SCE (64). Similar results were obtained by a tracer method on platinized platinum by Horanyi, et al., in HCl solution of varying concentration ( $1.3 \times 10^{-3}$  to  $2.6 \times 10^{-5}$  moles/L) (65,66). In the latter work, it was found that the adsorption curve was different for freshly prepared versus used electrodes and, also that hysteresis occurred upon reversal of the direction of voltage change.

Adsorption of halides decreases the surface coverage by oxygen as determined by Bagotzky, et al. (67,68). The fractional coverage ( $\theta$ ) of halide is an exponential function of concentration and linear with respect to voltage within a wide region on smooth Pt. However, a maximum surface coverage by chloride occurs above  $10^{-2}$  moles/liter at voltages between 0.3 to 0.7 volts versus NHE (0.5M  $H_2SO_4$ ) (67). Thus, it can be expected that in neutral chloride solutions (Ringer's, saline), overpotential characteristics will vary markedly when compared to studies in less strongly adsorbed electrolytes.

#### Composition of Interstitial Fluid

To assess the characteristics of porous cathodes or analyze the mechanism of oxygen reduction of platinum in biological media it is necessary to duplicate this media to whatever extent possible. Clearly, the electrolyte in which bio-fuel cells operate is extremely complex,



but its composition has been defined in a number of texts. In subcutaneous or intramuscular implantation, the fluid compartment of the body in which a cathode operates is considered to be interstitial fluid. Its composition is very similar to plasma except in protein concentration. This and other solute concentrations will now be described.

The approximate concentrations of the major anions and cations of interstitial fluid are shown in Table #2 (69). Non-electrolytes are given in Table #3 (70). There is relatively good agreement in the literature concerning the data shown with the notable exception of protein. This is, of course, a question of some concern since protein has been suspected as a possible "poison" for oxygen cathodes. Ruch and Patton state that "...interstitial fluid, unlike plasma, is nearly devoid of protein" (71, p. 887). On the other hand, Guyton puts the interstitial protein concentration at about 1.8 gm/100ml (gm%) (69) and Wiederhelm places it at about 2.1 gm% (72). Cater and co-workers used approximately 100 mg/100 ml serum protein in an artificial extracellular fluid mixture for testing a Clark-type oxygen (measuring) electrode (73). It is interesting to note that they found no effect on current from the protein at this concentration compared to tests without protein. However, at 2.5 gm%, the current was lowered by 15%. Since this type of electrode is operated in the limiting current region, it is not feasible to extrapolate to current values where the oxygen reaction is activation controlled. Also, at higher protein concentrations it is necessary to add anti-foaming agents which themselves decrease cathodic performance.

Table 2

## Electrolyte Composition of Interstitial Fluid (69)

Cations	conc. (meq/L)	Anions	conc. (meq/L)
Na <sup>+</sup>	145	Cl <sup>-</sup>	115
K <sup>+</sup>	4	HCO <sub>3</sub> <sup>-</sup>	30
Mg <sup>++</sup>	2	HPO <sub>4</sub> <sup>--</sup>	2
Ca <sup>++</sup>	3	SO <sub>4</sub> <sup>--</sup>	1
		organic acids	5
		Protein	?

Table 3

## Non-Electrolyte Composition of Interstitial Fluid (70)

Non-electrolyte	Conc. (mgm/100ml)
Phospholipids	280
Cholesterol	150
Neutral Fat	125
Glucose	100
Urea	15
Lactic Acid	10
Other	5

The amino acid concentration of interstitial fluid is another parameter which is rather elusive. Cater's artificial extracellular fluid included amino-acids as follows (73):

amino acid	mg/100ml	amino acid	mg/100ml
l-arginine	0.375	l-lysine	0.80
l-aspartic acid	0.300	l-methionine	0.25
l-cystine	0.07	$\beta$ -phenyl l-alanine	0.25
l-glutamic acid	0.75	l-proline	0.25
glycine	1.00	l-threonine	0.375
l-histidine	0.375	l-tryptophane	0.20
dl-isoleucine	0.25	l-tyrosine	0.40
l-leucine	0.25	dl-valine	0.50

The total from this list is 6.395 mg per 100 ml. Values of 4.84 and 4.90 mg/100ml have been given elsewhere for the total amino acid concentration of lymph and plasma, respectively, in dogs (74). Interstitial fluid is very similar to plasma and lymph in its concentration of low molecular weight species. Thus, these values probably are within a reasonable range for a first approximation.

## EXPERIMENTAL

In order to investigate the questions previously outlined in the Introduction, three separate experimental procedures were devised:

1. Analysis of oxygen reduction mechanism on platinized platinum.
2. Characteristics of an activated carbon cathode for oxygen reduction in neutral saline solution under (a) galvanostatic, (b) constant loading conditions.
3. Effects of products formed at hybrid fuel cell anodes and artificial interstitial fluid on an activated carbon cathode.

Each of these points has been treated individually in the hope that an increased understanding of in-vivo cathode operation will be reached. It remains now to describe the specific procedures that were undertaken toward this goal.

### Mechanism on Platinized Platinum

#### Electrode Material and Preparation

The oxygen reduction mechanism was studied on a pure platinum foil electrode, .005 cm (2 mil) thick (Fisher Scientific Company). The dimensions of all electrodes studied were 1 cm. x 2 cm. Initially, the foil was studied without platinization, but with different

pretreatments adapted from descriptions in the literature. One pretreatment consisted of heating the platinum to red hot, soaking in concentrated HCl and rinsing with distilled water. In another instance, the electrode was soaked in chromic sulfuric acid prior to the previous treatment. In a third case, trichloroethylene was used to degrease the electrode prior to following the steps in the first procedure. Each treatment also included a final cathodic polarization for fifteen seconds. The polarization behavior of electrodes prepared in this manner was observed in sulfuric acid solution to assess their performance as compared to data in the literature. Generally, similar voltage current curves were produced with this electrolyte. However, in these preliminary tests in neutral buffered saline solution the behavior of the platinum foil was not sufficiently reproducible. To overcome this difficulty a light platinization of the electrodes was required. Thus, the entire mechanistic study was carried out on such an electrode.

The platinum foil electrodes were platinized according to a procedure outlined in both Ives and Janz (75) and Feltham and Spiro (76). The foil was first welded to a 22 gauge (0.64 cm dia.) platinum wire by heating both to red hot and tapping lightly with a hammer. The wire was previously silver soldered to a three foot length of stranded copper wire and fitted into a 30 cm pyrex glass tube (5 mm I. D.). A glass to metal seal was formed leaving one cm of the platinum wire exposed. The wire in the seal was flattened to a thin crosssection in order to prepare a water tight joint. Pressure testing to 15 psi with compressed air ensured that no leaks were present. After welding, the foil and glass were rinsed

first in acetone, then in distilled water. The electrode was subjected to a ten minute cathodization with hydrogen evolution in 0.1 N sulfuric acid using a platinum foil counter electrode. After another distilled water rinse, platinization was carried out in a 2% chloroplatinic acid (Fisher Scientific Co.) in 2 N hydrochloric acid solution. The current was held constant at ten ma/cm<sup>2</sup> for fifteen minutes. The electrode was rinsed a number of times with distilled water and soaked in the same until ready for use. A scanning electronmicrograph (SEM) of the electrode surface is shown in Figure 3 and a close-up view of the electrode and glass seal in Figure 4.

#### Equipment

Procedures relating to the mechanistic investigation were performed in a pyrex glass "H-cell". A schematic diagram of the cell is shown in Figure 5 with an actual photo in Figure 6. The cell consisted of three compartments; one each for testing (working), counter, and reference electrodes. Separation between the three was by medium porosity glass frits (Ace Glass Inc.) with the additional capability of total closure with Teflon stopcocks. In order to fill the glass segments connecting the chambers, it was necessary to install relief valves as shown. Sampling of the electrolyte for pH measurements was afforded by a capillary tube extending into the test compartment. Gas for purging and/or stirring entered through a coarse glass frit located at the bottom of this section.

The counter electrode consisted of 4 cm x 4 cm piece of activated carbon on tantalum screen. It was spotwelded to a platinum

FIGURE 3

SCANNING ELECTRONMICROGRAPH OF  
PLATINIZED PLATINUM ELECTRODE

Magnification 3000X

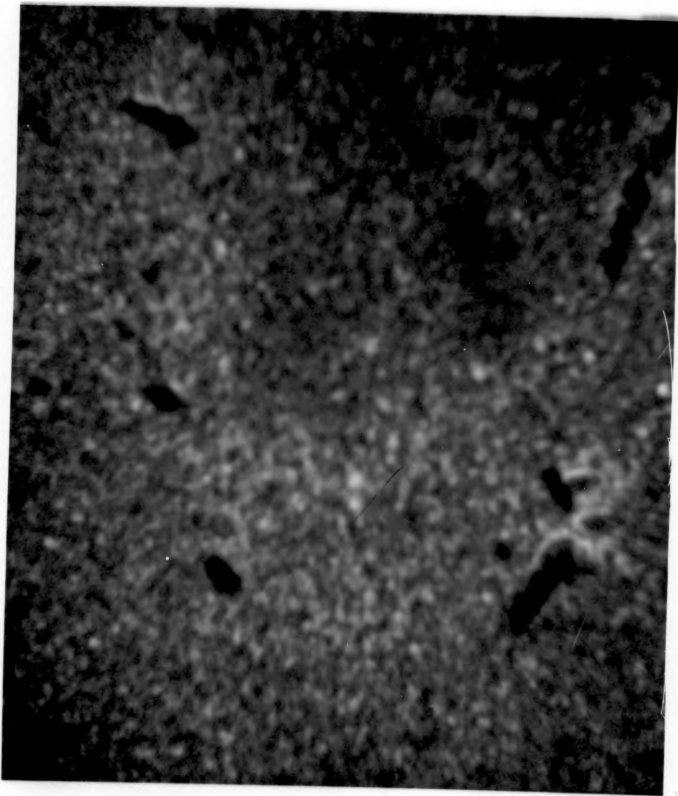




FIGURE 4

PHOTOGRAPH OF PLATINIZED PLATINUM ELECTRODE  
AND GLASS TO METAL SEAL

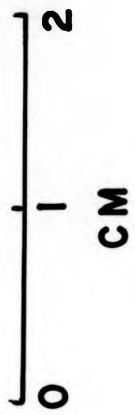


FIGURE 5

DIAGRAM OF GLASS "H-CELL"

FIGURE 5

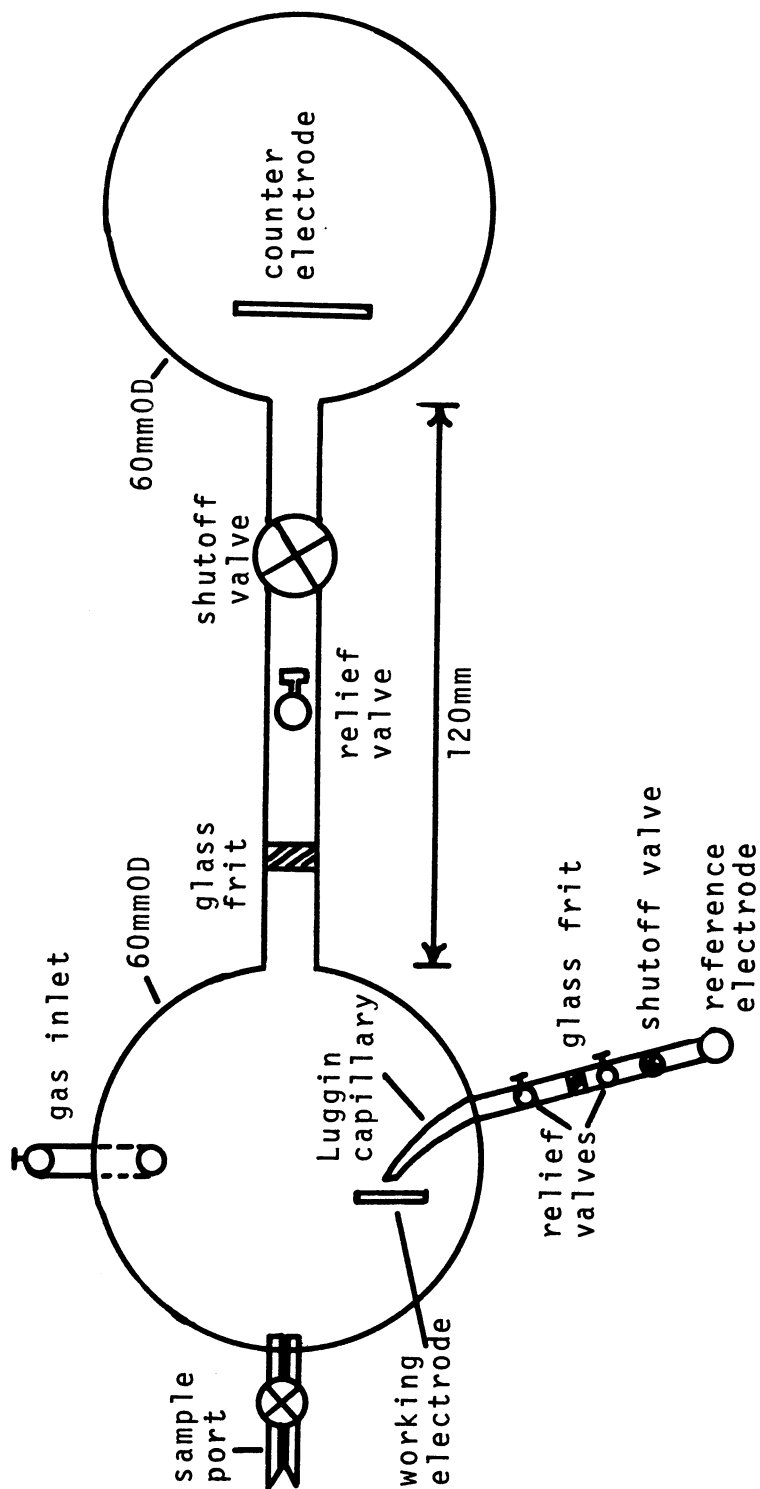
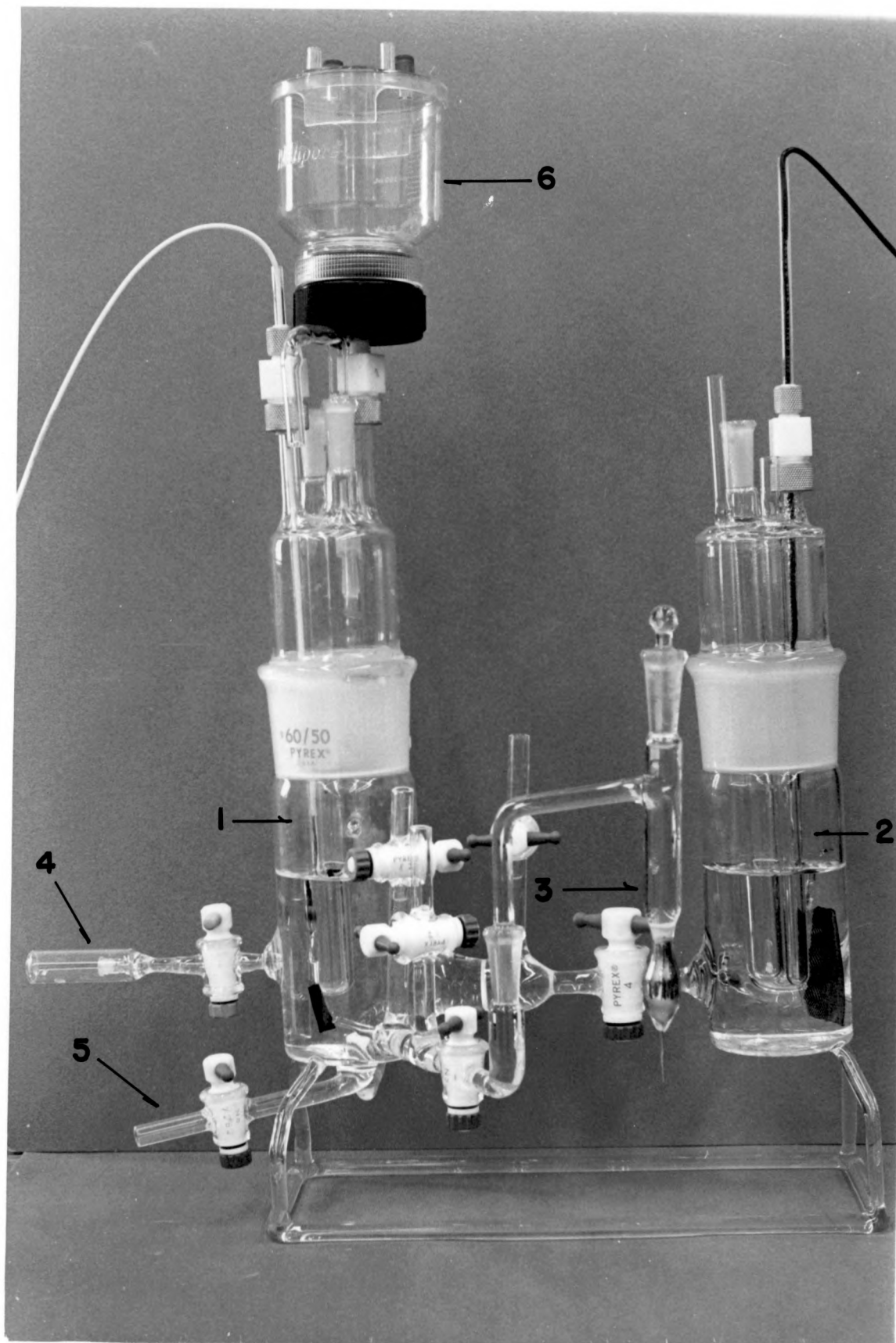


FIGURE 6

PHOTOGRAPH OF GLASS "H-CELL"

- 1 - Working electrode compartment
- 2 - Counter electrode compartment
- 3 - Calomel reference arm
- 4 - Sample port
- 5 - Drain
- 6 - Millipore filter holder



wire which had been sealed into a glass tube as described above. The reference half-cell was a saturated calomel electrode (SCE). Its voltage was frequently checked against a commercial SCE (Thomas #4857-F15) and always found to be within two millivolts. The reference electrode was connected to the test cell by means of a Luggin capillary, 1 mm I.D. x 3mm O.D.

Both the working and counter electrodes were held in place by Teflon connectors (Beckman #505). They were lowered through glass tubes sealed into the caps of the respective compartments. A glass tube sealed off at the bottom served as a well for temperature measurements in the test cell. Also on the upper section of the working compartment were two other protruding glass tube sections. One served as a gas exit from which sampling could be made for determination of oxygen partial pressure ( $PO_2$ ). The other was fitted with a Millipore filter holder (250 ml) through which the electrolyte was introduced into the cell. The filter was a Millipore, 0.4 micron pore size.

The working electrode voltage was controlled by means of a Tacussel PRT-30-01 potentiostat. Current was measured in the counter electrode loop with a Keithley Model 615 electrometer. A permanent record of the current was made with a Texas Instruments strip chart recorder, model FS02W6D. A Non-Linear Systems MX-3 digital voltmeter was used to monitor the cathode to reference voltage. All experimental electrical equipment, except the recorder, were housed in a copper screened cage to prevent interference from static and high frequency electrical fields in the surroundings. Also, the H-cell stood on a styrofoam pad and 75 pound steel table to

damp vibrational disturbances. The apparatus is shown in Figure 7 and a schematic diagram of the potentiostatic circuitry is given in Figure 8.

The shielding and grounding techniques are worthy of special attention. With potentiostatic control, measurement of currents below one microampere is subject to disturbances from surrounding equipment and power line switching transients. A special low resistance earth ground was available in the laboratory facility. All equipment chassis were tied to this ground as well as were all cable shieldings. Also, the copper cage and working electrode were similarly earth grounded. This system prevented for the most part, any current instabilities. However, occasional spike transients from unidentifiable sources were observed. These had no effect on the steady-state voltage and current measurements.

The partial pressure of oxygen in the inlet gas was controlled by means of Matheson gas proportioner. The gas was saturated with water vapor prior to entry into the test cell. Both  $PO_2$  and pH were measured using a Radiometer model PHM72 blood gas analyzer with a BMS3 electrode water bath housing.

#### Electrolyte and Gases

Buffered saline solution was prepared with doubly distilled water and reagent grade chemicals. The solute concentrations were 0.15 M NaCl and 0.05 M sodium phosphate buffer. The buffer consisted of a varied ratio of the dibasic and monobasic phosphate depending on the required initial pH. Experiments for determining pH dependency began at about pH 6 and the electrolyte was adjusted upwards with



FIGURE 7

PHOTOGRAPH OF POTENTIOSTATIC  
AND GALVANOSTATIC EQUIPMENT

- 1 - Gas proportioner
- 2 - Gas washing bottle
- 3 - Electrometer (current indicator)
- 4 - Potentiostat
- 5 - Multimeter (voltage indicator)
- 6 - "H-Cell"

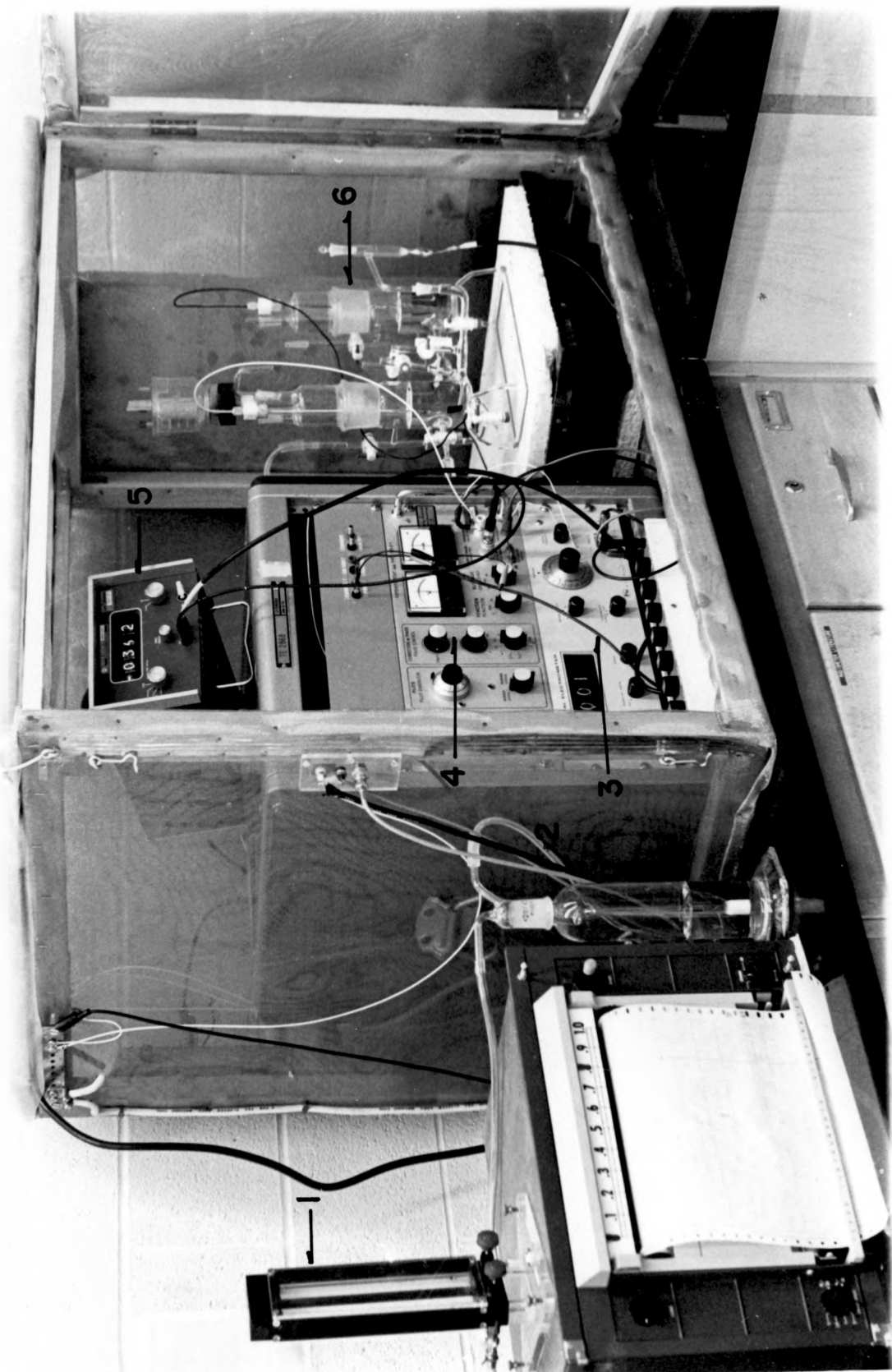
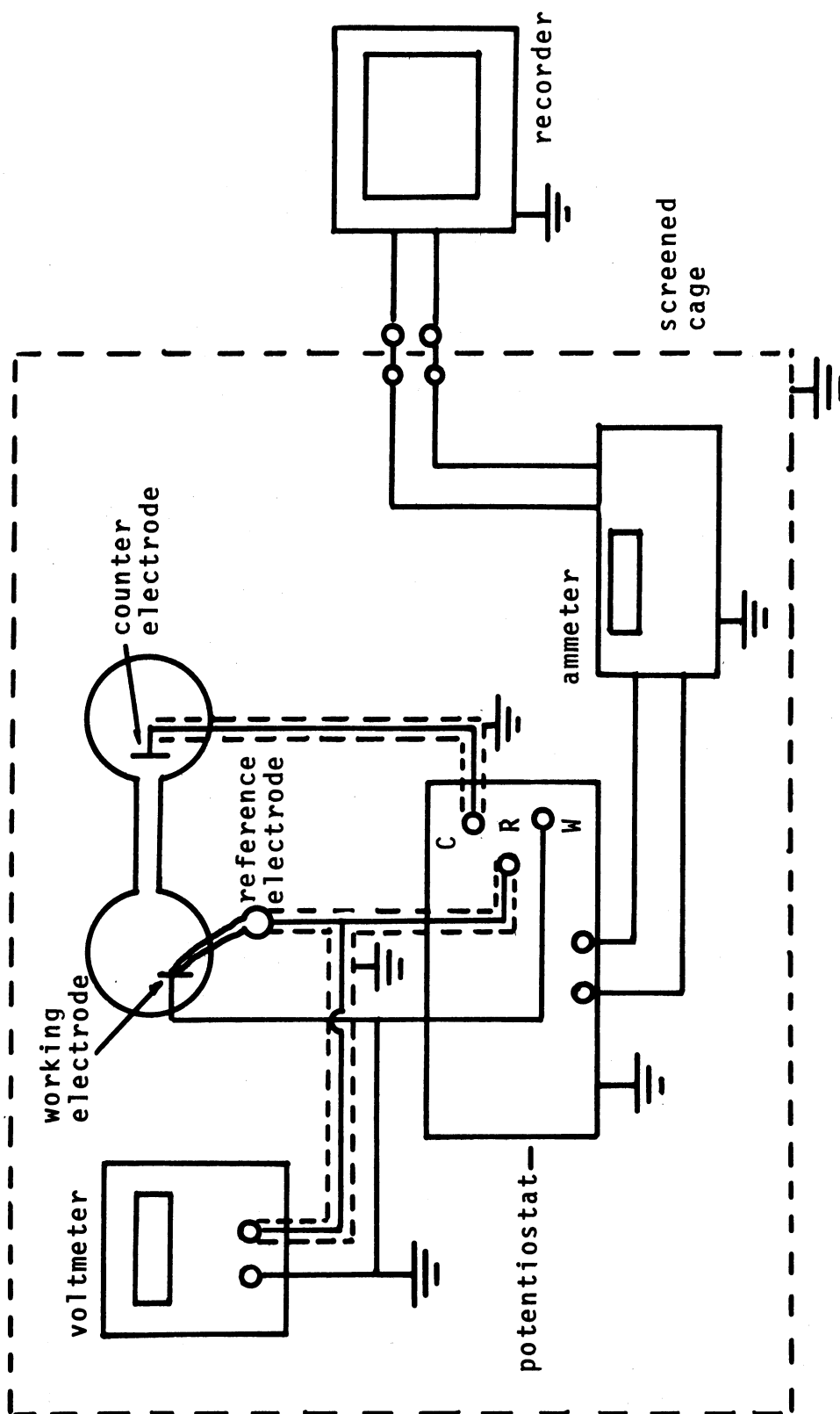


FIGURE 8

DIAGRAM OF POTENTIOSTATIC CIRCUIT

FIGURE 8



1 N NaOH additions. The ionic concentration increased less than 10% for the entire range of pH variation. Commercially available sulfuric acid solutions were used wherever this electrolyte is indicated. Prepurified nitrogen and extra dry grade oxygen (99.5%) were proportioned as required for control of  $P_{O_2}$ .

### Procedures

Pretreatment - The aim of this phase of experimentation was to determine the Tafel slopes and reaction order of  $H^+$  and  $O_2$ . In each case, the same general techniques were used for cell and electrode preparation. Prior to its first use, the cell was thoroughly washed with chromic sulfuric acid. Before each new series of tests, all glassware, including the cell, was cleaned with alcoholic KOH (100 gm KOH dissolved in 100 ml distilled water and 900 ml ethyl alcohol) and rinsed repeatedly with deionized water. The final rinsing was made with doubly distilled water and then 100 ml of the test electrolyte. Finally 250 ml of the test electrolyte were filtered into the working chamber by suction.

At the outset of a particular experiment, prepurified nitrogen was bubbled through the test chamber and the working electrode cathodically polarized. This was accomplished by potentiostating at -400 mv versus SCE for a 20 minute period. The potentiostat was then turned to the "off" position and the gas mixture adjusted to the required oxygen partial pressure. In preliminary tests, it was determined that a total gas flow above 500  $cm^3/min$ , did not alter the current at the greatest polarization voltage to be investigated (-400 mv vs. SCE). Thus, in experiments where the

entire range of currents was studied, this flow rate was used throughout. However, when only the Tafel region was under observation, lower flow rates were maintained for reasons of economy.

Tafel Slope - After cathodic treatment, the electrode was monitored at open circuit overnight by which time a stable potential was attained. For the investigation of Tafel slope at various oxygen partial pressures and pH's, a specific procedure was then followed. The working electrode was potentiostated at different voltage values beginning at 25 mv below its rest potential. Voltage step changes of 20 mv followed for at least one decade of current increase. Once out of the linear Tafel region, larger voltage steps were taken. When only the linear region was under study, the electrode was potentiostated for thirty minutes at -400 mv versus SCE at the end of each overvoltage run. Each potentiostat setting was maintained for thirty minutes. It must be noted that this interval did not necessarily produce a true steady state. Other reported investigations on oxygen reduction in acid and alkaline solution, utilize a variety of criteria for either potential or current change. Apparently, a steady state condition is not reached for a long period of time. In fact, at least twenty-four hours were required in neutral saline experiments for steady-state at intermediate current densities. The thirty minute criteria was determined arbitrarily and at the end of this time interval, the current had responded to at about 90% of its final value. Reproducible voltage-current curves were obtained under these conditions.

Reaction Orders - The determination of reaction order with respect to hydrogen ion and oxygen followed similar procedures. The

electrode was potentiostated at a voltage in the Tafel region overnight. For oxygen dependency, the pH was constant at a predetermined value (approximately 5.8 to 7.8) and the oxygen partial pressure was set to the lowest value to be measured. When pH was to be varied, oxygen concentration was maintained constant (at approximately 45 mm Hg) and the pH was initially set at approximately 5.8 by adjusting the buffer ratio of the electrolyte. The variable to be investigated was adjusted upwards in steps. This was accomplished by adjusting the gas proportioner (keeping total flow rate constant) or adding a measured amount of 1.0N NaOH. Both oxygen partial pressure and pH were measured during experiments and duplicate readings taken to assure reproducibility. The former was found to reproduce within  $\pm 2$  mm Hg and the latter by less than  $\pm 0.005$  pH units after a steady current was observed on the recorder. Also, in most cases, an intermediate data point was redetermined to demonstrate the validity of any particular run.

Experiments in this series were carried out at  $23 \pm 1^\circ\text{C}$ . Barometric pressure was monitored and used as a basis for calculation of oxygen partial pressure.

### Characteristics of Activated Carbon in Neutral Saline

#### Electrode Material and Preparation

The electrode material used throughout the experiments described in this section, was a platinum activated, carbon cathode furnished by ESB Research, Inc., Yardley, Pennsylvania. The method of its manufacture has already been described. All test electrodes were

1 cm x 2 cm and spotwelded to a platinum wire which had been sealed in glass in the same manner as were the platinized platinum electrodes. A scanning electronmicrograph of the electrode surface is shown in Figure 9 and a close view of the actual test configuration is in Figure 10. Pretreatment of the electrode consisted of a distilled water rinse followed by a three to five day warm-up period. During this time, current was maintained constant at  $20 \mu\text{a}$  ( $5 \mu\text{a}/\text{cm}^2$ ) by a Wenking potentiostat (Model #6250 TR) and voltage was monitored. The warm-up was carried out in a second pyrex glass H-cell. This cell was similar to the one used in the platinized platinum experiments except that separation between compartments was afforded by water-seal, ground glass stopcocks rather than glass frits.

#### Equipment

The highly porous nature of this particular material, prevents the use of potentiostatic control. Concentration and IR drop distributions in the pores cause a high degree of low frequency noise in the current signal. Also, in its capacity as a bio-power cell cathode, the electrode can be thought of as operating in either a constant current mode or under constant load conditions rather than at constant voltage. Thus, galvanostatic and constant load techniques have been used to assess the characteristics of the activated carbon cathode in a simulated biological environment.

The independent testing systems were developed to obtain performance data. A classical galvanostatic procedure was followed using the same all glass cell and equipment described in the platinized platinum experiments. This system is rather expensive and data



FIGURE 9

SCANNING ELECTRONMICROGRAPH OF ACTIVATED  
CARBON CATHODE

Magnification 3000X

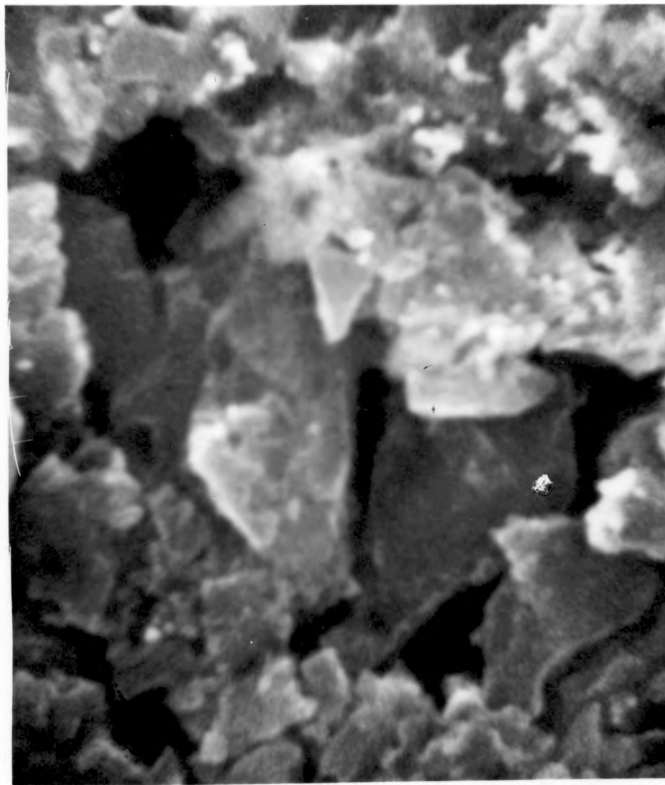
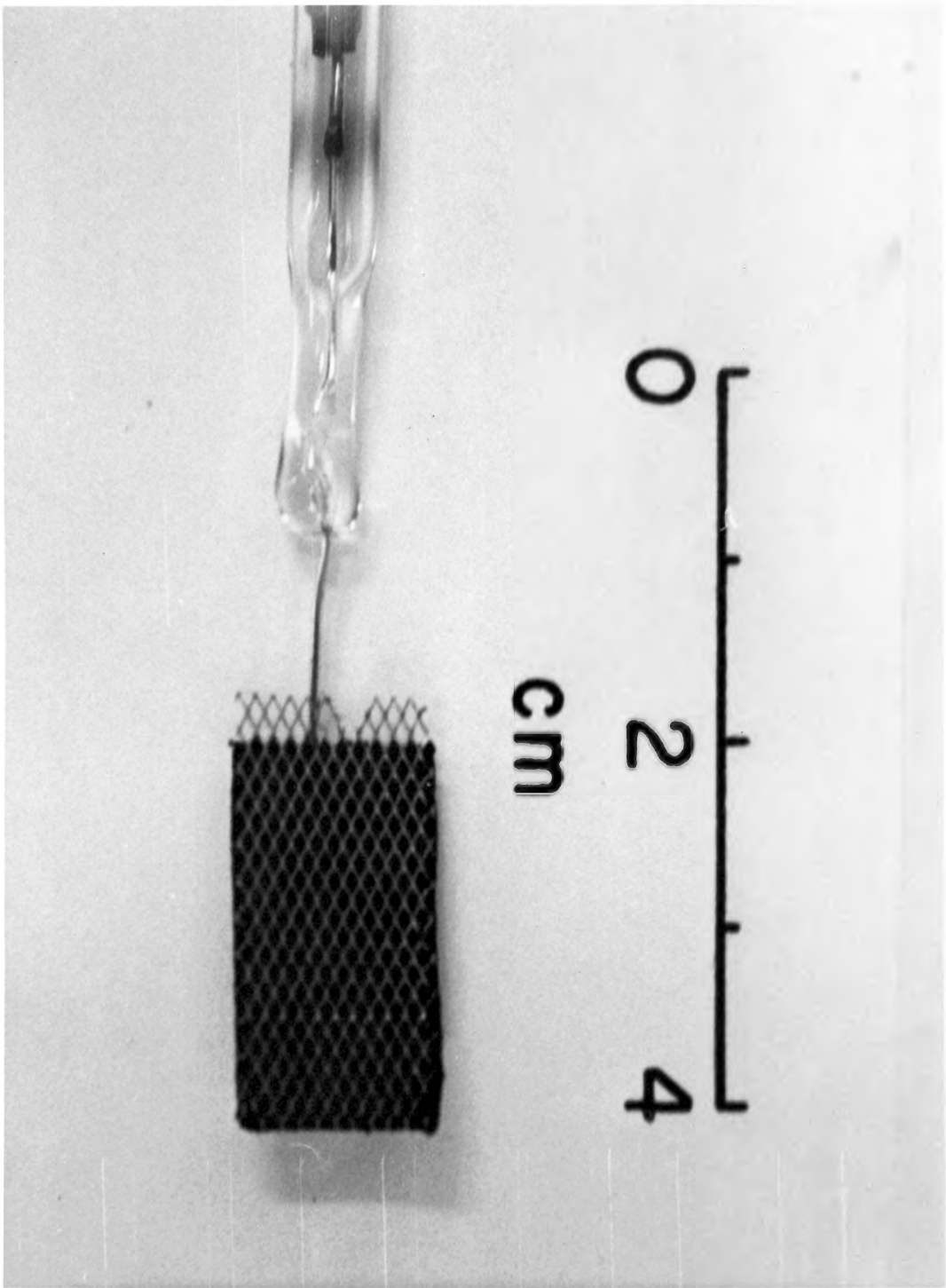


FIGURE 10

PHOTOGRAPH OF ACTIVATED CARBON CATHODE  
AND GLASS TO METAL SEAL



collection laborious. A computer operated screening technique briefly described by Cooper, et al. (35) was designed to speed testing of various cathode and anode materials for hybrid power cells (see Literature Review). The activated carbon cathode has been tested with this system in order to compare data generated by galvanostatic and constant load techniques. Both systems will now be described separately. This is the first time that the computer test system has been presented in any detail.

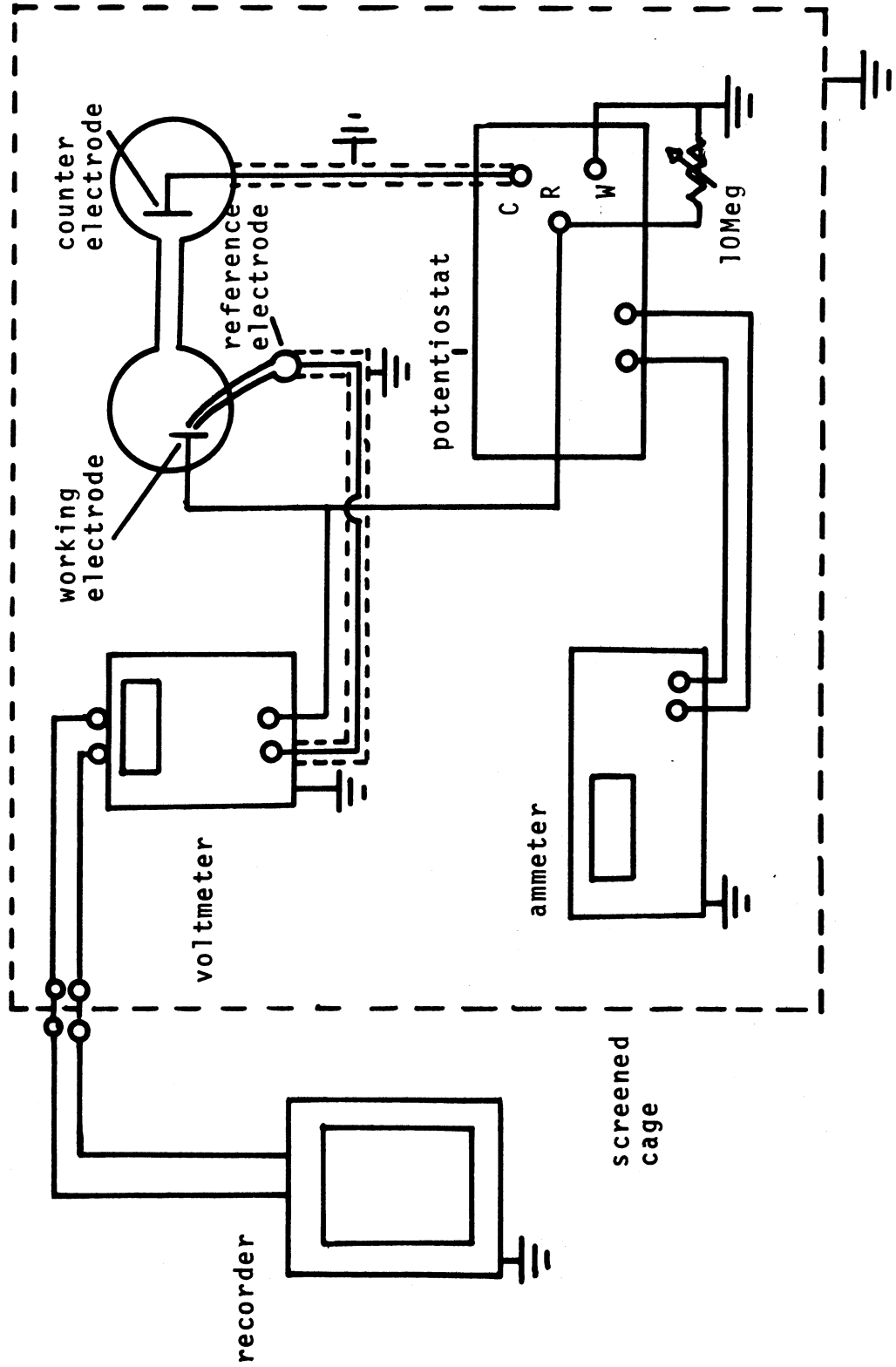
1. Galvanostatic equipment - In galvanostatic testing with the glass H-cell, the Tacussel potentiostat was used in a modified arrangement to maintain constant current. A diagram of the circuit is shown in Figure 11. All relevant equipment, i.e., voltmeter, recorder, ammeter, is the same as stated in the platinized platinum study. A 10 megohm decade resistance box was connected between the reference and working electrode inputs to the potentiostat. The controlled current was determined by the value of  $I=V/R$  where V is the voltage setting on the potentiostat. Using this arrangement, current could be maintained within  $\pm 0.5\%$  of the set value.

2. Computer test system - The automated data collection system was designed primarily to rapidly obtain voltage-current data for various cathode and anode materials. Although a great deal of data has been collected utilizing this system, the major emphasis in this presentation will be placed on its design and operation. The testing of the activated carbon cathode will serve as an example of its use comparing this rapid scanning system with the more precise galvanostatic technique.

FIGURE 11

DIAGRAM OF GALVANOSTATIC CIRCUIT

FIGURE 11



A particular anode-cathode pair was housed in a 1000 ml glass battery jar along with a silver/silver chloride reference electrode. The cathode was spotwelded to a length of platinum wire and the anode was arcwelded to a length of aluminum welding rod. The anode lead was then coated with a baked neoprene rubber to prevent corrosion. In the experiments concerning activated carbon cathodes, the anode was a 2 cm x 2 cm aluminum alloy (1% Mn, 0.3% Fe, trace Zn). The reference electrode is simply a length of silver wire (0.051 inch dia.) which was previously chlorided in 0.1 N HCl at  $10 \text{ ma/cm}^2$  for five minutes. The three electrodes are connected to a terminal strip atop the battery jar. All connections were gold plated with a chemical plating solution (Shipley #EL-221). A photo of the cell arrangement is shown in Figure 12. Although provisions were available for maintaining higher temperatures via a water circulation system, the experiments here were conducted at room temperature ( $23.0 \pm 1.0 \text{ }^\circ\text{C}$ ) for comparison with the galvanostatic observations.

Each of sixteen identical cells are wired to a three deck, eighteen position switch with two positions left as spares. A double pole, single throw switch acted to place either anode or cathode voltage versus the reference into the measuring circuit. A twenty-four position, sixteen deck switch was wired to place different resistive loads (1 Meg to 75 ohms) across each of the test cells. Each switch is activated by a solenoid which steps through the positions in sequence. The switching arrangement is shown diagrammatically in Figure 13.

Control of the load switching and collection of data were performed by a Linc-8 computer (Digital Equipment Corporation). Voltages



FIGURE 12

PHOTOGRAPH OF CELL BATH FOR AUTOMATED LOAD  
SWITCHING TESTS

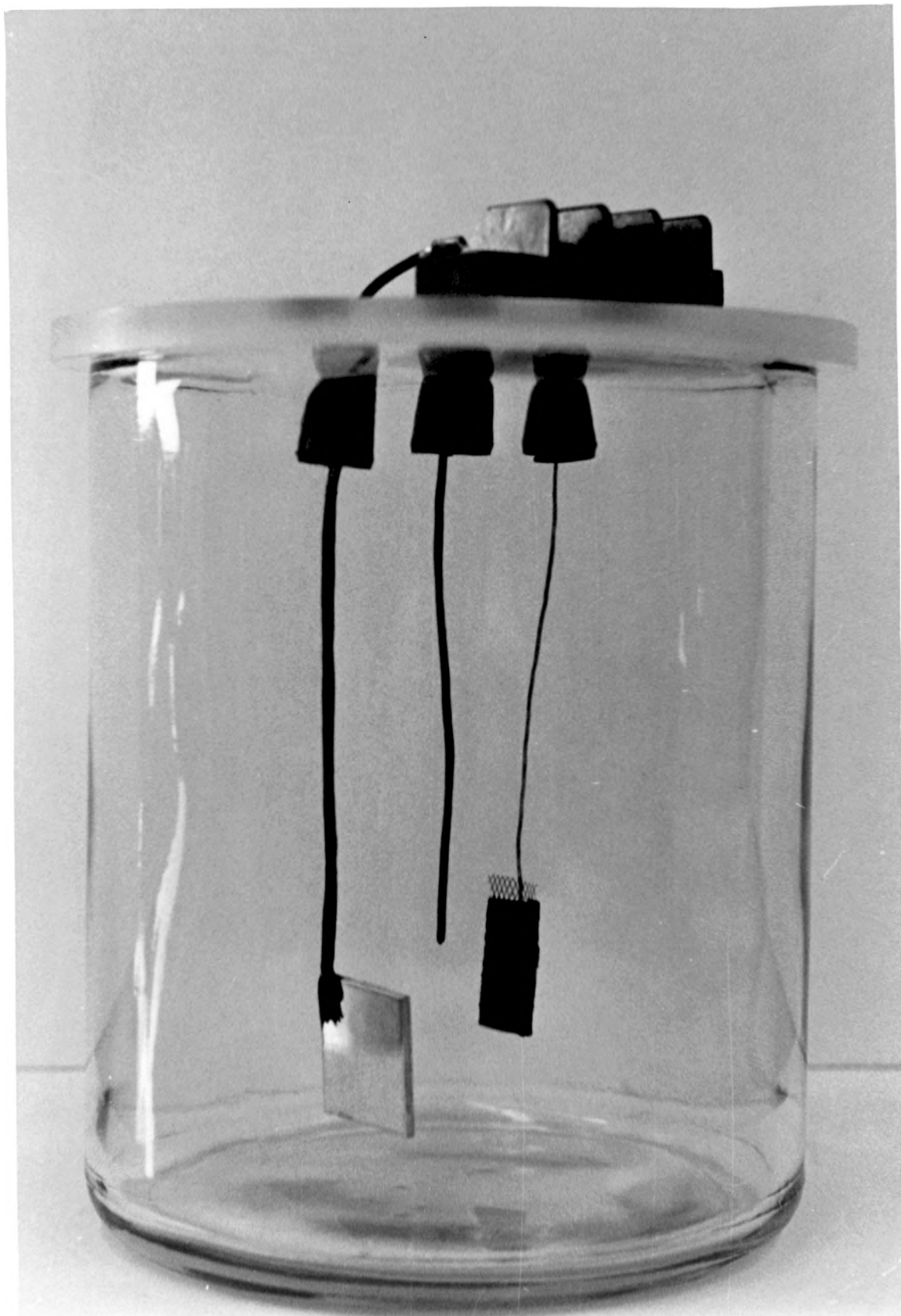
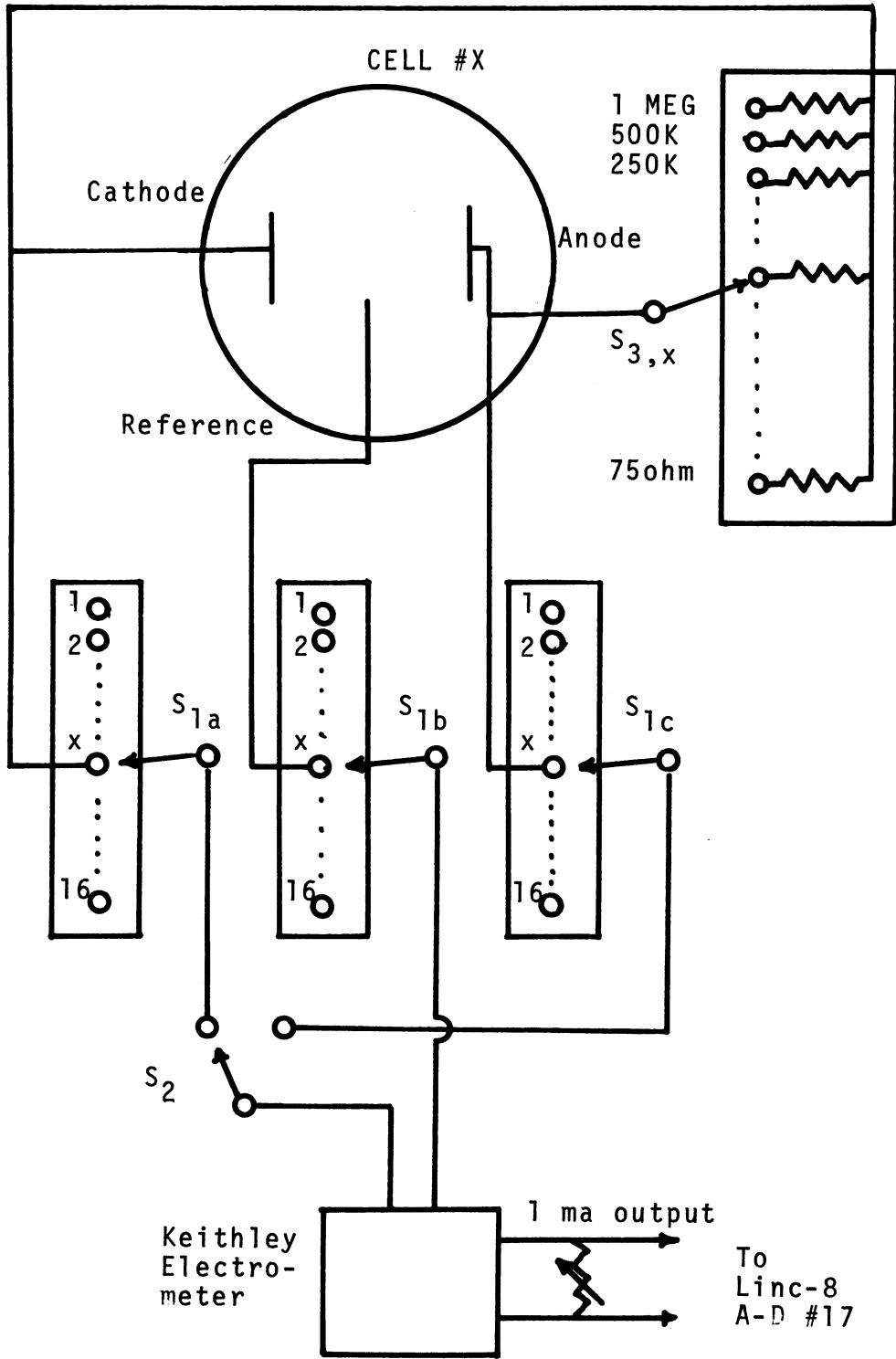


FIGURE 13

DIAGRAM OF SWITCHING ARRANGEMENT FOR  
AUTOMATED LOAD SWITCHING TESTS

FIGURE 13



were monitored by a Keithley Model 610C electrometer which acted as a buffer amplifier (gain = 1.0). The output signal from the electrometer was fed to an analog to digital converter channel in the computer. Accuracy, limited by the digitizing process ( $377_8 = 1000_{10} \text{mv}$ ), was within  $\pm 4 \text{ mv}$ . Another A-D Channel accepted a time pulse signal (1.0 volts every five minutes) and initiated the data collection sequence at preset intervals (multiples of five minutes).

Voltages versus current curves were determined by changing the load across each cell at fixed intervals. The time interval was chosen so that steady state conditions were reached at each point. By running at different intervals and comparing the curves, this criterion could be tested. Switching of load and sampling of individual half-cell voltages was accomplished by program controlled relays. These relays, in turn, activated a power relay which finally caused the solenoid of the respective cell, anode-cathode, or load switch to advance one position at a time. After the preset number of time pulses were sensed by the computer, one measurement cycle commenced. The cathode, then anode voltage of the first cell was read and the cell position advanced to cell #2. This loop was repeated sixteen times leaving the cell position indicator in its original position (two extra steps after the 16th cell to account for spare positions). After all sixteen cells were monitored, the load resistance was changed to the next lower position. This entire procedure was repeated until all twenty-three loads had been utilized. Data were stored in digital form on magnetic tape for subsequent manipulation and graphing. After a full operating cycle was completed,

data could be immediately evaluated by calculating the necessary quantities for plotting a  $V$  vs.  $\log i$  curve. For each set of points, the total voltage was determined by addition of half-cell voltages. Current was computed from  $i=V/R$  where  $R$  is the load value for a particular voltage reading. Total geometric surface area and the value of the silver chloride reference versus SCE were also entered into the program as parameters. The final output, is in the form of a graph of voltage versus SCE versus the logarithm of the current density expressed in microamps per square centimeter. This graph is plotted by a Calcomp 565 plotter under Linc-8 control.

A photograph of the insulated cell baths and switching unit is shown in Figure 14. The latter is in the foreground with the water circulating system in the rear. Details of the computer programming are not extremely pertinent to the discussions which will proceed this section and, thus, they will not be presented. However, all programs are available upon request.

### Procedures

1. Galvanostatic - These procedures were designed to evaluate all relevant parameters of the activated carbon cathode operating in neutral saline. This includes, (a) voltage-current characteristics (b) stirring artifacts (c) temperature dependency (d) oxygen dependency and (e) pH dependency. All experiments were carried out in a neutral buffered saline solution whose composition was previously described.

Voltage current relationships at various oxygen partial pressures were determined by observing steady-state voltage at various constant currents ranging from 0.1 to 80  $\mu\text{a}/\text{cm}^2$  of geometrical surface.

FIGURE 14

PHOTOGRAPH OF INSULATED CELL BATHS  
AND SWITCH BOX FOR AUTOMATED LOAD  
SWITCHING TEST SYSTEM

- 1 - Electrometer
- 2 - Decade resistance box for output calibration
- 3 - Timer
- 4 - Load indicator
- 5 - Cell indicator
- 6 - Anode - cathode indicator
- 7 - Cell bath
- 8 - Gas manifold

Throughout most of these tests, where atmospheric oxygen concentration was desired, filtered, humidified compressed air was bubbled into the test chamber. To examine the effect of stirring, the following procedure was implemented. Above 200 ml/min. of compressed air flow, increasing stirring did not effect the voltage and the voltage current plot was linear up to  $80 \mu\text{a}/\text{cm}^2$ . This was, then the stirring rate used throughout other phases of this test series. This is desirable so that factors other than oxygen diffusion can be examined. At each point taken in the course of a galvanostatic run, the flow rate was maintained at 200 ml/min. until a steady state was reached. The gas flow through the solution was then terminated, and the gas allowed to flow into the upper section of the test electrode chamber. Thus, the mass transfer process in solution is almost completely by diffusion (with some natural convection) and more closely simulated the biological situation. The oxygen concentration in the bulk of the electrolyte could then be considered to be directly proportional to the gas partial pressure above it (Henry's Law). The stirring artifact was examined at both atmospheric  $\text{PO}_2$  and approximately 3% oxygen.

Oxygen, pH, and temperature effects were all studied at a constant current in the linear portion of the voltage-current curve and in the vicinity of typical in-vivo operating current densities (4 and  $10 \mu\text{a}/\text{cm}^2$ ). Oxygen partial pressure and pH were varied in the same manner as described in the section on platinized platinum experiments. The variation of temperature produced some difficulties since heating tape wrapped around the test cell caused significant disturbances to the test electrode at low currents. This problem



was circumvented by use of a flexible, heat conductive, rubber tubing which could also be wrapped around the test chamber. Warm water was circulated through the tubing to elevate temperature. Experiments were carried out between 24°C and 43°C.

2. Automated Load Switching - Three runs at different time intervals were made with the computer test system to evaluate data gathered by this technique. Compressed air was bubbled at a constant flow rate (about 200 ml/min) through a porous air disperser and the pH of the buffered saline electrolyte was constant at  $7.22 \pm .02$ . Three, two, and one-half hour intervals were used. Open circuit voltage was monitored periodically before each run to insure a stable resting state.

#### Foreign Ion Effects on Activated Carbon Cathodes

The tests carried out in the preceding section were designed to evaluate cathode operation in an uncomplicated salt solution the ionic concentration of which closely resembles that of interstitial fluid. To complete the evaluation of simulated in-vivo operating characteristics, the effects of anode by-products and interstitial fluid components not present in saline solution were studied. Two different sets of experiments were performed.

#### Additions of By-Products From Hybrid Cell Anodes

Activated carbon cathodes were subjected to a constant current warm-up period in a glass H-cell. Here again, the electrolyte was buffered saline (pH = 7.2) and the current 20 microamperes. The voltage was monitored by a digital voltmeter and recorded on a strip

chart recorder. The counter electrode was a second activated carbon cathode,  $16 \text{ cm}^2$  geometrical area. Aluminum or zinc ions were added in the form of the respective chloride salt solutions. Experiments were first carried out by adding the ions in increasing steps. The solutions added were buffered saline plus  $2 \times 10^{-3}$ ,  $2 \times 10^{-2}$ , or  $2 \times 10^{-1}$  molar in either zinc or aluminum chloride. The additions were one ml each to a total of 200 ml of initial electrolyte solution. This yielded  $10^{-5}$ ,  $10^{-4}$ , and  $10^{-3}$  molar concentrations of the particular ion, respectively. Finally, additional amounts of the ions were added in order to exceed saturation conditions so that a milky white precipitate was observed. Voltage was recorded continuously on the strip chart recorder. The pH was also measured after each addition and found to change by less than 0.1 pH unit during the entire experiment.

Longer term (1 week) tests were also performed. Here, the electrolyte was immediately supersaturated with the respective ion after the warm-up period. The voltage was monitored daily on a Keithley electrometer, model 610C.

#### Interstitial Fluid Effect on Activated Carbon Cathode

Experiments were conducted in a simulated interstitial fluid environment using the galvanostatic procedures that have already been described. The maintenance of aseptic conditions was required since the electrolyte is an excellent media for growth of organisms.

The basic electrolyte for these tests was a commercial culture media which contains most of the constituents of interstitial fluid. This includes glucose, thirteen amino acids, magnesium, potassium,

and calcium salts, and other assorted organics. The media (BME, Basal Medium with Hanks' salts) is purchased in the form of a sterile 10 X concentrate and was diluted aseptically with a phosphate buffer to produce the same buffer molarity as the buffered saline of previous experiments. The actual electrolyte composition is listed in Appendix A.

The glass cell shown in Figure 6 was used with only slight modification. All relief valves and other openings were plugged with cotton and gauze. A stainless steel tube packed with fiberglass was placed in the gas inlet line to remove bacteria laden dust particles which could contaminate the system. The reference arm contained saturated KCl and the counter electrode chamber buffered saline as previously.

An activated carbon cathode was first subjected to a warm-up period and a complete voltage-current curve determined. The entire system was then sterilized in an electric autoclave at 121°C for thirty minutes. The inlet gas filter was autoclaved separately and dried in vacuo for thirty minutes. The calomel reference arm required special attention since the saturated KCl could not be left in place during sterilization. Instead, the mercury and calomel were added as usual and subjected to sterilization. Using a careful aseptic technique, sterile saturated KCl was then added from a reservoir bottle which has provisions for transferring the KCl under pressure. Thus, no section of the test apparatus was exposed to the atmosphere for more than a brief moment.

A second voltage-current curve was then run in the buffered saline after the first sterilization. After a second sterilization, 250 ml of the culture media was added to the test chamber by suction through the 0.4 micron Millipore filter. After a stable open circuit potential was observed (twelve hours), a third polarization run was carried out. In addition, oxygen dependency was determined from 0.02 to 0.97 atmosphere at a current of  $10 \mu\text{a}/\text{cm}^2$ .

The pH was periodically measured and a daily sample taken for bacteriological examination. Sterile petri dishes were poured with a mixture of yeast agar (5 gm yeast to 1 liter water and 15 gm agar). The dishes were incubated for 48 hours at  $37^{\circ}\text{C}$  to test for sterility of the preparation. A 0.2 sample was drawn from the test chamber with a 1 cc disposable tuberculin syringe. Half of the sample was injected onto the plate and the other half measured for pH. The former was then spread carefully to afford an even distribution. The spreading was performed with a glass rod which had been previously dipped in isopropyl alcohol and flashed with a flame. Plates were incubated at  $37^{\circ}\text{C}$  for at least 48 hours.

Polarization curves were also taken in a culture media electrolyte to which had been added 1.0 gm% bovine serum albumin (Cohn Fraction V, Sigma Chemical Co.). Difficulties arise with protein solutions in that severe foaming and protein denaturation can occur when the saturating gas is bubbled through the solution. These tests were carried out in a stagnant electrolyte and must be compared to buffered saline experiments taken under the same conditions.

## RESULTS

### Platinized Platinum

Generally reproducible results were obtained for the Tafel slope and reaction orders of  $H^+$  and  $O_2$  on platinized platinum in neutral chloride solution. There is a marked difference in the order of magnitude of current density in this solution as compared to other investigations carried out in strongly acid or basic solution. Thus, some preliminary data on time response of the electrode and its characteristics in sulfuric acid will be of interest.

In Figure 15, a semilogarithmic voltage versus current density\* plot is shown for platinized platinum in 1.0 N sulfuric acid at one atmosphere oxygen partial pressure. The upper curve is from a freshly platinized electrode and the lower curve is from an electrode which had been operated in buffered saline for a series of pH dependency tests. Both electrodes were cathodically treated for twenty minutes prior to starting the polarization cycle. The fresh electrode had a stable open circuit potential of +742 mv versus SCE; i.e. 986 mv versus the normal hydrogen electrode.\*\* This is the 0.98 potential

---

\*Current density in all proceeding figures is based on total face area of electrode surface; i.e., 1 cm x 2 cm electrode includes 4 cm<sup>2</sup> surface area.

\*\*The standard half-cell potential of the saturated calomel electrode at 25°C is +0.244 volts and varies less than one millivolt per degree centigrade between 20°C and 30°C (75).

FIGURE 15

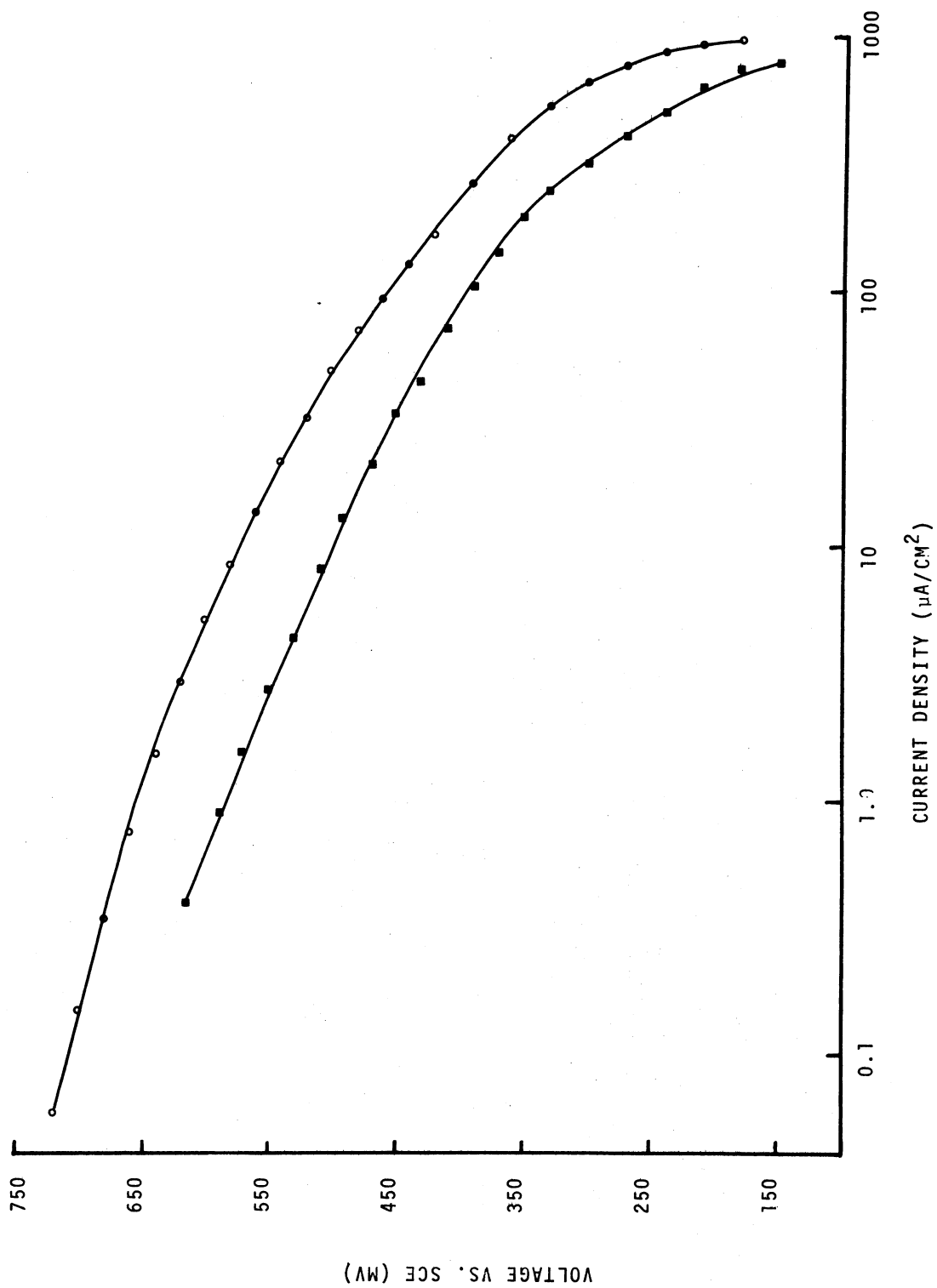
VOLTAGE VERSUS CURRENT DENSITY  
PLATINIZED PLATINUM ELECTRODE

1.0 N H<sub>2</sub>SO<sub>4</sub>

P<sub>O</sub><sub>2</sub> ≅ 0.97 atm

- Fresh electrode
- Used electrode

FIGURE 15



which was discussed earlier. On the other hand, the "used" electrode had an open circuit potential of only 640 mv versus SCE. The shape of the two curves and the limiting current are generally the same. The important point to be made is that the platinized platinum electrode, prepared and treated as described, has the same general characteristics of platinum electrodes described in the literature. It is difficult to strictly define a "typical" platinum electrode even in acid solution because of the variety of pretreatments used. However, the relatively linear region from about  $0.5 \mu\text{a}/\text{cm}^2$  and a diffusion limiting current of about  $1 \text{ ma}/\text{cm}^2$  are usually seen in voltage-current curves of this type.

The response of the electrode current to a step voltage change is shown in Figure 16 for operation in buffered saline. It is interesting that most investigators fail to elaborate on the question of steady state at platinum electrodes in acid or basic solutions. Thus, this curve cannot readily be compared to other data except for that of Bianchi and Mussini. (48). Their studies on smooth platinum in 1.0 N  $\text{H}_2\text{SO}_4$  showed a similar shape for the current versus time response at constant voltage. However, they do not describe the method by which their voltage versus current plots were obtained; i.e., the time interval between points. Thus, ambiguity exists as to the steady state conditions for voltage-current curves on platinum in general. It can be seen from Figure 16 that from thirty to three hundred minutes there is only a 13% change in current density. Thus, the determination of Tafel slopes and their subsequent interpretation are based on the assumption



FIGURE 16

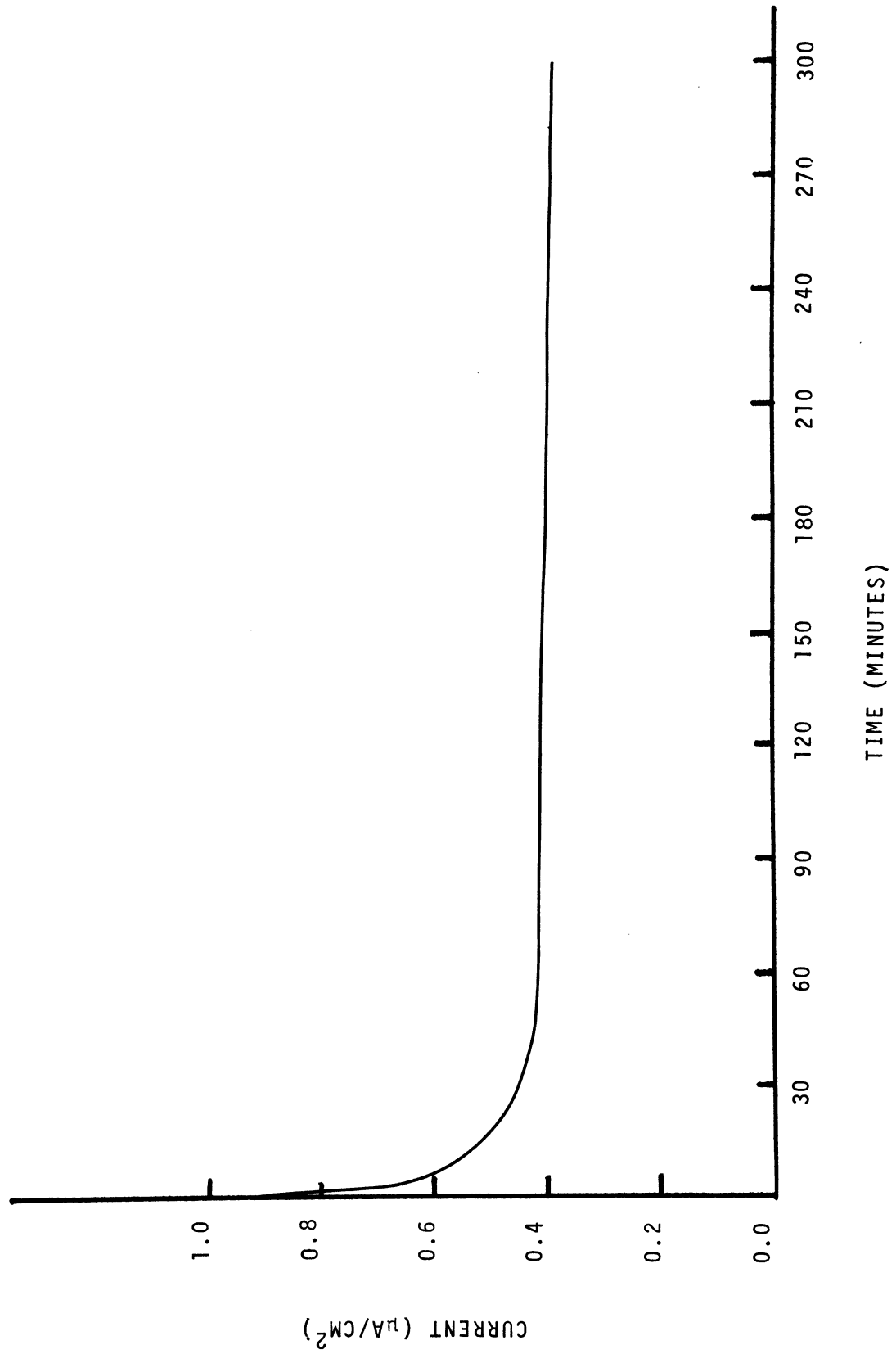
CURRENT RESPONSE TO VOLTAGE STEP CHANGE

PLATINIZED PLATINUM ELECTRODE

$P_{O_2} \cong 0.055 \text{ atm}$

$\text{pH} = 6.81$

FIGURE 16



that for thirty minutes at each step change of voltage, the conditions at the electrode are relatively close to being steady.

From the following five figures, the pertinent parameters for elucidation of the oxygen reduction mechanism can be obtained. In Figure 17, five voltage versus log current density curves are shown for different oxygen partial pressures at a total pressure of one atmosphere. The pH was constant throughout at  $6.81 \pm .01$ . The percentages of oxygen were 1.5, 5.5, 22.5, and 97 per cent respectively. A duplicate of the curve for the lowest percent oxygen concentration in the Tafel region only is also shown to demonstrate reproducibility. The highest oxygen percentage has been corrected for the partial pressure of water vapor at  $23^{\circ}\text{C}$ . No IR drop correction was made because of the extremely low magnitude of the currents and the use of a Luggin capillary.

In Figure 18, a voltage-current plot in the Tafel region only is shown for three different values of the pH; 6.08, 6.91 and 7.55, respectively. Here the partial pressure of oxygen was constant at  $46 \pm 3$  mm Hg. These curves have the same general characteristics of those in Figure 17 with a linear region of about one decade and, in this case, an upwards shift with decreasing pH. The average Tafel slope for nine different runs for oxygen and pH dependency was calculated to be  $-135 \pm 18$  (s.d.) millivolts. This slope was calculated in the same arbitrary manner for each curve. The first point chosen was at a polarization of 100 mv from the open circuit voltage which had been observed at the start of a run at any particular conditions. In this way, the error introduced from the current of

FIGURE 17

VOLTAGE VERSUS CURRENT DENSITY  
PLATINIZED PLATINUM ELECTRODE

VARIABLE  $P_{O_2}$

pH = 6.81

- 0.015 atm 1st run
- ▣ 0.015 atm 2nd run
- 0.055 atm
- ▼ 0.225 atm
- ▲ 0.97 atm

FIGURE 17

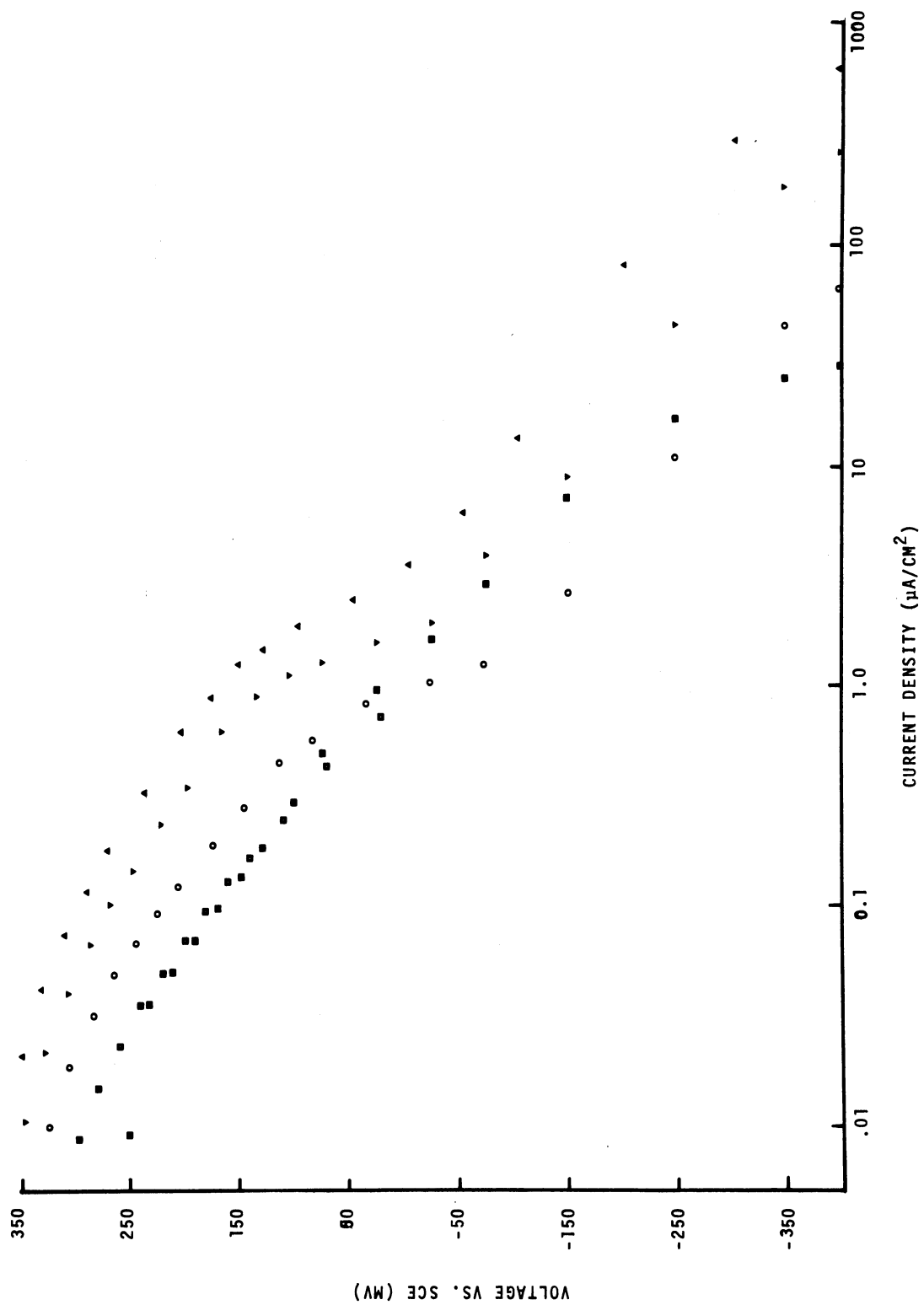


FIGURE 18

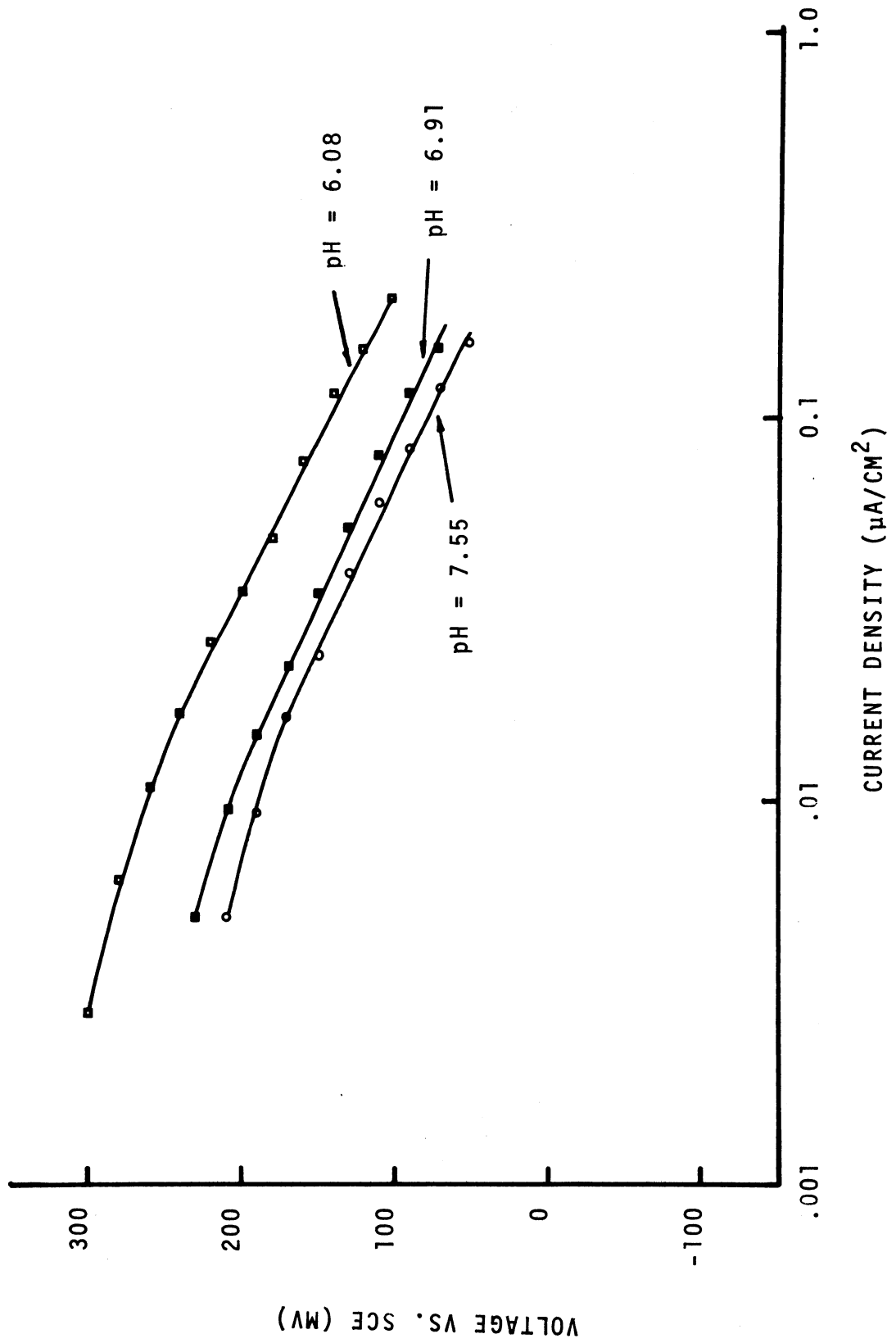
VOLTAGE VERSUS CURRENT DENSITY  
PLATINIZED PLATINUM ELECTRODE

VARIABLE pH

$P_{O_2} = 0.055 \text{ atm}$

- pH = 7.55
- pH = 6.91
- ▣ pH = 6.08

FIGURE 18



the reverse reaction is only about 2%.\* The data points for one decade of current following the 100 mv polarization level were used for evaluation of the slope. Calculations were performed with an Olivetti Underwood Programma 101 calculator using a standard regression analysis routine supplied by the manufacturer.

In Figure 19, three sets of data are plotted for the variation of log current with changes in log  $P_{O_2}$  at constant voltage. The pH values are, again, 6.08, 6.91, and 7.55 from top to bottom. The constant voltage for each curve was +175 mv at pH 6.08 and 150 mv at pH's 6.91 and 7.55. Referring to Figure 18, it can be seen that these voltages were chosen to be somewhere near the center of the Tafel region so that the reaction would be under activation control throughout the range of oxygen partial pressures. The average of five oxygen dependency runs at varying pH was  $1.10 \pm 0.15$  (s.d.). As a check on the determination of reaction order by the potentiostatic technique, a galvanostatic experiment was run at pH 6.85 with the current fixed at  $4 \times 10^{-8}$   $\mu\text{a}/\text{cm}^2$ . The oxygen partial pressure was varied as before. The results are shown in Figure 20 with voltage plotted versus log  $P_{O_2}$ . The circled point was taken from Figure 19 at pH = 6.91 to demonstrate that the two experiments were, in fact, complementary. The slope of the regression line is 115 mv/decade. In Figure 21, two curves are shown for the pH dependency at constant voltage;  $V = +125$  mv (upper) and +150 mv (lower). The log of current is plotted versus pH in the range 5.8 to pH 7.6. The average slope of the curves is  $-0.19 \pm 0.006$  (s.d.)

---

\*The interested reader is referred to Delehay (77) for the derivation of the Tafel slope and an analysis of the error introduced by its use below various values of polarization.



FIGURE 19

CURRENT DENSITY VERSUS OXYGEN PARTIAL PRESSURE  
PLATINIZED PLATINUM ELECTRODE  
VARIABLE pH

- pH = 7.55 150 mv
- pH = 6.91 150 mv
- ▣ pH = 6.08 175 mv

FIGURE 19

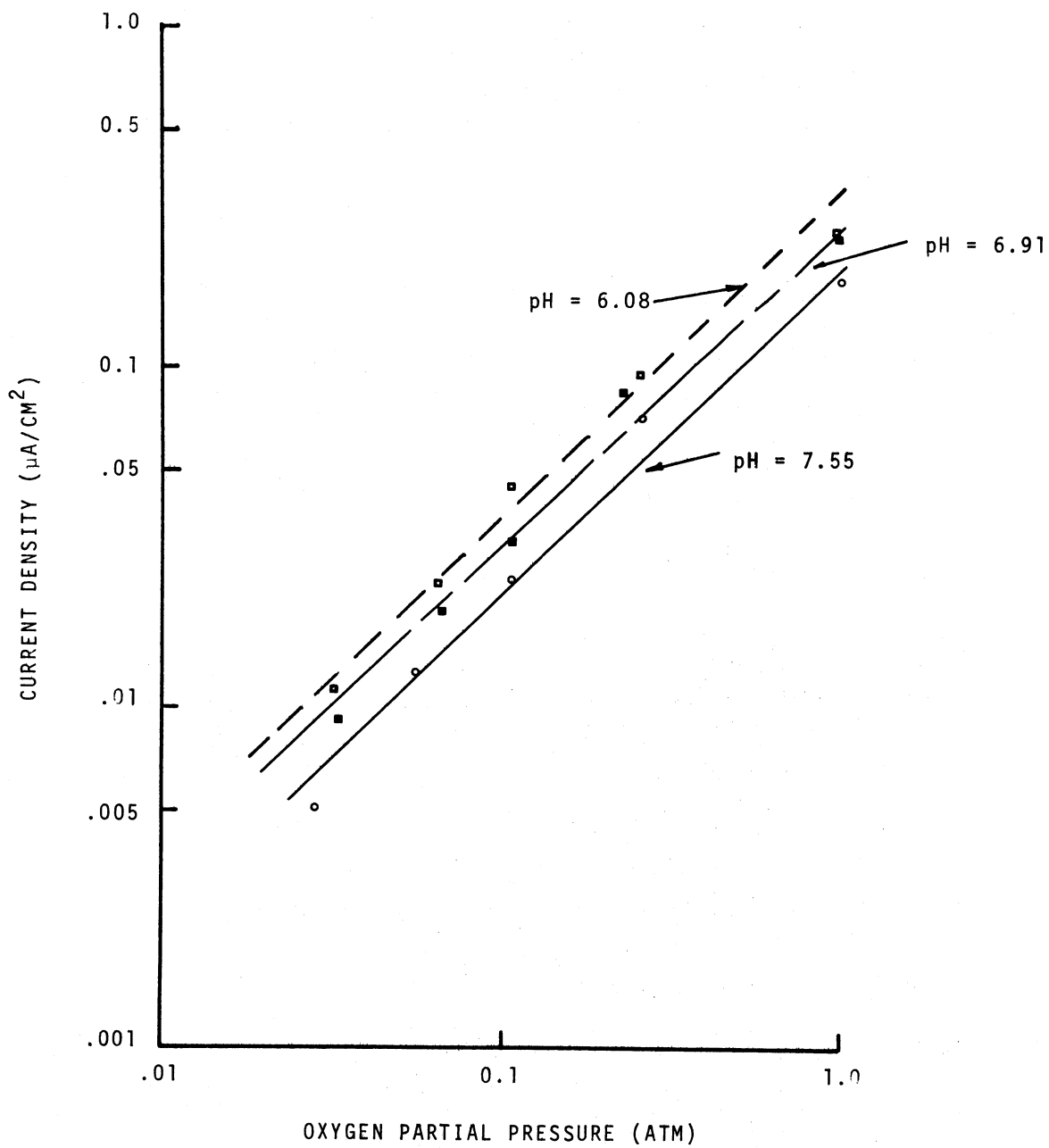


FIGURE 20

VOLTAGE VERSUS OXYGEN PARTIAL PRESSURE  
PLATINIZED PLATINUM ELECTRODE

$$i = 4.0 \times 10^{-8} \text{ a/cm}^2$$

$$\text{pH} = 6.81$$

- from Figure 19 (potentiostatic technique)

FIGURE 20

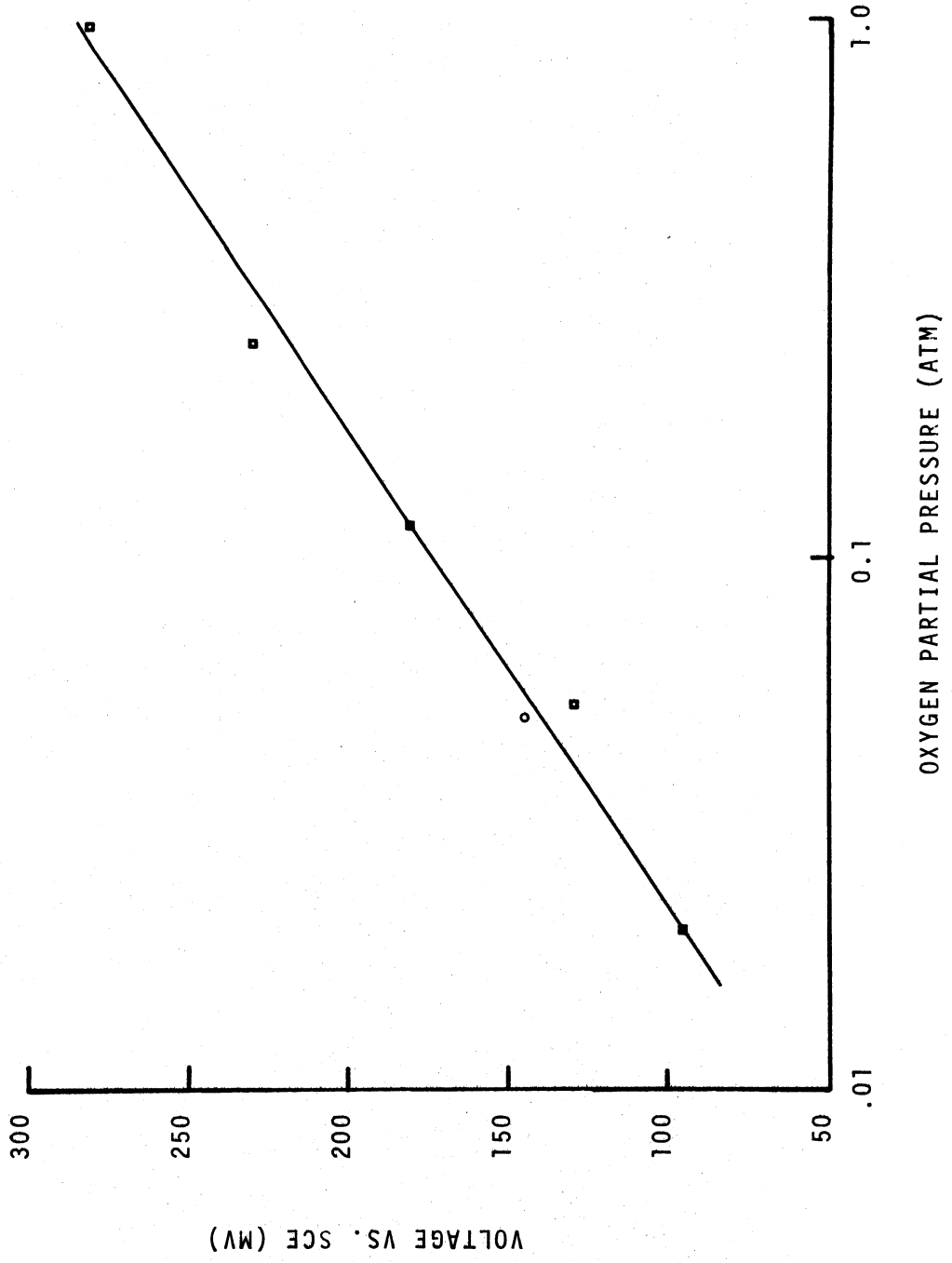


FIGURE 21

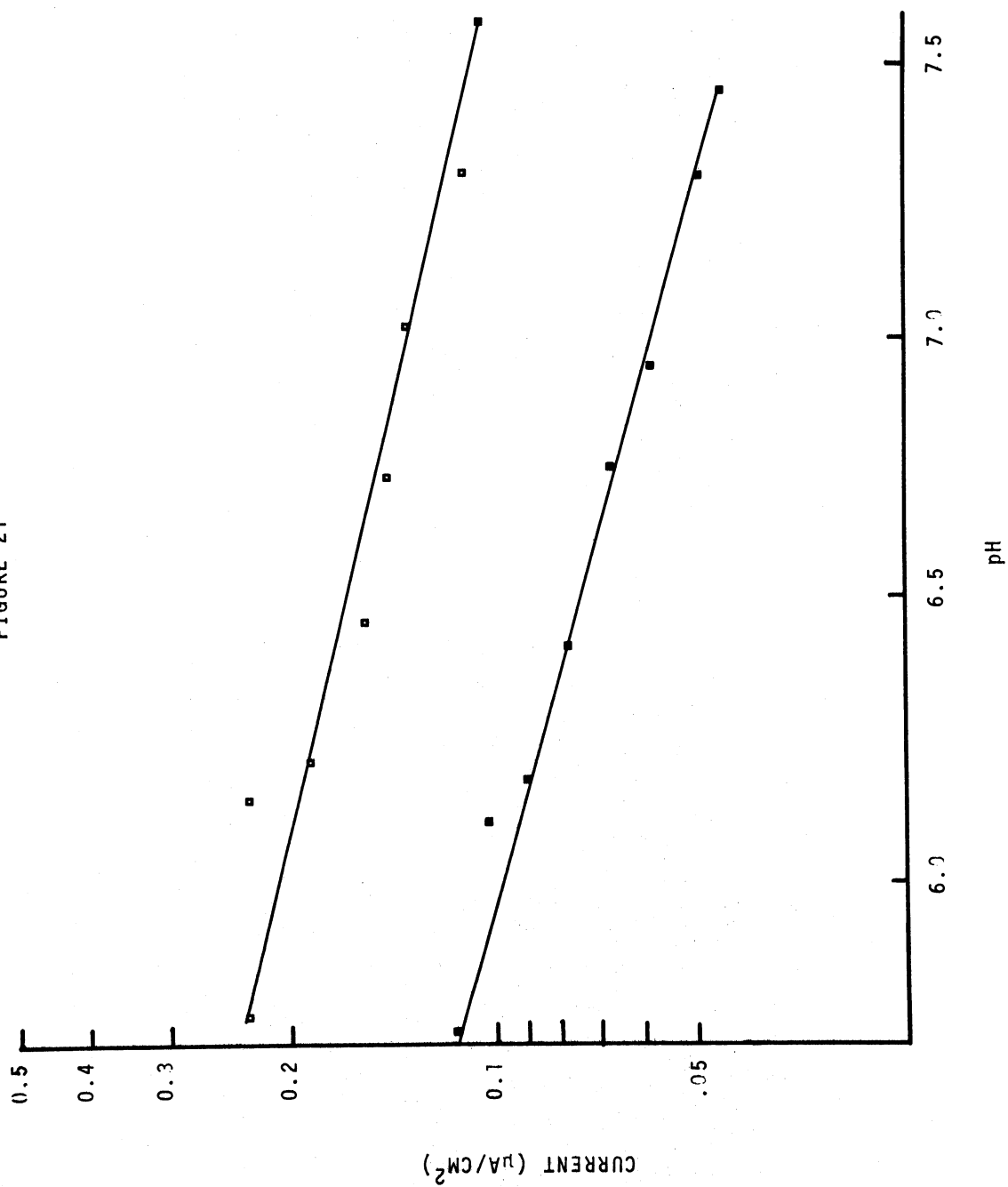
CURRENT VERSUS pH AT CONSTANT VOLTAGE  
PLATINIZED PLATINUM ELECTRODE

$$P_{O_2} = 0.055 \text{ atm}$$

$$\blacksquare V = 125 \text{ mv}$$

$$\blacksquare V = 150 \text{ mv}$$

FIGURE 21



The analysis and interpretation of these results will be left for the Discussion section.

### Activated Carbon in Neutral Saline

#### Galvanostatic

As in the case of platinized platinum, it was found that surprisingly long times were required for attainment of steady state after each step change. As previously described, the procedures were galvanostatic and, thus, step current changes rather than voltage changes were made. In Figure 22, a voltage versus time curve is shown for a step current change from  $1 \mu\text{a}/\text{cm}^2$  to  $2.5 \mu\text{a}/\text{cm}^2$  at  $\text{pH} = 7.22$  and atmospheric oxygen. It can be seen that about twenty hours was required before steady-state conditions were observed. Since these data are intended to be a measure of performance rather than a mechanistic study, all data points were measured only after the voltage had reached a distinct plateau region on the strip chart recorder. At higher current densities ( $80 \mu\text{a}/\text{cm}^2$ ) this criteria was met in as little as four hours. Typically, one complete voltage current curve required three to four days for completion.

Voltage versus current density is graphically displayed in Figure 23 for three different oxygen partial pressures. A different cathode was used in each case all having been subjected to a break-in period. The stirring rate was constant at  $200 \text{ cm}^3/\text{min}$  of the saturating gas. Individual points were repeatable within  $\pm 10 \text{ mv}$  for any one cathode. At the conclusion of the break-in periods (constant  $20 \mu\text{a}$  total current) for six different cathodes, the stable average cathode voltage was  $271 \pm 17$  (s.d.) mv. with a

FIGURE 22

VOLTAGE RESPONSE TO CURRENT STEP CHANGE

ACTIVATED CARBON CATHODE

$P_{O_2} = 0.202 \text{ atm}$

$\text{pH} = 7.22$



FIGURE 22

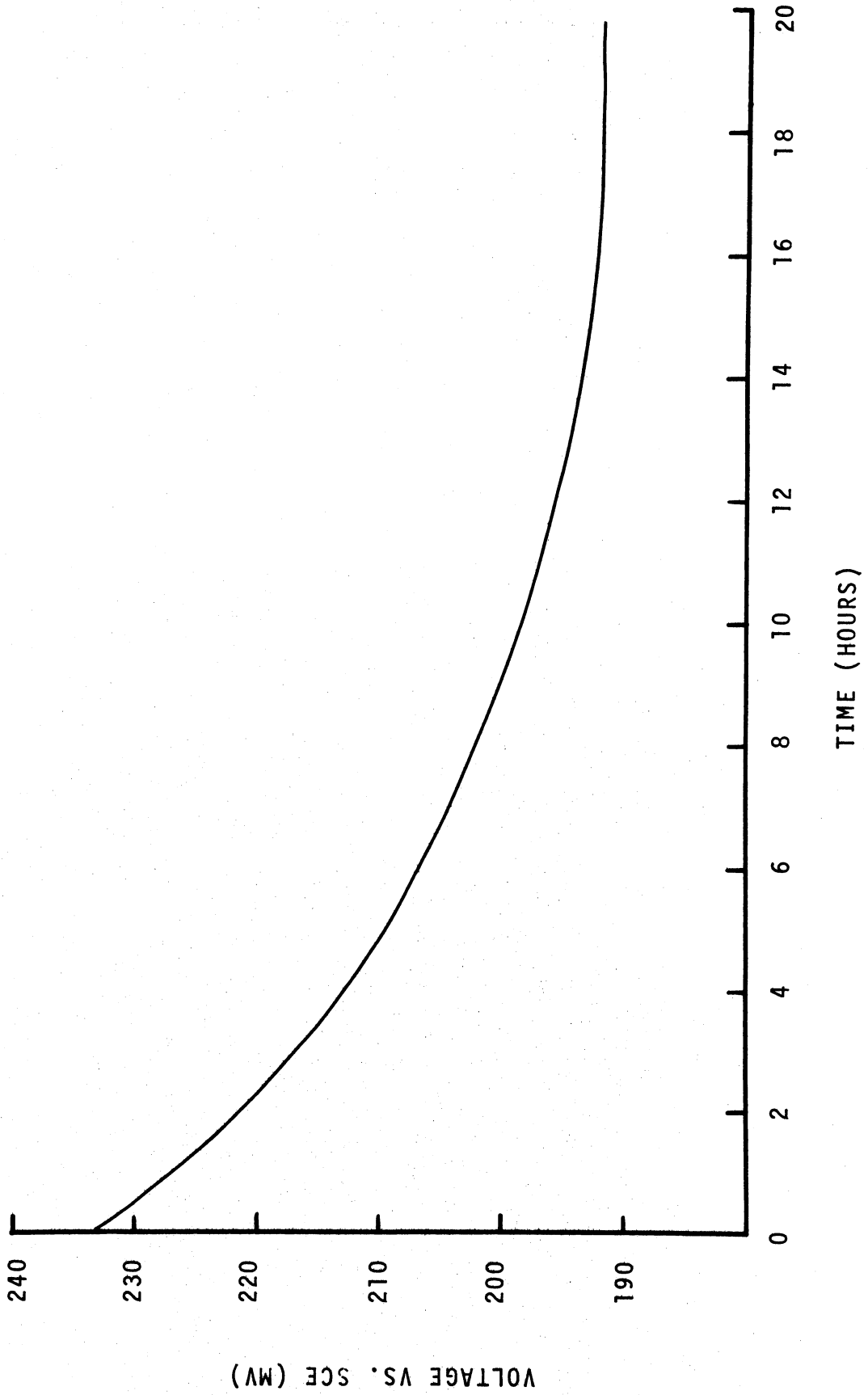


FIGURE 23

VOLTAGE VERSUS CURRENT DENSITY  
ACTIVATED CARBON CATHODE  
VARIABLE OXYGEN PARTIAL PRESSURE

pH = 7.22

- 0.202 atm
- 0.059 atm
- 0.032 atm

FIGURE 23

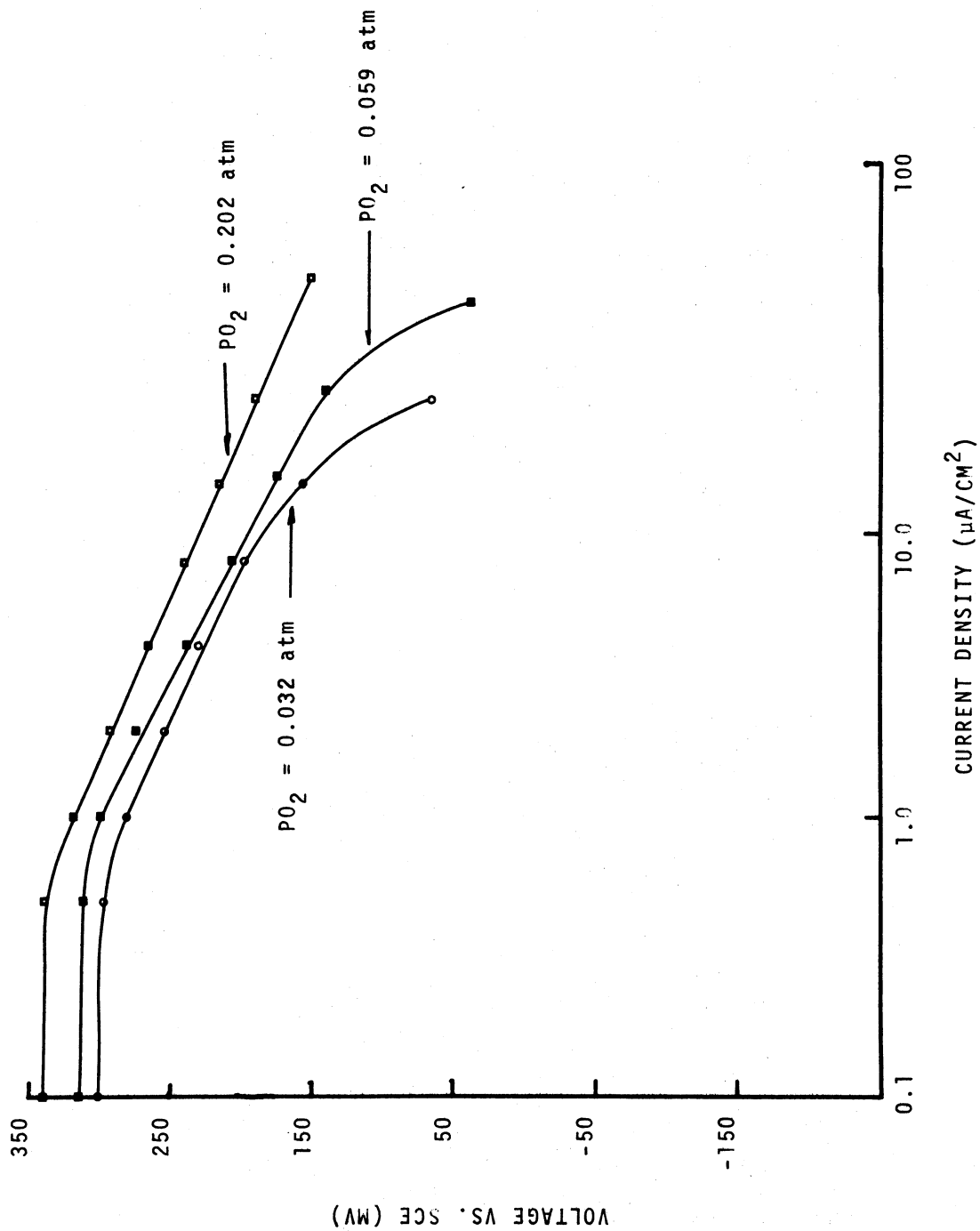


FIGURE 24

VOLTAGE VERSUS OXYGEN PARTIAL PRESSURE  
ACTIVATED CARBON CATHODE

○ and ▼  $4 \mu\text{a}/\text{cm}^2$

◻ and ■  $10 \mu\text{a}/\text{cm}^2$

FIGURE 24

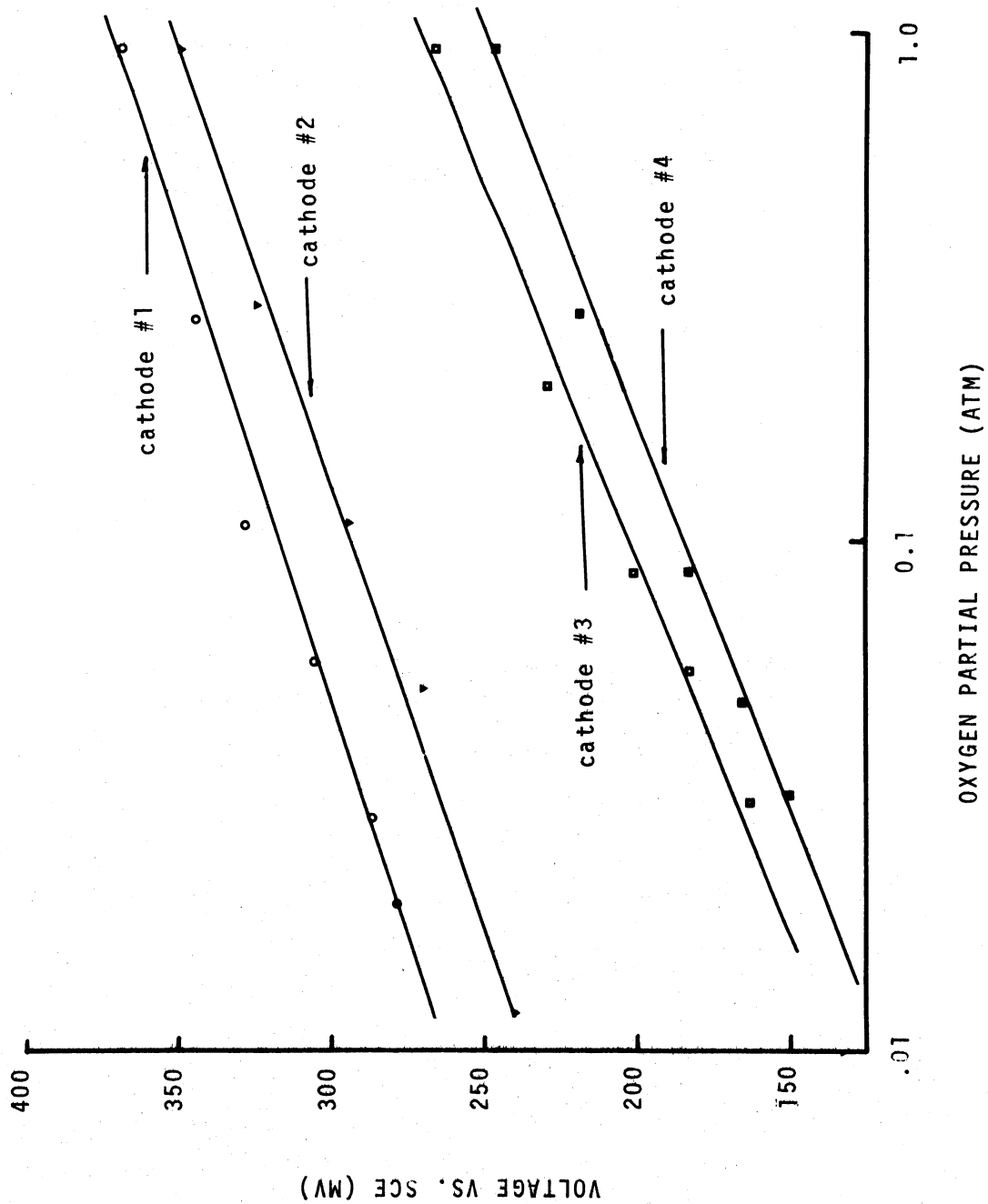


FIGURE 25

VOLTAGE VERSUS pH

ACTIVATED CARBON CATHODE

▪  $P_{O_2} = 0.202 \text{ atm}; i = 4 \text{ } \mu\text{a/cm}^2$

▪  $P_{O_2} = 0.055 \text{ atm}; i = 10 \text{ } \mu\text{a/cm}^2$

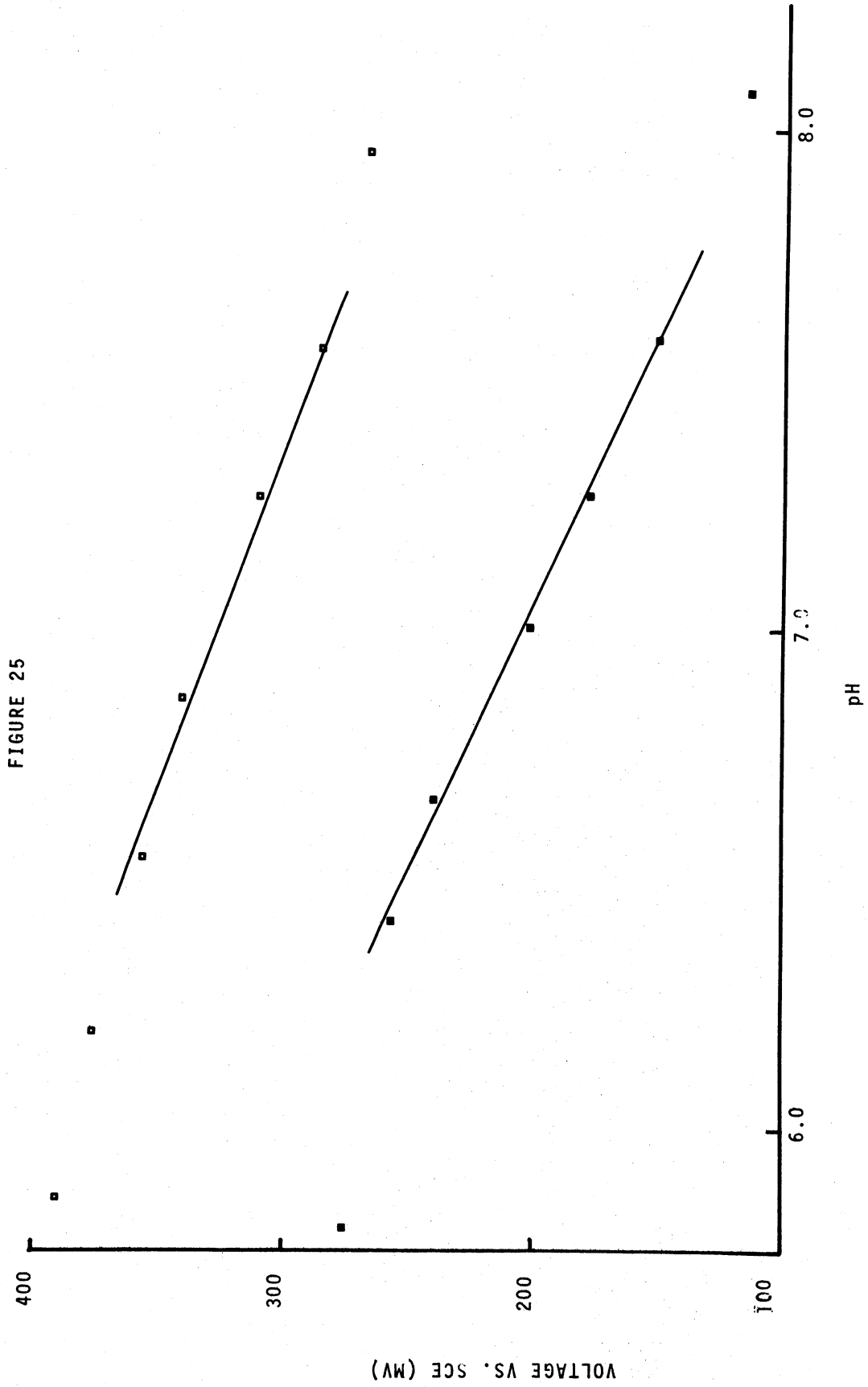


FIGURE 26

VOLTAGE VERSUS TEMPERATURE  
ACTIVATED CARBON CATHODE

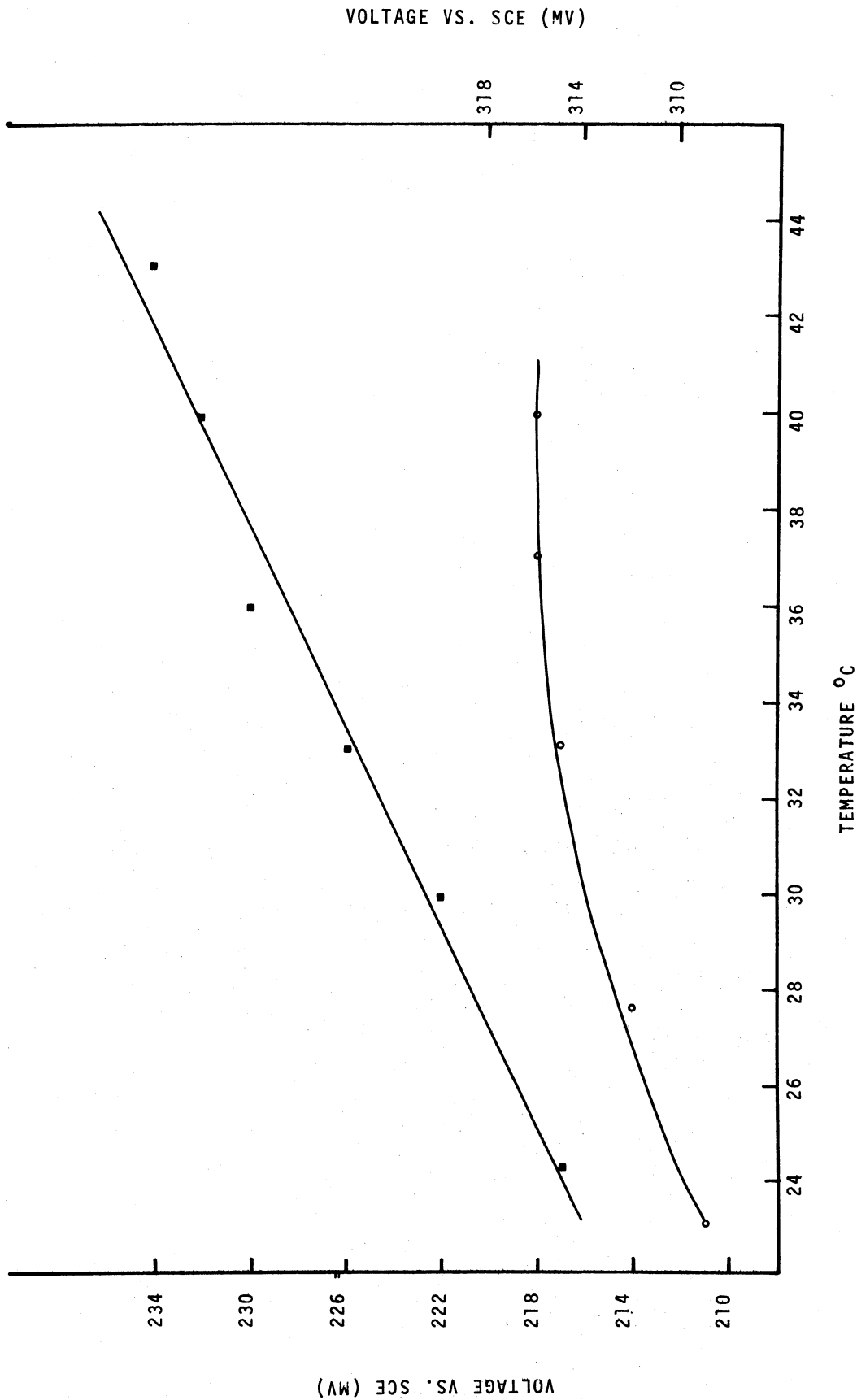
$P_{O_2} = 0.202 \text{ atm}$

■  $i = 10 \text{ } \mu\text{a/cm}^2$

○  $i = 4 \text{ } \mu\text{a/cm}^2$



FIGURE 26



VOLTAGE VS. SCE (MV)

318

314

310

range of 252 to 292 mv. This is a good indication of the reproducibility between different electrodes. The polarization curves show a distinctly linear region varying in length depending on  $PO_2$ . The average slope for six runs at varying oxygen partial pressures was  $135 \pm 22$  (s.d.) mv/decade. It should be noted, that when current was increased beyond the last point shown in each curve, the voltage rapidly decreased towards highly negative values. When this occurred, the polarization cycle was terminated.

The oxygen dependency at two different current densities (4 and  $10 \mu\text{a}/\text{cm}^2$ ) is displayed in Figure 24. Each curve was taken with a different cathode. The response to a step increase in  $PO_2$  (at constant gas flow rate) was relatively rapid when compared to a step current change. Typically, about two to three hours was required to reach a steady state. Data points interpolated from V versus log i curves to their corresponding V versus log  $PO_2$  curves fall within 10 mv of the regression line at  $10 \mu\text{a}/\text{cm}^2$ . Although any one experimental point did reproduce within 10 mv during the course of a particular run, at  $4 \mu\text{a}/\text{cm}^2$ , interpolation from the V versus log  $PO_2$  curve was not extremely favorable. Discrepancies were as great as 50 mv at individual points. The average slope from six experiments of this type was  $64 \pm 10$  (s.d.) mv per decade  $PO_2$  change.

The pH and temperature dependencies are given in Figures 25 and 26 respectively. Again, the response of the test system to changes in either variable was extremely slow. For pH, eight to ten hours was required to attain steady state. The pH of the electrolyte became stable very rapidly after addition of sodium hydroxide; i.e.,

within one to two minutes. Thus, the slow response was due to the electrode itself. However, in the case of temperature variation, the electrode potential followed approximately the same time course as did the temperature change. Therefore, the slow response was due more to the experimental temperature control mechanism than the electrode. It can be seen from both figures that both pH and temperature effect a linear change in half cell voltage at constant current within certain regions. The slope of the two pH plots between pH 6.5 and 7.5 are 91 mv/pH unit ( $10 \mu\text{a}/\text{cm}^2$ ) and 71 mv/pH unit ( $4 \mu\text{a}/\text{cm}^2$ ). At  $10 \mu\text{a}/\text{cm}^2$  the electrode voltage changes by  $0.94 \text{ mv}/^\circ\text{C}$  (pH = 7.24,  $\text{P}\text{O}_2 = .202 \text{ atm}$ ) and is linear throughout the entire temperature range. However, at  $4 \mu\text{a}/\text{cm}^2$ , the temperature versus voltage curve behaves rather oddly, exhibiting a plateau in the physiological temperature range.

The effects of stirring are clearly indicated by the voltage current curves in Figure 27. At both 0.202 and 0.03 atm  $\text{P}\text{O}_2$ , the voltage decreases in a distinctly linear manner with the log of current density in the stirred electrolyte. At the lower  $\text{P}\text{O}_2$ , a diffusion limited current begins to set in above  $8 \mu\text{a}/\text{cm}^2$ . As would be expected, when no forced convection is present, severe concentration polarization begins to occur at relatively low currents. The limiting currents without stirring are on the order of 2 and  $20 \mu\text{a}/\text{cm}^2$  for the 0.03 and 0.202 atm  $\text{P}\text{O}_2$  curves, respectively. The implications of these results are rather significant and will be discussed in detail in the following chapter.

FIGURE 27

VOLTAGE VERSUS CURRENT DENSITY  
ACTIVATED CARBON CATHODE  
STIRRED AND UNSTIRRED SOLUTION

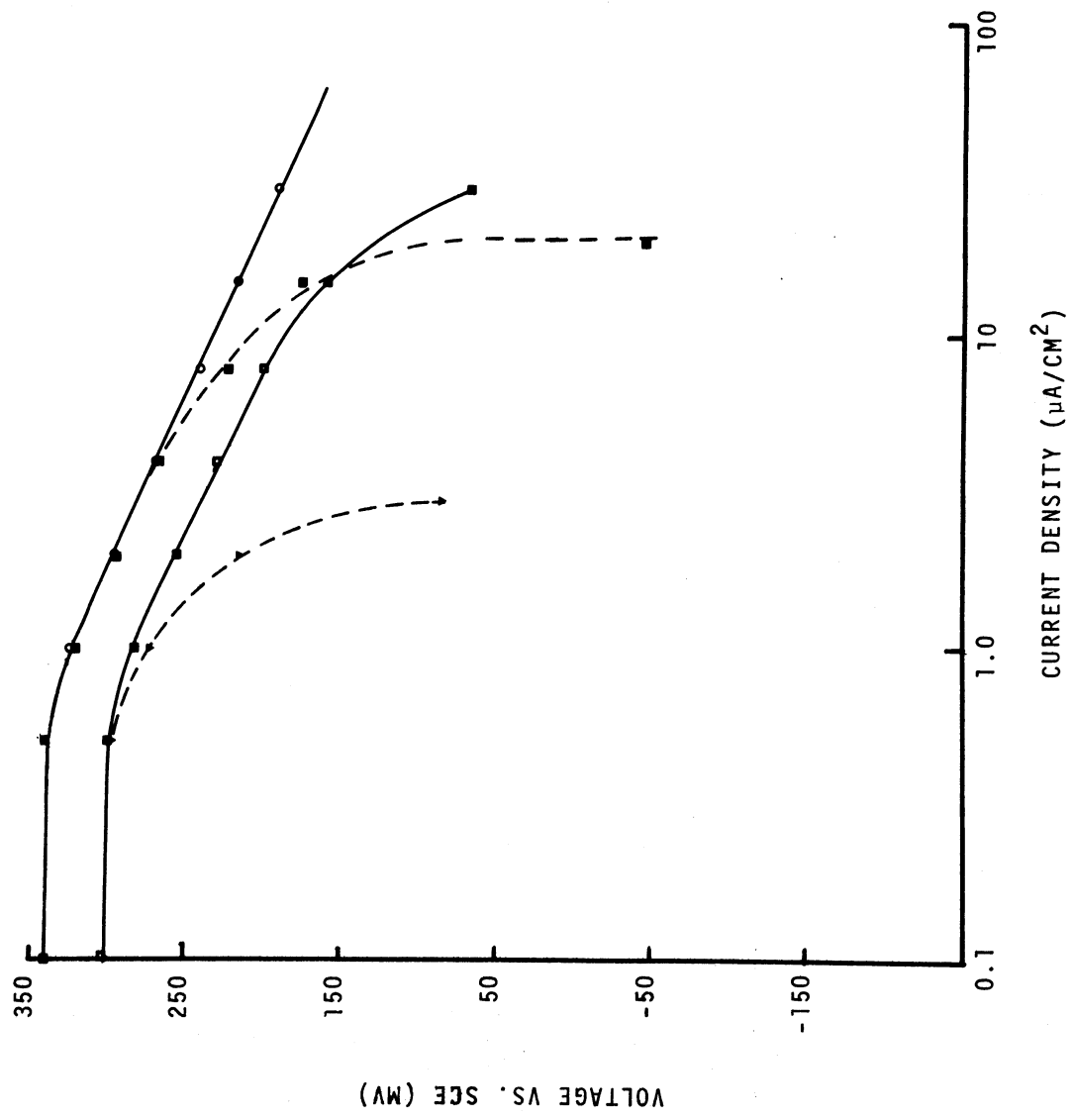
◦ and ◼  $PO_2 = 0.202$  atm

▼ and ◻  $PO_2 = 0.030$  atm

solid - stirred

dashed - unstirred

FIGURE 27



## Constant Load

Four identical activated carbon-aluminum cells were repeatedly tested via the automated load switching system. The results are quite reproducible as evidenced from Figure 28. The data shown are the superposition of one run from each cell taken simultaneously (actual photograph of computer drawn graph). The time interval between individual points is three hours. The largest deviation between any two points below the limiting current is about 40 millivolts. Limiting currents fall in the range of 100 to 200  $\mu\text{a}/\text{cm}^2$ . Open circuit voltages monitored prior to the start of 12 different runs averaged  $318 \pm 12$  (s.d.) mv versus SCE. It was found that reference voltage values (vs. SCE) decreased with increasing current and at the end of a run had fallen by as much as 10 mv. An average reference voltage was used for plotting the data shown in Figure 28 and in subsequent figures in this section.

In Figure 29, three runs at different time intervals are shown for one cell. The time intervals were 1/2, 2, and 3 hours. Some difficulty was experienced with maintenance of a steady pH throughout repeated runs of a particular cell. The buffer capacity of the cell electrolyte is, of course, finite and when a number of long (2 or 3 day) experiments are performed, the pH will begin to rise. The largest pH increase in these tests was 0.5 pH unit in one cell which had been run through six complete overvoltages cycles. From Figure 25 of the previous section, it can be seen that this pH change could correspond to a voltage decrease on the order of 35 to 45 millivolts. Thus, at least some of the downward shift in the voltage current plot is due to this factor.

FIGURE 28

VOLTAGE VERSUS CURRENT DENSITY  
ACTIVATED CARBON CATHODE  
AUTOMATED LOAD SWITCHING

Cells 1 thru 4

3 hour switching interval

FIGURE 28

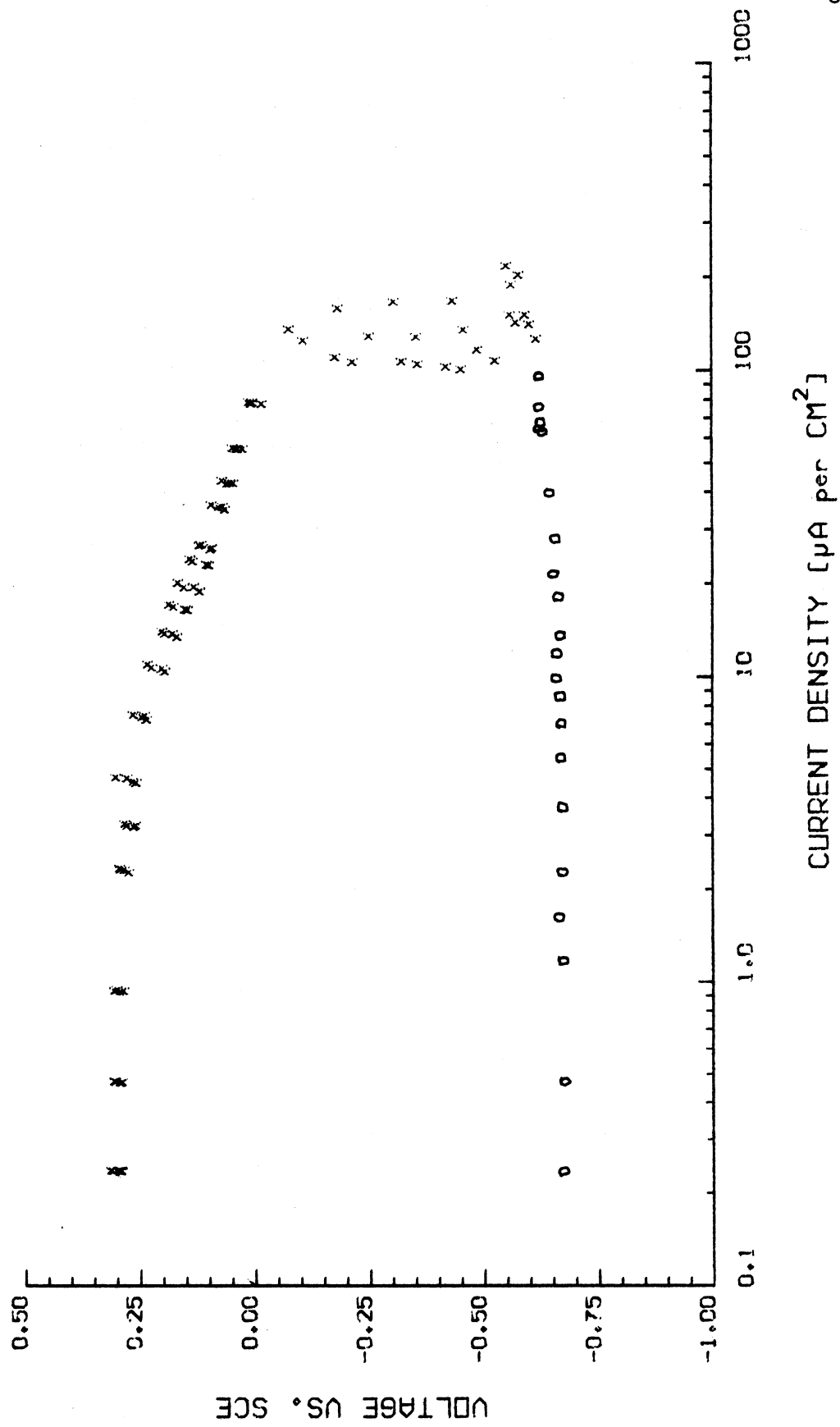




FIGURE 29

VOLTAGE VERSUS CURRENT DENSITY

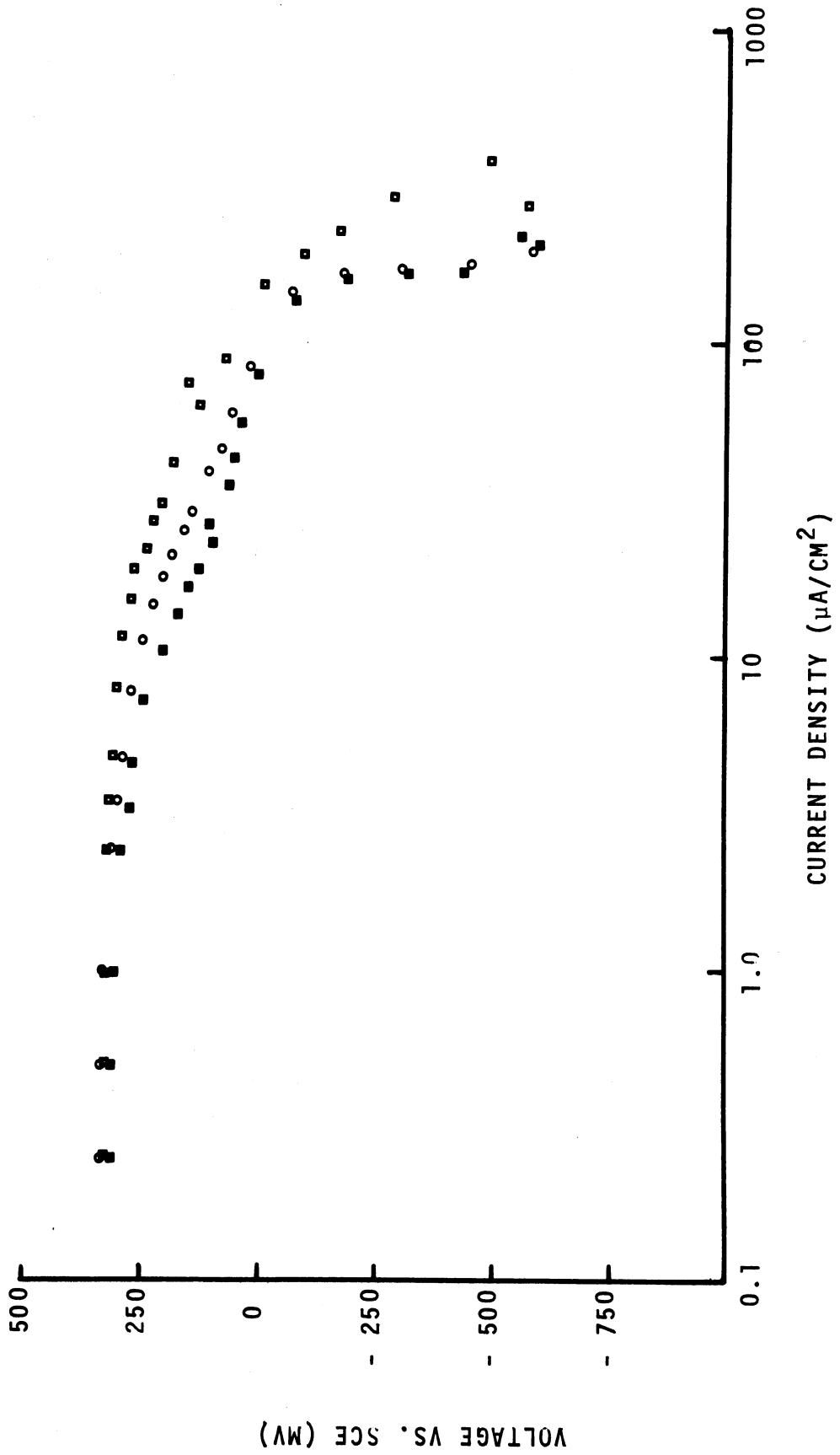
ACTIVATED CARBON CATHODE

AUTOMATED LOAD SWITCHING

CELL #1

- $\frac{1}{2}$  hour switching interval
- 2 hour switching interval
- 3 hour switching interval

FIGURE 29



It may also be of interest to note the anodic overvoltage data in Figure 28 which is taken from only one cell. Aluminum anodes typically exhibit little polarization when subjected to currents as high as  $400 \mu\text{a}/\text{cm}^2$ . Although this fact is only incidental to these discussions, it is an important consideration in the design of the total power cell package.

Figure 30 illustrates the relationship between the galvanostatic and automated constant load techniques. Agreement between the two is satisfactory up to about  $30 \mu\text{a}/\text{cm}^2$  at which point the computer drawn constant load curve begins to dip below that taken by galvanostatic means. At  $80 \mu\text{a}/\text{cm}^2$ , the difference between the cathode voltages is about 80 millivolts. It might be suspected that a portion of this discrepancy is due to IR drop between the reference (Ag/AgCl) and working electrodes in the constant load cell bath. A rough calculation of resistance polarization can be made with the assumptions:  $i = 100 \mu\text{a}/\text{cm}^2$ ;  $1/\kappa$  (specific conductance) = 50 ohm cm\*; and distance between cathode and reference = 2 cm. The resistance polarization would then be only about 10 mv. This approximation was confirmed by operating an activated carbon-aluminum cell galvanostatically at  $100 \mu\text{a}/\text{cm}^2$ . The cathode-reference voltage was monitored on a Tektronix 564B storage oscilloscope. After a stable voltage was reached, the current was interrupted by opening the galvanostatic circuit. The instantaneous voltage increase is due to resistance effects and was found to be slightly less than 10 mv (45).

---

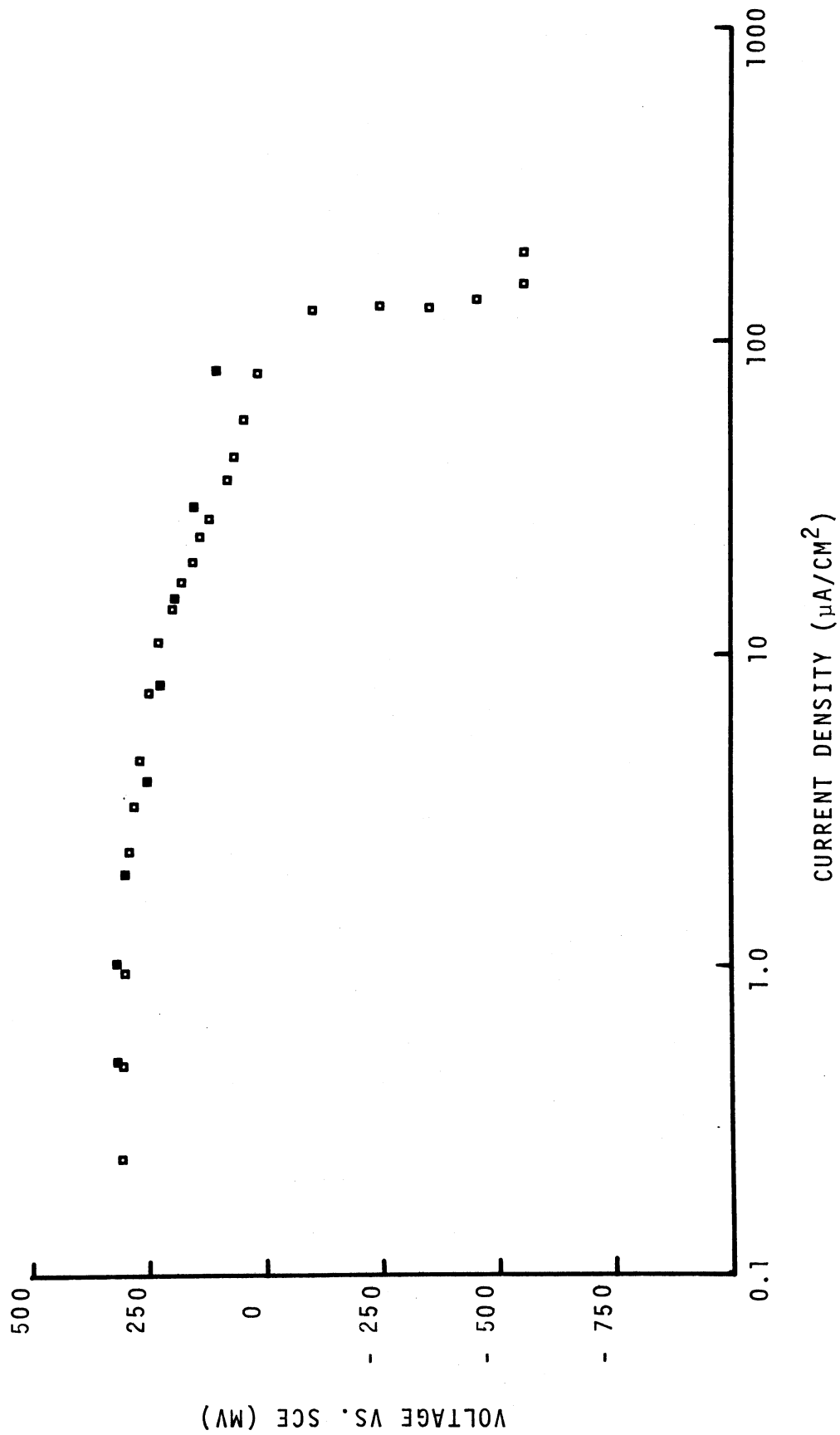
\*measured via conductance cell

FIGURE 30

VOLTAGE VERSUS CURRENT DENSITY  
ACTIVATED CARBON CATHODE  
AUTOMATED LOAD SWITCHING VERSUS GALVANOSTATIC

- Galvanostatic
- Automated load switching

FIGURE 30



Thus, IR polarization can only account for a portion of the downward shift exhibited by the computer generated data.

### Foreign Ion Effects on Activated Carbon

#### Effects of Products Produced at Hybrid Fuel Cell Anodes

Addition of either zinc or aluminum ions to the electrolyte of an operating activated carbon cathode had no effect on half-cell voltage. This was demonstrated in both short and long term test runs. The stirring rate was maintained at a very low level so that a precipitate would form on the electrode, thus simulating conditions that could occur in-vivo. The data for the long term exposures are given in Table 4.

Table 4

ion	days in saline	$V_{avg} \pm \text{range}$	days in ion sat. solution	$V_{avg} \pm \text{range}$	$\Delta pH$
Al	5	293+3	7	296+7	-0.07
Zn	4	267+1	9	268+4	-0.10

#### Artificial Interstitial Fluid

The results of one experiment in the artificial interstitial fluid are displayed in Figure 31. The three curves represent galvanostatic runs made in buffered saline (a) after six day warm up at  $5 \mu a/cm^2$  (b) in buffered saline after 30 minutes steam sterilization at  $250^{\circ}C$  (buffered saline), and (c) in artificial interstitial fluid (AIP) after a second 30 minute steam sterilization. It can be seen that sterilization has the effect of slightly increasing the open

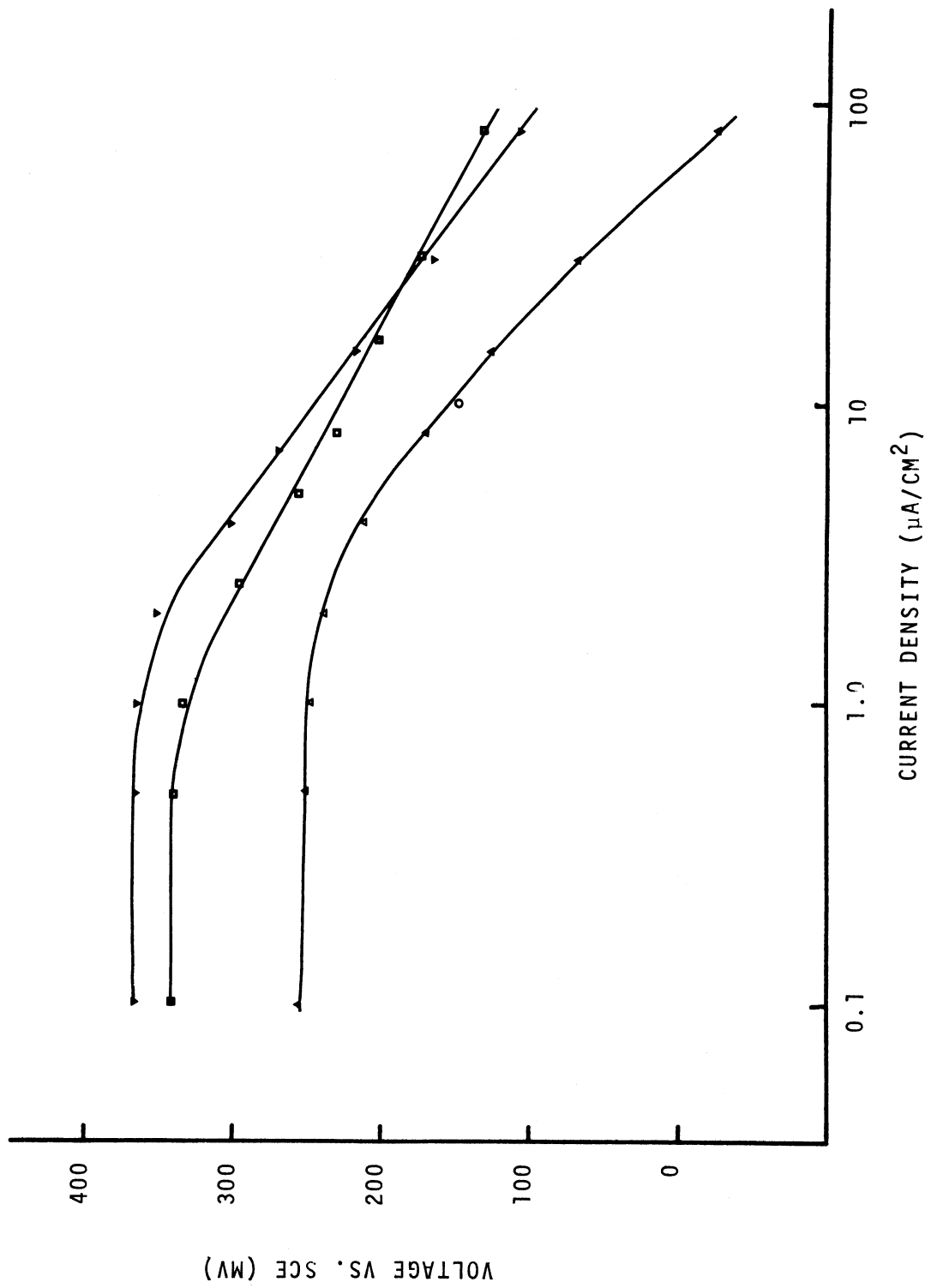
FIGURE 31

VOLTAGE VERSUS CURRENT DENSITY

ACTIVATED CARBON CATHODE

- ▣ Presterilization (buffered saline)
- ▼ Poststerilization (buffered saline)
- ▲ Artificial Interstitial Fluid

FIGURE 31





circuit potential. However, upon polarization the presterilization and post sterilization curves approach one another and overlap. When the electrolyte is AIF, the stable open circuit potential is reached overnight as is the case with buffered saline, and it lies about 100 mv below the former two curves. The voltage versus current plot exhibits a slightly curved shape rather than the distinctly linear relationship of curves taken in saline. The circled data point in the AIF plot was interpolated from Figure 32, the voltage dependency on oxygen partial pressure. This point lies within less than 10 mv of its expected value and was actually taken more than 72 hours after the cathode first operated in that current density region. Thus, reproducibility is exhibited even after a number of days of operation in the simulated biological environment. This entire set of experiments was highly reproducible. Upon repeating the complete testing cycle, individual points were duplicated within about 10 mv utilizing a different activated carbon cathode.

The dependence of cathode voltage on oxygen partial in AIF is shown in the semilogarithmic plot of Figure 32. Results of two experiments are illustrated. The slopes of the regression lines are 77 and 92 mv/decade  $PO_2$ .

The pH of the artificial interstitial fluid mixture was  $7.15 \pm .02$  (range); i.e. about .07 pH units below that of the buffered saline. This would account for only a very minor difference in cathode voltage between the two electrolytes.

Cultures taken daily (as described in the Experimental section) indicated no sign of bacterial growth until the sixth day of operation in AIF. At this time, a number of bacteria were present in the 0.1 ml

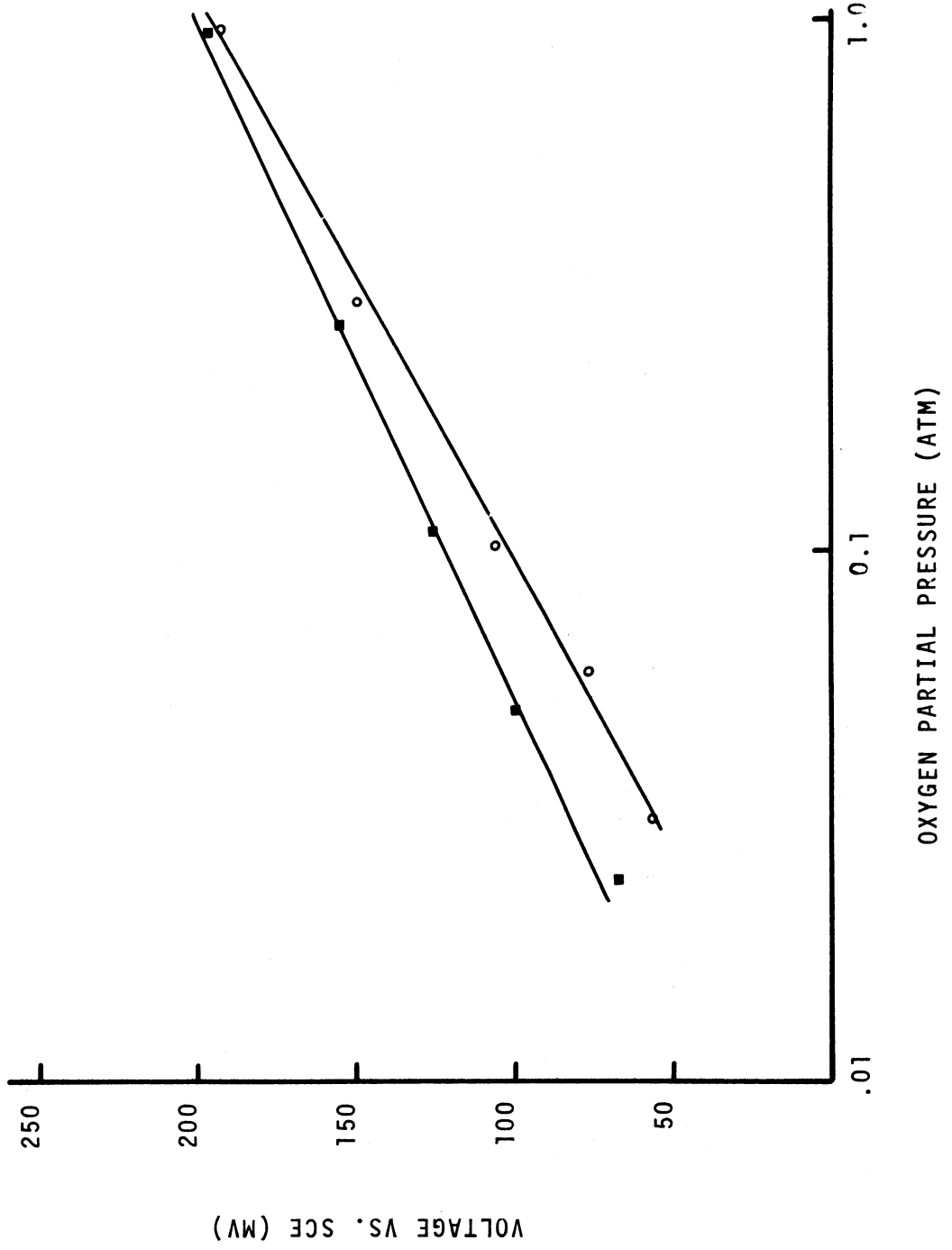
FIGURE 32

VOLTAGE VERSUS OXYGEN PARTIAL PRESSURE  
ACTIVATED CARBON CATHODE  
ARTIFICIAL INTERSTITIAL FLUID

$$i = 10 \mu\text{a}/\text{cm}^2$$

- Electrode #1
- Electrode #2

FIGURE 32



culture sample. First indications are that these were gram positive rods. Also, after the sixth day the solution became slightly cloudy and a pungent odor could be detected in the gas outlet stream. These signs all indicate the initial stages of what would rapidly become severe contamination. This was, however, of no consequence, since the sequence of procedures in this electrolyte were completed within five days. Thus, the aseptic techniques were sufficient for the purpose of collecting the required data without the interference of bacterial growth.

In Figure 33, a voltage versus current density plot in unstirred solution ( $P_{O_2} = 0.202 \text{ atm}$ ) is shown for the AIF plus protein media. A curve taken with the same electrode in buffered saline is also given for comparison. It is apparent that the voltage is shifted downward in the same manner as was that with AIF alone. In another experiment with the same electrode, current density was maintained constant at  $2.0 \mu\text{a}/\text{cm}^2$  for a five day period in the AIF plus protein solution. Stabilization of the voltage occurred after thirty-six hours at about 230 mv and remained within  $\pm 5 \text{ mv}$  for about four and one half days. At this time, contamination became evident (slightly cloudy solution, positive culture) and the voltage began a slow decline. It is interesting to note that stirring of the solution caused an increase in voltage and did not result in severe foaming after contamination. The latter was probably due to the fact that the proteins had denatured. It is also very likely that a stirring artifact at this low current density was caused by a decrease in the solution oxygen concentration because of its utilization by bacterial contaminants.

FIGURE 33

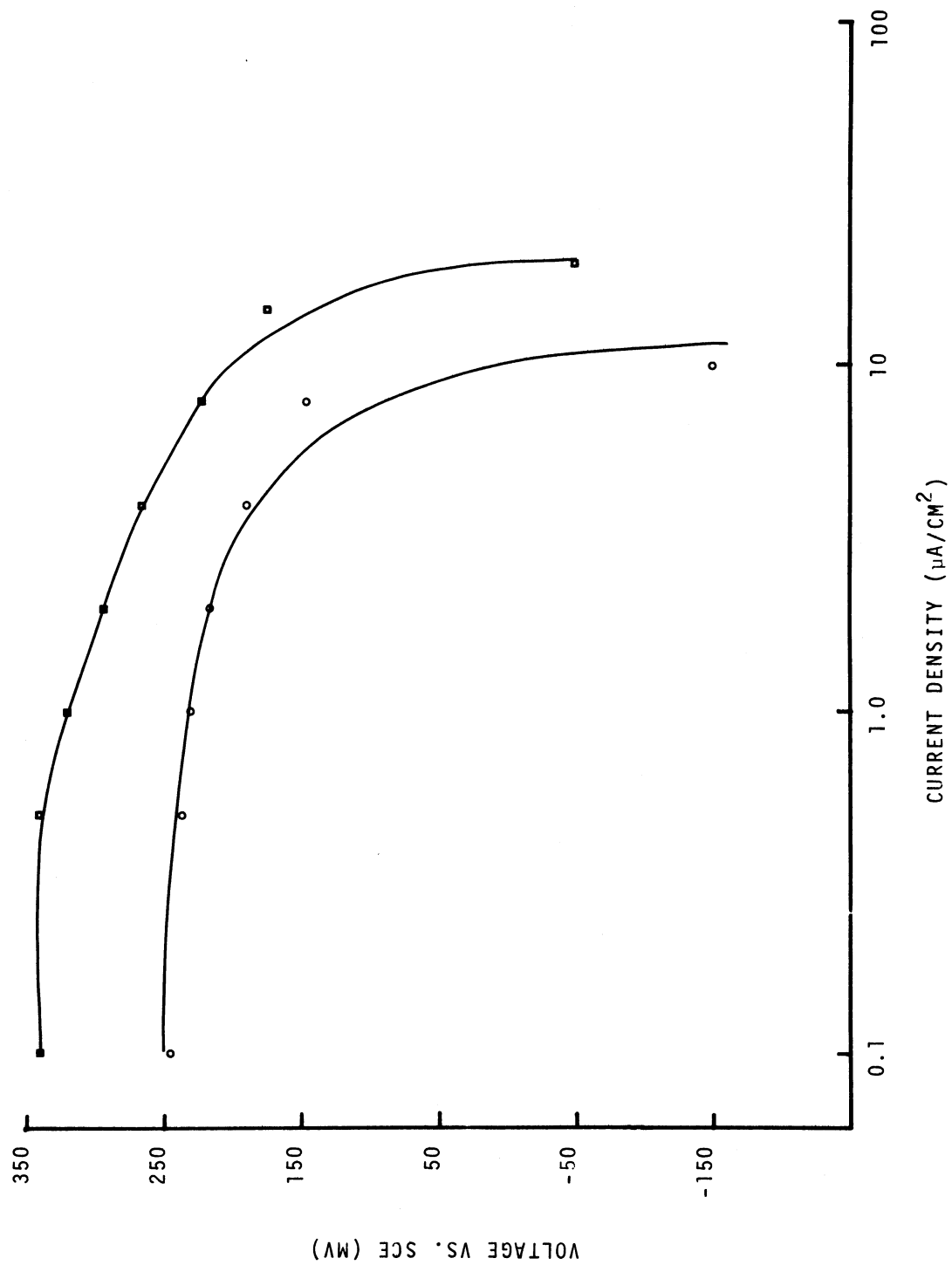
VOLTAGE VERSUS CURRENT DENSITY

ACTIVATED CARBON CATHODE

$PO_2 = 0.202 \text{ atm}$

- Artificial interstitial fluid
- Buffered saline

FIGURE 33



## DISCUSSION

## Oxygen Reduction on Platinized Platinum

Utilizing the results of the experiments on platinized platinum, it is possible to propose a mechanism for oxygen reduction on this surface in neutral saline solution. Of course, there are a number of simplifying assumptions which must be made and the question of the validity of such assumptions must also be justified. The development of a mechanism requires the use of a variety of theoretical equations and an understanding of the thermodynamic and kinetic nature of electrochemical processes. These topics have been presented in detail by many authors (43,45,78,79,80,81). Rather than reiterate the complex derivations which have already been given numerous times in the texts referenced, this discussion will describe only those equations which are specifically pertinent to the oxygen reduction mechanism. For a more complete treatment of electrochemical theory, it is suggested that the interested reader consult the literature, especially the work of Conway (78) and the Bockris review series (43,80,81).

The elucidation of an electrochemical reaction mechanism usually begins with the formulation of the rate equation for the electrode process. For a multistep process, an equation can be written for each step relating the rate of reaction (or current) to the concentration of reactants and the potentials which affect the activation energy for the process. The simple case of a step involving an

electron transfer can be represented by:



where O and R represent a reactant and product respectively. If mass transfer effects can be neglected; i.e., the reaction is strictly under activation control, then a general equation for the forward reaction current can be written as (78):

$$\vec{i} = \tau \frac{kTzF}{h} C_o (1-\theta) \exp\left[-\frac{zF\psi_1}{RT}\right] \exp\left[-\frac{\Delta G_f^*}{RT}\right] \exp\left[-\frac{(1-\beta)(\phi_m - \psi_1)zF}{RT}\right] \quad (2)$$

where

$\tau$  = transmission coefficient

$k$  = Boltzmann constant

$h$  = Plank constant

$F$  = Faraday constant

$z$  = Number of electrons involved in charge transfer step

$C_b$  = Bulk concentration of "O"

$\theta$  = Fractional surface coverage

$\psi_1$  = Potential at outer Helmholtz layer

$\Delta G_f^*$  = Activation energy for forward reaction

$\phi_m$  = Potential at electrode surface

A similar equation can be written for the reverse reaction and, at equilibrium, the exchange current,  $i_o$  is defined as:

$$i_o = \overset{\rightarrow}{i} - \overset{\leftarrow}{i} \quad (3)$$



Another quantity typically defined in discussions of this type is the overpotential,  $\eta$ , which is the potential beyond the reversible value required to drive the current in the forward direction at the net rate,  $i$ . Thus:

$$\eta = \phi_m - \phi_{R,M} \quad (4)$$

where  $\phi_{R,M}$  is the reversible potential of the electrode operating under reversible conditions.

For values of  $\eta > 0.050$  volts, the equation for the net current can be approximated by the form known as the Tafel relationship:

$$\eta = a - b \ln |i| \quad (5)$$

$$a = \frac{RT}{(1-\beta)F} \ln i_0$$

$$b = \frac{2.3 RT}{(1-\beta)F}$$

for a cathodic process.

There are a few points which require clarification before entering into the problem of deriving an entire multi-step reaction mechanism. The activation energy,  $\Delta G_f^*$ , shown in equation (2) may or may not be constant depending on the type of reactant and/or product adsorption which is occurring. The two adsorption isotherms most often considered are those of Langmuir and Temkin. In the former, the free energy of adsorption is considered to be constant. The coverage of a particular species is related to its partial pressure in the bulk phase,  $P$ , by:

$$\frac{\theta}{1-\theta} = KP \quad (6)$$

where  $l$  is a constant.

For the Temkin isotherm, it is assumed that the free energy of adsorption is a function of coverage which leads to a relationship of the form:

$$\theta = \frac{l}{f} \ln l_0 P, \quad (7)$$

where  $f$  is a proportionality factor relating the free energy at coverage  $\theta$  to the free energy at zero coverage.

The adsorption isotherm becomes important when an adsorbed reactant or product is taking part in an electron transfer step. Thus, the coverage,  $\theta$ , of the adsorbed species rather than its bulk concentration or activity, is the variable to be considered. It can be shown that the Langmuir isotherm will tend to be approached at low coverages ( $\theta \ll 1$ ) (78). If low coverage conditions are in effect, then the coverage of the reacting species can be regarded as being a function only of its partial pressure in solution. Langmuir adsorption conditions simplify matters considerably, however, Temkin-type adsorption can also be dealt with, should the need arise.

It is important to carefully consider the potentials,  $\phi_m$  and  $\psi_1$ . The variable that one usually measures in an electrochemical process is actually the potential of the electrode (Galvani potential) versus a suitable reference. The voltage measurements given in the Results section are all referred to the saturated calomel electrode which can be referred to the normal hydrogen scale. The problem that arises with this type of reference system is that the charge on the working electrode is not accounted for. It is known that this electrode charge can play an important role in the ad-

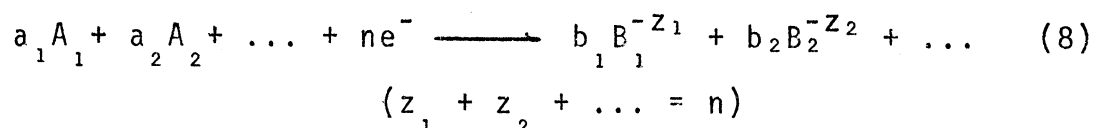
sorption of species. The potential at which the charge on the metal surface is zero has been defined as the "potential of zero charge" (p.z.c.). Bockris and Conway (43) have treated in detail the significance and measurement of the p.z.c. on various surfaces. Suffice it to say, that on most electrode surfaces (excepting mercury) the p.z.c. is not a value which is easily obtained and varies markedly with the nature and concentration of the electrolyte. However, as these authors have pointed out, it can be useful to examine the potential dependence of electrode reactions by referencing the potential to the p.z.c. and applying whatever knowledge is available about its characteristics. Electrode potentials referred to the p.z.c. have been termed "rational" electrode potentials.

The p.z.c. has been measured on smooth and platinized platinum in a number of different solutions. In acidic,  $10^{-3}$  N NaCl solution, a value of 0.14 volts has been found versus NHE (82). In 0.1M KCl in basic solution (pH = 12), the p.z.c. was determined to be -0.40 volts versus NHE (83). Although it is impossible to say exactly where the p.z.c. lies for the electrode and electrolyte of the present study, the Tafel region is apparently well above it. From Figures 17 and 18, it can be seen that the linear regions are all above + 0.05 volts versus SCE; i.e., + 0.29 volts versus NHE. Later in this section the significance of p.z.c. in the interpretation of the data collected in this study will be shown.

The potential difference  $\phi_m - \psi_1$  is what actually determines the effect of potential on the activation energy for a given electrode process. This is referred to as the potential across the compact

double layer (45). It may become necessary, in certain instances, to account for changes in the potential of the outer Helmholtz plane,  $\psi_1$ . However,  $\psi_1$  can usually be considered constant when an excess of indifferent electrolyte ( $> 0.1 M$ ) is present and when  $\phi_m$  is sufficiently far from the p.z.c. (45,78).

Equations similar to equation (2) can be written for each step of a proposed mechanism. With the assumption that the activation energy is a function only of potential and  $\psi_1$  is constant, a rate equation for the generalized reaction:



can be written in the forward direction as:

$$i = k' \prod_{i=1} (C_{A_i})^{a_i} \exp\left[-\frac{(1-\beta)\Delta\phi_m nF}{RT}\right] \quad (9)$$

An analogous equation can be written for the reverse reaction. A strictly chemical reaction step (no electron transfer) would not include the exponential term since the activation energy for such a process would be unaffected by potential changes. The factor,  $k'$ , contains all terms from equation (2) which have been assumed to be constant. In the case of an adsorbed reactant, the concentration,  $C_{A_i}$ , must be replaced by the appropriate coverage,  $\theta_{A_i}$ .

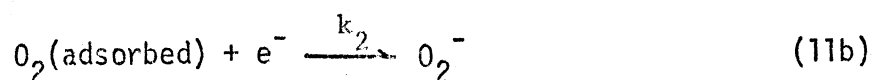
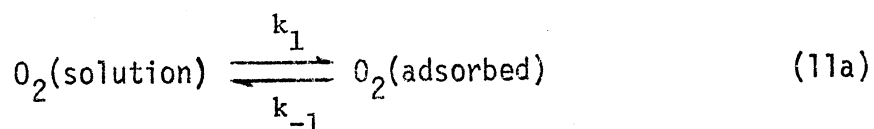
In deriving the diagnostic criteria for a multi-step mechanism, the quasi-equilibrium approach can be taken. Steps prior to the rate determining one are considered to be in equilibrium and the appropriate equilibrium relation can be written. Such an assumption is valid if the rate constants for the quasi-equilibrium reactions are

at least an order of magnitude greater than that of the rate determining step. Thus, the concentrations of the reactants in the latter can be written as a function of equilibrium values for the preceding steps. Examples of this procedure have been given by Conway (78) and Vetter (45).

The data presented in the Results section, yield diagnostic criteria which fit a relatively simple sequence of steps up to the rate limiting step. It will be recalled that the Tafel slope was 135 mv and the reaction order was 1.1 with respect to oxygen and about 0.19 with respect to  $[H^+]$ . The kinetic parameters can be stated approximately as:  $\partial V / \partial \log i = (2)(2.3)RT/F$ ;  $\partial \log i / \partial \log PO_2 = 1$ ; and  $\partial \log i / \partial \log [H^+] = 0.2$ . Expressing this in equation form gives:

$$i = k'' [O_2] [H^+]^{0.2} \exp\left(-\frac{F\phi}{2RT}\right) \quad (10)$$

where  $\phi$  is now the potential of the cathode versus the SCE reference. The Tafel slope and oxygen reaction order fit a consecutive adsorption and electron transfer sequence:



which has been proposed by other authors (see Literature Review, P. 25) However, the pH dependence is not accounted for if the electron transfer step (11b) is rate limiting. There is a convenient explanation for this apparent conflict if one considers the shift of the p.z.c.

with pH in chloride solution. Petrii, et al. have reported that the p.z.c. shifts in the negative direction with increasing pH (84). Quantitatively, this shift was given as being 30 mv/pH units. Thus, if  $\phi$  in equation (10) is to be relative to the potential of zero charge it must be replaced by

$$\phi = \phi - [\phi_{pzc}^0 - (0.03) \text{ pH}] \quad (12)$$

where  $\phi_{pzc}^0$  is the potential of zero charge at pH = 0.

From equations (11a) and (11b) and with the assumption that (11b) is rate determining, the rate equation can be developed. For equation (11a):

$$k_1 P O_2 (1 - \theta_{tot}) = k_{-1} \theta_{O_2} \quad (13)$$

For low coverages ( $\theta_{O_2} \ll 1$ ), this gives:

$$\theta_{O_2} = K_1 P O_2 \quad (14)$$

From equations (9), (11b), (12), and (14)\*:

$$\bar{i} = k_2 K_1 P O_2 \exp\left[-\frac{(1-\beta)F(\phi - \phi_{pzc}^0 + 0.30 \text{ pH})}{RT}\right] \quad (15)$$

$$\bar{i} = k_1' P O_2 \exp\left[-\frac{(1-\beta)F(\phi + 0.03 \text{ pH})}{RT}\right] \quad (16)$$

\*It is assumed here that the rate of the reverse reaction is negligible compared to the forward reaction. This is acceptable when  $\eta > 0.05$  volts (77).

The symmetry factor,  $\beta$ , (which is often used interchangeably with  $\alpha$ , the transfer coefficient) is frequently assumed to have a value of one-half. It has the significance of indicating the fraction of the overpotential which affects the activation energy for a process in the anodic direction. Similarly,  $(1-\beta)$  is the fraction of the overpotential which affects the cathodic activation energy. An explanation of the symmetry factor has been given by Conway (78).

Thus, with  $\beta = \frac{1}{2}$ , equation (16) gives:

$$\log i = \text{constant} + \log P_{O_2} - \frac{FV}{(2)(2.3)RT} - \frac{0.03 F}{(2)(2.3)RT} \text{ pH} \quad (17a)$$

Since  $2.3 RT/F = .059$  volt (at  $25^\circ\text{C}$ ):

$$\log i = \text{constant} + \log P_{O_2} - 0.25 \text{ pH} - \frac{V}{.118} \quad (17b)$$

The kinetic parameters from equation (17b) are:

$$\frac{\partial V}{\partial \log i} = - 0.118 \text{ V}$$

$$\frac{\partial V}{\partial \log P_{O_2}} = + 0.118 \text{ V}$$

$$\frac{\partial \log i}{\partial \log P_{O_2}} = 1.0$$

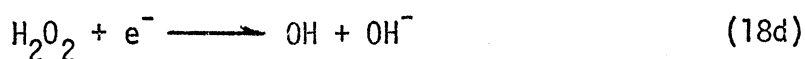
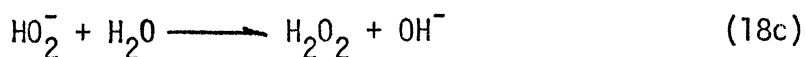
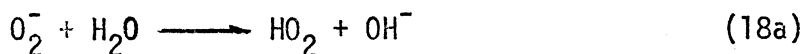
$$\frac{\partial \log i}{\partial \text{pH}} = - 0.025 \text{ V}$$

These compare favorably with the empirical values. The experimental oxygen dependency, both by galvanostatic ( $\partial V/\partial \log P_{O_2} = 115$  mv) and potentiostatic ( $\partial \log i/\partial \log P_{O_2} = 1.1$  means indicates that either

technique permits similar conclusions to be drawn.

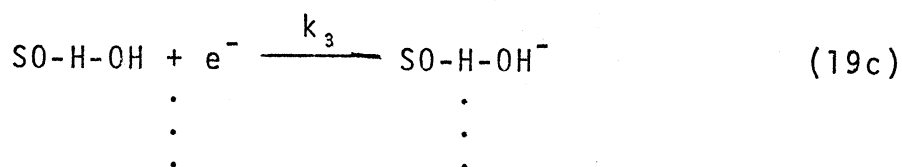
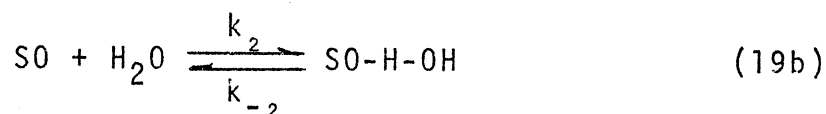
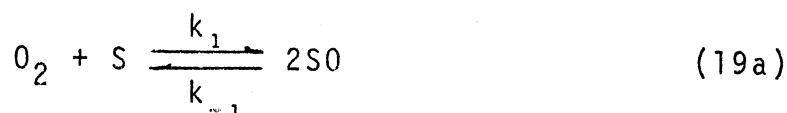
It has been assumed in this analysis that low coverage conditions prevail. In fact, it has been shown that oxygen coverage on oxide free platinum is quite low ( $\theta < 0.2$  in  $\text{HClO}_4$  solution) in the over-potential region in which the Tafel relationship holds (54). The assumption becomes even more justifiable when consideration is given to the additional coverage which would occur in a chloride ion environment (see Literature Review). There is likely even less active surface area for oxygen reduction in saline solution. This could well account for the extremely low currents encountered in the experiments carried out in this study.

The methods which have been used in this investigation cannot elucidate steps following the rate-determining one. Techniques such as the rotating ring-disc electrode might be implemented to give further information about the reaction sequence. As has been already stated, hydrogen peroxide is almost always detected as an intermediate product when oxygen is reduced except when the solutions are ultra-pure. Considering the electrolytes utilized here,  $\text{H}_2\text{O}_2$  would probably be formed and the adsorbed  $\text{O}_2^-$  could then follow the series of steps (79).





Of course, this is quite speculative and a more elaborate investigation beyond the scope of the present study would be required for its confirmation. Many reaction mechanisms have been proposed for oxygen reduction over the years. Sixteen possible paths with the associated diagnostic criteria, have been listed by Damjanovic, et al. (54). When one considers all the parameters from this study, each path presents some conflict. For instances, it is often suggested that oxygen reduction is accompanied by a splitting of the  $O_2$  molecule prior to an electron transfer. Besides the argument from tracer experiments, this type of step can be eliminated by considering the following analysis. For the mechanism beginning with:



(where S denotes an active site on the catalyst)

$$K = \frac{[SO]^2}{[O_2]} \longrightarrow [SO] = K_1' [O_2]^{1/2}$$

$$K_2 = \frac{[SO-H-OH]}{K [O_2]^{1/2}} \quad (20b)$$

$$i = k_3 K_2 K_1' [O_2]^{1/2} \exp[-(1-\beta)F\phi/RT] \quad (20c)$$

Thus, such a mechanism could only be accounted for by a reaction order of one-half with respect to oxygen. Similar arguments can be presented

for other mechanisms involving splitting of  $O_2$ . Mechanisms involving a combination of  $H^+$  during the electron transfer are ruled out by virtue of the experimental pH dependence. Thus, it would seem that oxygen reduction on platinized platinum in neutral saline is rate controlled by an electron transfer to the adsorbed oxygen molecule as suggested in the reviews of Hoare (44) and Eyring (74) for the case of acid electrolytes and smooth platinum.

### Activated Carbon Cathodes

With the data from the activated carbon cathode, some very interesting conclusions can be drawn with respect to in-vivo operation of hybrid biogalvanic fuel cells. There is now enough evidence at hand to explain, with reasonable certainty, the causes of the low cathode voltages which are detrimental to the successful operation of such power sources. An evaluation of automated power cell testing can also be made with suggestions for improvement of the method.

### Interpretation of In-Vivo Performance From In-Vitro Data

Without doubt, cations produced at either a zinc or aluminum anode have little effect on cathode performance. Even with the growth of a precipitate film on the activated carbon surface, no significant changes in voltage were observed. Thus, this factor cannot be used as a basis of suitability for choosing between these materials.

On the other hand, some of the constituents of interstitial fluid will act to decrease the cathode voltage. However, the magnitude of this effect is not of such proportions that it should be worthy of

much attention. The artificial interstitial fluid with or without albumin, lowered the voltage by only about 100 mv from its presterilization values throughout most of the polarization curve. The curvature in the AIF curves can be attributed to changes in factors involved in the diffusional processes and is inconsequential in the region of typical operating current densities, i.e., below  $10\mu\text{a}/\text{cm}^2$ . This particular type of catalyst, then, can be improved upon very little from the standpoint of so-called "poisoning" by those species with which it comes in contact upon implantation. The introduction of membranes to prevent poisoning would not result in a significant gain in power output, but would serve to make available an additional mode of failure. It must be pointed out that these conclusions can only be drawn for teflon bonded platinum activated carbon. Any other type of cathode material would have to be tested under similar circumstances to determine its characteristics in a simulated biological environment.

The curves in Figure 27 show that oxygen concentration and mass transfer phenomena play the key role in determining in-vivo power levels. It would be difficult from theoretical considerations to predict the concentration polarization that will occur in a subcutaneous or intramuscular implantation for at least two reasons. First, the bulk oxygen concentration in-vivo can vary dramatically depending on the exact nature of the vascular supply to an implant site and the surgical implantation technique. Secondly, the manner in which oxygen is transported to the electrode surface involves not only diffusion and natural convection, but also some component of forced convection. The latter would be due to the movement of

tissues and fluid surrounding the implant site as a result of muscular contractions and arterial pulsations. To estimate the thickness of the diffusion boundary layer under such conditions is almost an impossible task. However, by examining the limiting conditions of the stagnant and the well mixed electrolytes, one can estimate what the lower and upper limits of concentration polarization might be.

The limiting current densities in buffered saline\* for the stirred electrolyte were  $100\text{-}200\mu\text{a}/\text{cm}^2$  at  $0.21\text{ atm PO}_2$  and about  $30\mu\text{a}/\text{cm}^2$  at  $0.032\text{ atm PO}_2$ . In stagnant solution the respective limiting currents were approximately  $20$  and  $3\mu\text{a}/\text{cm}^2$ . Before discussing the significance of these measurements, it is necessary to have some estimate of the oxygen partial pressure in the in-vivo environment. Subcutaneous and intramuscular partial pressures have been recorded in dogs utilizing Clark type electrodes. Cater, *et al.*, reported a  $\text{PO}_2$  of  $14.1 \pm 1.5$  mm Hg in skeletal muscle and  $16.9 \pm 4.7$  subcutaneously (85). Somewhat higher values have been determined by Jones and co-workers using a perforated capsule technique which probably yields a more meaningful value of mean tissue  $\text{PO}_2$  (86). In skeletal muscle they found a  $\text{PO}_2$  of  $21.7 \pm 1.5$  and in subcutaneous tissue the  $\text{PO}_2$  was  $33.3 \pm 2.1$ . The lower value of  $\text{PO}_2$  in Figure 27 was  $0.032\text{ atm}$  (approximately  $25\text{ mm Hg}$ ) which is of the same order of magnitude as those values obtained for tissues where hybrid cells are typically implanted.

It can be seen then, that at normal tissue  $\text{PO}_2$  levels a hybrid cell operating above  $2\mu\text{a}/\text{cm}^2$  will encounter significant concentration

---

\*See Figures 27 and 28

polarization if the transfer of oxygen is strictly diffusional (stagnant fluid). It will be recalled from Figure 2 that Roy, et al., reported a current density of about  $18 \mu\text{a}/\text{cm}^2$  and that Hahn, et al., operated hybrid cells at approximately 1 and  $2 \mu\text{a}/\text{cm}^2$  (25,26). The cathode voltages in these studies differed by only about 200 mv which is less than would be expected if the power cells were operating near the limiting current region. There would seem, then, to be some conflict between the two investigations. However, wide variation in oxygen transfer rates to the cathode are to be expected and could account for the discrepancies. This point can be supported to some extent when the previously mentioned study by Cater, et al., is considered (85). Although they reported a mean  $\text{PO}_2$  of 14.1 mm Hg in skeletal muscle, this mean value did not include two abnormally high readings of 51 and 46 mm Hg. It was found upon necropsy of the implant site that the actual placement of the oxygen electrode was very near a relatively large vessel. It is just such a variation in actual electrode placement that can account for differences in concentration polarization in hybrid power cells. Since it is difficult, if not impossible, to determine a priori what the mean tissue  $\text{PO}_2$  will be for any one implantation, the limiting low case must be used as a basis for prediction of minimum power output and estimation of required cathode surface area.

It may be of interest to examine the nature of the mass transfer processes which can occur when concentration polarization becomes an important factor in limiting power output. The cases of the stirred and unstirred electrolytes have been treated extensively and reviewed (45,87). A most important point, which, is often not

considered, is that limiting currents are not necessarily in direct proportion to electrode area with either forced or natural convection. For a vertical electrode in an unstirred solution, the average limiting diffusion current density depends on  $L^{-1/4}$  where  $L$  is the height of the electrode (45). For the simplified case of laminar flow parallel to a surface, a non-linear dependency on surface area is also found. Turbulent flow conditions involve considerable difficulties, but again "... in general, the current is not proportional to the area of the electrode" (87). Thus, when the cathode voltage is under the influence of oxygen mass transfer limitations, scaling up from laboratory size test electrodes to full size cathodes must be considered with extreme caution.

Assuming that a cardiac pacemaker would require a current of approximately  $100\mu\text{a}$ , a  $50\text{ cm}^2$  cathode, operating at  $2\mu\text{a}/\text{cm}^2$  should be sufficient. From Figure 27, the voltage at  $2\mu\text{a}/\text{cm}^2$  with  $\text{PO}_2 = 0.032\text{ atm}$ , is about  $+200\text{ mv}$  versus SCE in the stagnant solution. With an additional loss of about  $100\text{ mv}$  due to biological contaminants (Figures 31 and 33), the activated carbon cathode should operate at about  $+100\text{ mv}$  versus SCE. Data from Hahn, et al., indicate that this type of cathode, in-vivo, actually operated at about  $-100$  to  $+100\text{ mv}$  versus SCE in this current density region (25). It would seem, then that the case of the stagnant electrolyte at low  $\text{PO}_2$  still does not yield a conservative lower limit for the estimation of the in-vivo mass transfer processes. There are a few factors, including those previously mentioned, that can account for this discrepancy. The scale-up from a  $1\text{ cm} \times 2\text{ cm}$  test cathode to the  $5\text{ cm} \times 9\text{ cm}$  cathode\* used in Hahn's investigation can certainly introduce some errors.

Moreover, this error is unpredictable when it is considered that the in-vivo mass transfer process does not lend itself to modeling. In addition, the tissue  $PO_2$  could be slightly less than 0.032 atm further shifting the diffusion limited region to the left in the in-vitro polarization curve. Furthermore, the diffusion coefficient and oxygen solubilities vary somewhat between the testing situation and in-vivo operating conditions. These effects can best be seen from analyzing the simplified case of the Nernst diffusion layer theory.

According to the diffusion layer theory, a partially stationary layer of liquid (stagnant film) exists in front of the electrode surface whether the electrolyte is stirred or unstirred (45). Diffusion of a component through this layer of thickness,  $\delta$ , occurs by virtue of the concentration gradient (more correctly, activity gradient),  $dC_j/dx$ , where  $C_j$  is the concentration of species  $j$ , and  $x$  is the distance coordinate. This is shown in Figure 34 for the simple case of a linear diffusion gradient to a smooth planar electrode. The dashed line represents the case of the limiting diffusion current density, i.e., when the concentration of species  $j$  at the electrode surface is zero. The mass transfer of oxygen during its reduction can be represented in terms of the current density,  $i$ , by:

$$i = \frac{-D_o nF(C_b - C_o)}{\delta}$$

---

\*This cathode was<sub>2</sub> folded over on itself and wrapped around the anode. Thus, only 45 cm<sup>2</sup> were actually exposed to tissue surface.

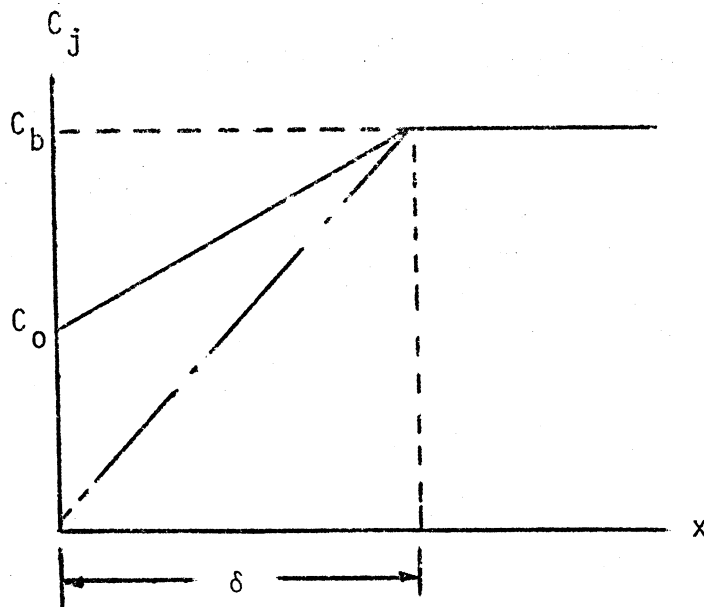


FIGURE 34

Nernst diffusion layer model

where  $C_b$  and  $C_0$  are the bulk solution and surface concentrations, respectively and  $D_0$  is the diffusion co-efficient.

The thickness of the diffusion layer is usually estimated at  $10^{-2}$  to  $10^{-3}$  cm for a well stirred electrolyte (45,87,89). The diffusion coefficient for oxygen in water at  $25^{\circ}\text{C}$  has been given as  $2.6 \times 10^{-5}$   $\text{cm}^2/\text{sec}$  (44). The concentration of oxygen in saline can be determined from interpolation of data for the Ostwald co-efficient given by Linke (90). Using these data and equation (21), a value for the limiting current density with atmospheric  $\text{PO}_2$  in stirred saline solution would be about  $500 \mu\text{a}/\text{cm}^2$  (see Appendix C). This is within an order of magnitude of the  $100 - 200 \mu\text{a}/\text{cm}^2$  shown in Figure 28.



The variation in limiting current from stirred to unstirred solution and from high to low oxygen partial pressures is also of the expected order of magnitude. The ratio of partial pressures (0.202/0.032) is about 6.3 and the ratio of limiting current densities is about 5.0 (150 $\mu$ a/30 $\mu$ a) for the case of the stirred electrolytes. Since the thickness of the diffusion boundary layer is about an order of magnitude less in stagnant solutions than in well stirred solutions (45), one would expect a ten fold decrease in limiting current in going from one situation to the other. Such is the case since at 0.202 atm:

$$\frac{i_{L,\text{stirred}}}{i_{L,\text{stagnant}}} \doteq \frac{150}{20} = 7.5$$

and at 0.0302 atm:

$$\frac{i_{L,\text{stirred}}}{i_{L,\text{stagnant}}} \doteq \frac{30}{3} = 10$$

The diffusion coefficient for oxygen in saline is certainly different from that in tissue or interstitial fluid. This fact is shown in Figure 33 where overpotential curves in the AIF and protein solution and saline are compared. The limiting currents vary by about a factor of two which could be accounted for partially by a lower  $D_o$  for oxygen in the artificial media and also a lower oxygen solubility in the same. The latter factor is probably not significant as shown by Cater, et al. (73).

Although equation (21) may hold at the limiting current, it cannot be applied in the region below this because of the porous

structure of and the non-uniform concentration distribution through the electrode. It would be difficult to define an equation describing the total overvoltage characteristics of the activated carbon electrode in-vivo, again, because of lack of complete data concerning the various parameters involved. Generally speaking, though, one can use the data collected in this study to estimate the required cathode area for driving a particular implantable device. This is provided that a conservative approach is taken and possible sources of error are accounted for.

#### Analysis of Automated Test System

The collection of performance data from hybrid cells (or any other type power source) is greatly facilitated by the use of an automated system. However, the overall system must be analyzed in terms of its two major components, i.e., that part which serves to collect and manipulate data and that part which serves to simulate the in-vivo environment. The former has proven itself to save many man-hours of labor while the latter is subject to improvement.

The accuracy and reliability of the computer system is more than satisfactory. The major limit on accuracy is the type of buffer amplifier in the measuring circuit. In the present study, the Keithley 610C, one of the better instruments of its class, is still only a  $\pm 2\%$  (of full scale) device. Thus the  $\pm 4\text{mv}$  resolution of the analog to digital converter of the Linc-8 computer does not introduce errors of great significance. The convenience of the data

manipulation and graphing programs is certainly beneficial when large numbers of experiments are performed.

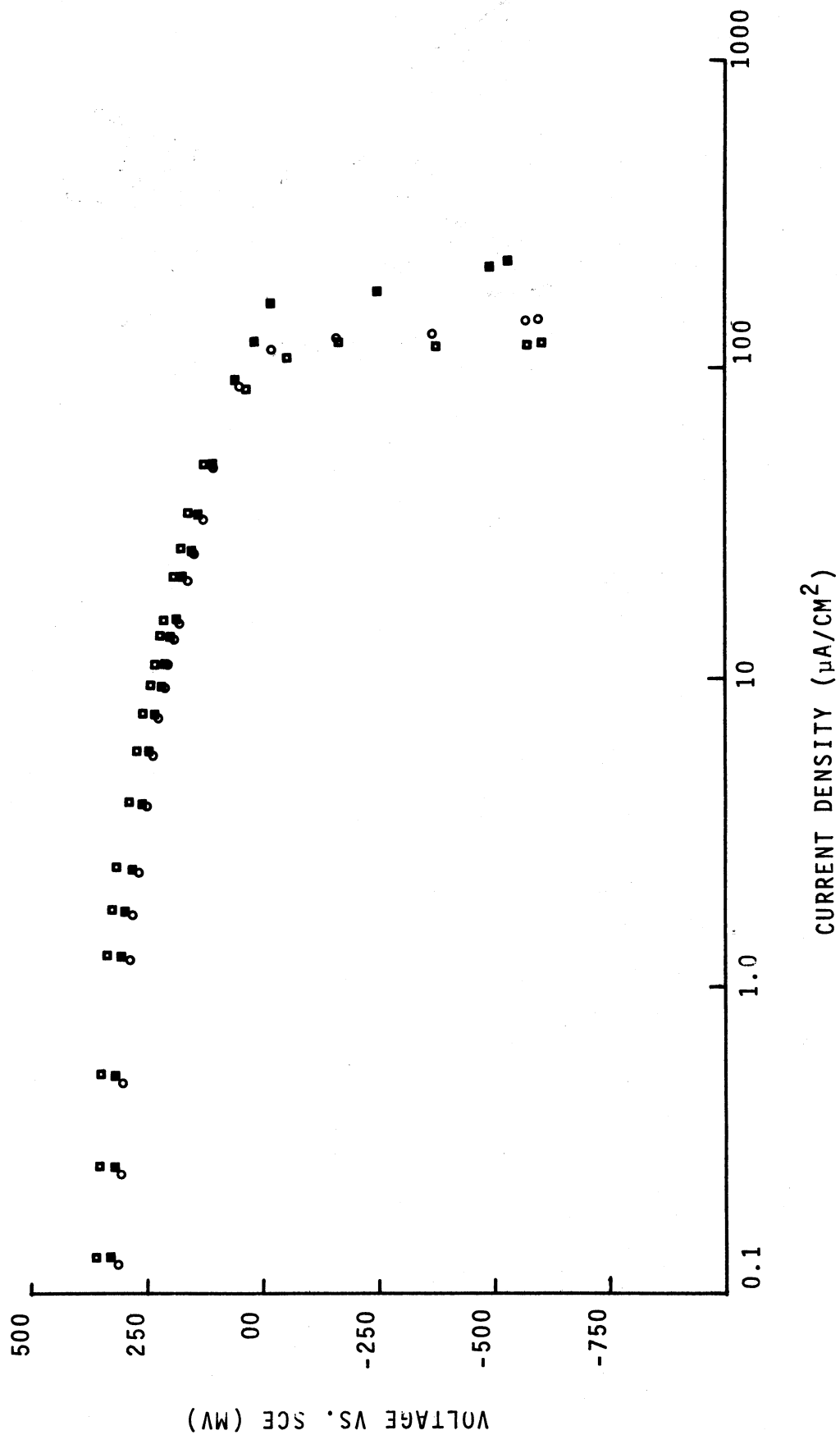
Concerning the environmental conditions to which hybrid cells are subjected in automated screening tests, a reevaluation of criteria is necessary. The cell bath electrolyte, and stirring used for the automated testing do serve to demonstrate the nature of the catalytic properties of different cathode materials. Thus, materials which are poor candidates in well stirred neutral saline at atmospheric  $PO_2$ , are probably not suitable for in-vivo application. However, as shown in the previous section, the in-vivo situation is governed by mass transfer limitations. Differences in the porous structure of cathodes could then prove to be important at low oxygen partial pressures in a relatively stagnant electrolyte. That such differences do exist can be seen by comparing the response time of the activated carbon cathode and a teflon bonded platinum black cathode. Three polarization curves for the latter are shown in Figure 35 (91). These curves were taken with  $\frac{1}{2}$ , 1, and  $1\frac{1}{2}$  hour switching intervals. It can be seen that after  $\frac{1}{2}$  hour, a steady state has been reached with no significant differences occurring between the three time intervals. This contrasts markedly with Figure 29 in which at least a three hour interval was required for a steady state with the activated carbon cathode. It may be that the thicker, more densely packed activated carbon presents a significantly greater resistance to oxygen transfer than the relatively thin, loose Teflon bonded Pt-black. At low  $PO_2$  values in the bulk solution, the interior of the activated carbon is probably depleted of oxygen greatly lowering the current capabilities of the overall electrode. For a more complete evaluation

FIGURE 35

VOLTAGE VERSUS CURRENT DENSITY  
TEFLON BONDED PLATINUM BLACK ELECTRODES (91)  
AUTOMATED LOAD SWITCHING  
 $P_{O_2} = 0.202 \text{ atm}$

- $\frac{1}{2}$  hour switching interval
- 1 hour switching interval
- $1\frac{1}{2}$  hour switching interval

FIGURE 35



of the characteristics of a specific cathode material, testing must be carried out under stagnant conditions at low oxygen partial pressures. These factors have not been extensively considered in any in-vitro testing of biological power cells.

#### Platinized Platinum Versus Platinum Activated Carbon

The initial assumption that platinized platinum would be similar to the active surface of platinum activated carbon is probably open to question. The former exhibited severe polarization at very low current densities which may suggest that it was not an active surface for oxygen reduction. However, the voltage-current curves taken in sulfuric acid both before and after tests in saline, were similar to curves found in the literature. This would indicate that the low activity of the platinized platinum is peculiar to neutral saline and not sulfuric acid.

Although differences between the two types of electrode materials can be partly attributed to unequal specific surface areas, other factors must be involved when the pH and oxygen dependencies are considered. There is a good possibility that oxygen reduction does not take place by the same mechanism on both surfaces. A variety of reasons could account for this, however, data from this investigation are not sufficient to attempt an explanation. It would be wise to prepare an activated carbon surface, say on pyrolytic graphite, which was smooth enough to warrant kinetic interpretation.

## CONCLUSIONS AND RECOMMENDATIONS

Although much has been learned with respect to the characteristics of hybrid fuel cell cathodes, there remain many questions which are yet to be answered. The initial goals of this investigation have been achieved as outlined in the Introduction. It now remains to suggest the future direction for development of a viable hybrid biogalvanic fuel cell power supply for cardiac pacemakers.

It has been shown that the major problem concerning the cathode of the hybrid biogalvanic fuel cell is related to availability of oxygen and its transport to the electrode surface. Thus, the understanding of the mechanism of the reaction would probably not contribute a great deal from the practical aspect of increasing the power generating capabilities of this type of power source. The most important conclusion which can be drawn from the results of the experiments which have been described, is that current densities should be kept at the lowest possible level; i.e., below  $2 \mu\text{a}/\text{cm}^2$ , if this is feasible. In this manner, variations which would occur from one implant to another would still permit the cathode to operate at a suitable voltage. Conservatively speaking, a power cell package should be designed with the expectation that the cathode voltage would be about -100 mv versus SCE. When coupled with a pure zinc anode, the total voltage available would then be approximately 900 mv. This should be sufficient to drive a properly designed cardiac pacemaker or transmitter device. There is, of course, the possibility

that an increase in overall cell performance can be gained from improvement of the anode half-cell voltage through the use of alloy materials. This should be the topic of an investigation in the near future.

The study of the reduction of oxygen in neutral chloride media does have a direct application when mass transport processes are not limiting. There are, at present, investigations into the development of a fuel cell power source for an artificial heart in which blood is the electrolyte. In this case, the oxygen partial pressure at the cathode would be much higher when compared to that of interstitial fluid. Also, the flow-through arrangement of such a device would add a great deal of forced convection to the overall transport process. It would be helpful to have not only a knowledge of the rate limiting step, but also a measurement of chloride adsorption and its relation to the p.z.c. on various cathode materials. The formation and subsequent reaction of intermediates (specifically hydrogen peroxide) is also an important consideration. Although a mechanism has been proposed for oxygen reduction on platinum in neutral chloride media, it has only opened the door to further investigations into answering the above mentioned questions. There is apparently a marked difference between platinized platinum and activated carbon. A thorough understanding of this difference could lead to the development of a suitably active catalyst for large power output fuel cells.

A study concerned with the effects of cathode dimensions on mass transport limitations would be of importance at this time. It would be of interest to measure polarization characteristics at low  $PO_2$  in stagnant solutions with various size electrodes so that length and width parameters could be related to concentration polarization. Hopefully,



a consistent relationship would arise that would aid in design of full power cell cathodes from data taken on smaller test electrodes.

One of the more important conclusions which has arisen from the experiments and discussion presented in this writing pertains to the utility of in-vitro testing and the direction of future efforts towards the development of a hybrid fuel cell power supply. In-vitro testing of cathode materials can give a good indication of the general characteristics of a particular catalyst structure. At the present time, there are too many unknown factors involved in the in-vivo mass transport phenomena to warrant direct interpretation of purely in-vitro results. Thus, in-vivo testing under loading conditions equivalent to that of a cardiac pacemaker (including pulsed mode operation), must be the final and most critical means of judging a complete power cell package. The platinum activated carbon cathode which has been examined in this study is a suitable cathode material from all aspects which need be considered. It is believed that further, long-term in-vivo experiments will prove that, when coupled with a sufficiently active and efficient anode, platinum activated carbon can, indeed, serve as a cathode for a hybrid fuel cell cardiac pacemaker power source.

## BIBLIOGRAPHY

1. Roy, O.Z., "Biological Energy Sources: A Review," IEEE Trans. Bio.-Med. Eng., 6(6):250-56, 1971.
2. Nose, Y., ed., Cardiac Engineering, Interscience (New York), 1970.
3. Salkind, A.J., and Raddi, W., "Primary and Secondary Cells," Ann. N.Y. Acad. Sci., 167(2):635-44, 1969.
4. Meyers, G.H., Parsonnet, V., Zucker, R.I., and Lotman, H.A., "Biologically Energized Cardiac Pacemakers," Am. J. Med. Elec., p. 233-36, Oct., 1964.
5. Enger, C.C., and Simeone, F.A., "Biologically Energized Cardiac Pacemaker: In-Vivo Experience with Dogs," Nature, 218(5137): 180-81, 1968.
6. Lewin, G., Meyers, G.H., Parsonnet, V., and Raman, K.V., "An Improved Power Source for Cardiac Pacemakers," Trans. Amer. Soc. Artif. Int. Org., 14:215-19, 1968.
7. Hursen, T., and Kolenik, S., "A Reliable Nuclear Battery for Cardiac Pacemaking," Abs. 23rd ACEMB, p. 286, Nov., 1970.
8. Greatbatch, W., Lee, J.H., Mathias, W., Eldridge, M., Moser, J.R., and Schneider, A.A., "The Solid-State Lithium Battery: A New Improved Chemical Power Source for Implantable Cardiac Pacemakers," IEEE Trans. Bio.-Med. Eng., 18(5):317-24, 1971.
9. Schaldach, M., "Bioelectric Sources for Cardiac Pacing," Ann. N.Y. Acad. Sci., 167:1016-24, 1969.
10. Roy, O.Z., and Wehnert, R.W., "Biological Energy Sources," Ann. N.Y. Acad. Sci., 167(2):645-60, 1969.
11. Schaldach, M., "An Electrochemically Activated Pacemaker," Wiederbelebung und Organersatz, 5(2):75-84, 1968.
12. Schaldach, M., "Practical Experiences with Biogalvanically Operated Heart Pacemakers," Thoraxchirurgie und Vasculare Chirurgie, 17:541-45, 1969.
13. Wolfson, S.K., Yao, S.J., Geisel, A., and Cash, H.R., "A Single Electrolyte Fuel Cell Utilizing Permselective Membranes," Trans. Amer. Soc. Artif. Int. Org., 16:193-98, 1970.

14. Appleby, A.J., Ng, D.Y.C., Wolfson, S.K., and Weinstein, H., "An Implantable Biological Fuel Cell with an Air-Breathing Cathode," Intersociety Energy Conv. Conf., P. 346-53, Sept., 1969.
15. Drake, R.F., Kusserow, B.K., Messinger, S., and Matsuda, S., and Matsuda, S., "A Tissue Implantable Fuel Cell Power Supply," Trans. Amer. Soc. Artif. Org., 16:199-205, 1970.
16. Wolfson, S.K., Gofberg, S.L., Prusiner, P. and Nanis, L., "The Bioautofuel Cell: A Device for Pacemaker Power from Direct Energy Conversion Consuming Autogenous Fuel," Trans. Amer. Soc. Artif. Org., 14:198-203, 1968.
17. Massie, H., Racine, P., Pasker, R., Hahn, A.W., and Sun, H.H., "Study of Power Generating Implantable Electrodes," Med. Biol. Eng., 6:503-16, 1968.
18. Plank, G.R., Hahn, A.W., Beard, R.B., and Cooper, J.B., "Chronic Implantation of Biological Power Cells," J. Assoc. Adv. Med. Inst., 4(1):28-32, 1970.
19. Reynolds, L.W., "Implantable Power Source Employing a Body Fluid as an Electrolyte," U.S. Pat. 3,345,989, 1967.
20. Frasier, J.D., "Implantable Electrical Device with Biological Power Supply," U.S. Pat. 3,421,512, 1969.
21. Satinsky, V., Cassel, J., and Salkind, A.J., "Bioelectric Energy by Reduction of Tissue Oxygen," J. Assoc. Adv. Med. Inst., 5(3):184-87, 1971.
22. Roy, O.Z., Whitelaw, W., and Wehnert, R.W., "Biogalvanic Energy Sources," Digest 7th Int. Conf. on Eng. Med. Biol., p.519, Stockholm, 1967.
23. Strohl, C.L., Scott, R.D., Frezel, W.J., and Wolfson, S.K., "Studies of Bioelectric Power Sources for Cardiac Pacemakers," Trans. Amer. Soc. Artif. Int. Org., 12:318-28, 1966.
24. Tseung, A.C.C., and King, W.J., "An Encapsulated Implantable Metal-Oxygen Cell as a Long Term Power Source for Medical and Biological Applications," Med. Biol. Eng., 9:175-84, 1971
25. Cooper, J.B., Hahn, A.W., Hoffer, R.E., and Salkind, A.J., "Continued Development of Hybrid Power Cells for Cardiac Pacemakers," Abs. 24th ACEMB, p. 282, Nov., 1971.

26. Hahn, A.W., Cooper, J.B., Cywinski, J., and Salkind, A.J., "Implantable Hybrid Cells for Biological Applications," Ext. Abs. Electrochem. Soc. Fall Meet., p. 203-05, 1970.
27. Sonne, J., "The Oxygen Dependency of Implantable Electrodes," M.S. Thesis, Drexel Univ., 1969.
28. Kozawa, A., Zilionis, V.E., and Brodd, R.J., "Electrode Materials and Catalysts for Oxygen Reduction in Isotonic Saline Solution," J. Electrochem. Soc., 117(12):1474-78, 1970.
29. Fishman, J. and Henry, J., "Oxygen Reduction on Gold-Palladium Alloys in Neutral Media," Proc. Art. Heart Prog. Conf., p. 825-38, June, 1969.
30. Cywinski, J.K., Hahn, A.W., and Cooper, J.B., "Implantable Transmitters Powered by Biogalvanic Cells," 1972 San Diego Biomedical Symp., in publication.
31. Cooper, J.B., "Application of Oxygen Permeable Membranes to Hybrid Biogalvanic Fuel Cells," M.S. Thesis, Drexel Univ., 1970.
32. Giner, J., and Hunter, C., "The Mechanism of Operation of Teflon Bonded Gas Diffusion Electrode: "A Mathematical Model," J. Electrochem. Soc., 116:1124-30, 1969.
33. Vogel, W.M., and Lundquist, J.T., "Reduction of Oxygen on Teflon Bonded Platinum Electrodes," J. Electrochem. Soc., 117(12): 1512-16, 1970.
34. Yeager, E., Krouse, P. and Rao, K., "Kinetics of the Oxygen-Peroxide Couple on Carbon," CITCE Meeting, Moscow, Aug, 1963; Tech. Rep. 16, Western Reserve Univ., U.S. Office of Naval Res., Cont. Nonr 2391 (00), June, 1963.
35. Cooper, J.B., Hahn, A.W., and Hoffer, R.E., "Electrode Screening Techniques for Hybrid Power Cells," 23rd ACEMB, p. 285, Nov., 1970.
36. DeRosa, J.F., Beard, R.B., and Hahn, A.W., "Fabrication and Evaluation of Cathode and Anode Materials for Implantable Hybrid Cells," Trans IEEE Bio-Med. Eng., 17(4):324-30, 1970.
37. \_\_\_\_\_, Monsanto Research Corporation, "First Ann. Sum. Rep. Implant. Fuel Cell for an Artif. Heart." Contract PH43-66-976, NHI, DHEW, PHS, NIH, 1968.
38. Brodd, R.J., Kozawa, A., Zilionis, V.E., and Kalnoki-Kis, T., "On Oxygen Electrodes for a Biological Fuel Cell", Ext. Abs. Electrochem Soc. Fall Meet., p. 200-01, 1970.

39. Henry, J.F., and Fishman, J.H., "Oxygen Reduction in Near Neutral Electrolytes," Ext. Abs. Electrochem. Soc. Fall Meet., p. 200-01, 1970.
40. Hahn, A.W., "Engineering Studies of a Biological Fuel Cell," Final Progress Report HE-12,975-01, NIH, 1971.
41. Cywinski, J.K., and Hahn, A.W., "Monitoring the Output of Implanted Hybrid Power Cells," 23rd ACEMB, p. 298, Nov., 1970.
42. Hahn, A.W. and Cooper, J.B., to be published.
43. Bockris, J. O'M., and Conway, B.E., eds., Modern Aspects of Electrochemistry, No. 5, Plenum Press (London), 1969.
44. Hoare, J.P., The Electrochemistry of Oxygen, Interscience (New York), 1968.
45. Vetter, K.J., Electrochemical Kinetics, Academic Press (New York), 1967.
46. Delehay, P., "A Polarographic Method for the Indirect Determination of Polarization Curves for Oxygen Reduction on Various Metals, I Case of Platinum," J. Electrochem. Soc., 97:108-204, 1950.
47. Hoar, T.P., "The Mechanism of the Oxygen Electrode," Proc. Roy. Soc., A143:628-646, 1933.
48. Bianchi, G., and Mussini, T., "Cathodic Reduction of Oxygen on Smooth Platinum in Acid Solution," Electrochim. Acta., 10:445-55, 1965.
49. Damjanovic, A., and Bockris, J. O'M., "The Rate Constant for Oxygen Dissolution on Bare and Oxide Covered Platinum," Electrochim. Acta., 11:376-77, 1966.
50. Bockris, J. O'M., and Hug, A.K.M.S., "The Mechanism of the Electrolyte Evolution of Oxygen on Platinum," Proc. Roy. Soc., A237:277, 1956.
51. Watanabe, N., and Devanathan, A.A.V., "Reversible Oxygen Electrodes," J. Electrochem. Soc., 111(5); 615-19, 1964.
52. Hoare, J.P., "Oxygen Overvoltage Measurements on Bright Platinum in Acid Solutions, III," J. Electrochem. Soc., 112(8):849-53, 1965.
53. Wroblowa, H., Rao, M.L.B., Damjanovic, A., and Bockris, J. O.M., "Adsorption and Kinetics at Platinum Electrodes in the Presence of Oxygen at Zero Net Current," J. Electroanal. Chem., 15:139-50, 1967.

54. Damjanovic, A., and Brusic, V., "Electrode Kinetics of Oxygen Reduction on Oxide-Free Platinum Electrodes," Electrochim. Acta., 12:615-28, 1967.
55. Hoare, J.P., "Oxygen Overvoltage Measurements on Bright Platinum in Acid Solutions, I. Bright Platinum," J. Electrochem. Soc., 112:602-07, 1965.
56. Damjanovic, A., Dey, A., and Bockris, J. O.'M., "Kinetics of Oxygen Evolution and Dissolution on Platinum Electrodes," Electrochim. Acta., 11:791:814, 1966.
57. Damjanovic, A., and Genshaw, M.A., "Dependence of the Kinetics of  $O_2$  Dissolution at Pt on the Conditions for Adsorption of Reaction Intermediates," Electrochim. Acta., 15:1281-83, 1970.
58. Hoar, T.P., "The Mechanism of the Oxygen Electrode in Alkaline Solution," Proc. 8th Meet. Int. Comm. Electrochem. Thermo. and Kin., p. 439-44, 1958.
59. Winkelmann, D., "Untersuchungen uber das elektrochemische Verhalten von  $O_2$ -  $H_2O_2$  -  $H_2O$  am blanken und platinieren Platin," Zeit. für Elektrochem., 60(7):731-40, 1956.
60. Damjanovic, A., Genshaw, M.A., and Bockris, J. O.'M., "The Role of Hydrogen Peroxide in Oxygen Reduction at Platinum in  $H_2SO_4$  Solution," J. Electrochem. Soc., 114:466, 1967.
61. Davies, M.O., Clark, N., Yeager, E., and Hovorka, F., "The Oxygen Electrode: Isotopic Investigation of Electrode Mechanism," J. Electrochem. Soc., 106:56: 1959.
62. Rao, M.L.B., Damjanovic, A., and Bockris, J. O.'M., "Oxygen Adsorption Related to the Unpaired d-Electrons in Transition Metals," J. Phys. Chem., 67:2508-09, 1963.
63. Kozawa, A., "Effects of Anions and Cations on Oxygen Reduction and Evolution Reactions on Platinum Electrodes," J. Electroanal. Chem., 8:20-39, 1964.
64. Popat, P.V., and Hackerman, N., "Capacity of the Electrical Double Layer and Adsorption at Polarized Platinum Electrodes," J. Phys. Chem., 62:1198-1203, 1958.
65. Horanyi, G., Solt, J., and Nagy, F., "Investigation of Adsorption Phenomena on Platinized Platinum Electrodes by Tracer Methods," J. Electroanal. Chem., 31:87-93, 1971.
66. Horanyi, G., Solt, J., and Nagy, F., "Investigation of Adsorption Phenomena on Platinized Platinum by Electrodes by Tracer Methods, V, Potential Dependence of Chloride Ion Adsorption," Acta. Chim. Acad. Sci. Hung., 68:29-38, 1971.

67. Bagotsky, V.S., Vassilyev, B., Weber, J., and Pirtskhalova, J.N., "Adsorption of Anions on Smooth Platinum Electrodes," J. Electroanal. Chem., 27:31-46, 1970.
68. Weber, J., Vassilyev, B., and Bagotsky, V.S., "Effect on Anions on the Adsorption of Hydrogen, Oxygen, and Methanol on a Platinum Surface," Elektrokhimya, 5(3):323-26, 1969.
69. \_\_\_\_\_, Abbott Laboratories, Fluid and Electrolytes, 1970.
70. Guyton, A.C., Textbook of Medical Physiology, W.B. Saunders Co. (Philadelphia), 1966.
71. Ruch, T.H., and Patton, H.D., Physiology and Biophysics, W.B. Saunders Co. (Philadelphia), 1965.
72. Wiederhielm, C.A., "Dynamics of Transcapillary Fluid Exchange," J. Gen Physiol., 52:29s-63s, 1968.
73. Cater, D.B., Silver, I.A., and Wilson, G.M., "Apparatus and Techniques for the Qualitative Measurement of Oxygen Tension in Living Tissue," Proc. Roy. Soc., B151:256-276, 1959.
74. Altman, P.L., Blood and Other Body Fluids, Federation of American Societies for Experimental Biology, 1961.
75. Ives, D., and Janz, G.J., Reference Electrodes, Academic Press (New York), 1969.
76. Feltham, A.M. and Spiro, M., "Platinized Platinum Electrodes," Chem. Rev., 71:177-93, 1971.
77. Delehay, P., Double Layer and Electrode Kinetics, Interscience (New York). 1966.
78. Conway, B.E., Theory and Principles of Electrode Processes, Ronald Press (New York). 1965.
79. Eyring, H., ed., Physical Chemistry, An Advanced Treatise, V IXB, Academic Press (New York), 1970.
80. Bockris, J. O.'M., ed., Modern Aspects of Electrochemistry, Plenum Press (New York), 1954.
81. Bockris, J. O.'M., ed., Modern Aspects of Electrochemistry No. 3 Butterworths (London). 1964.
82. Balashova, N.A., and Kazarinov, V.E., "Investigation of the Relation Between Cation and Anion Adsorption on Platinum in Acid Solution at Various Potentials," Elektrokhimya, 1(5):512-16, 1965.
83. Perkins, S., and Eyring, H., "Zero Charge Potentials of Solid Metals," J. Am. Chem. Soc., 86:4496, 1964.

84. Petrii, O.A., Frimkin, A.N., and Kotlov, Yu. G., Dependence of Constant Charge Potential of Platinum and Rhodium Electrodes on Solution pH," Elektrokhimiya, 5(4):476-79, 1969.
85. Cater, D.B., Hill, D.W., Nunn, I.F., and Silver, I.A., "Oxygen Washout Studies in the Anesthetized Dog," J. Appl. Physiol., 18:888-94, 1963.
86. Jones, C.E., Crowell, J.W., and Smith, E.E., "Determination of Mean Tissue Oxygen Tensions by Implanted Perforated Capsules," J. Appl. Physiol., 26(5):630-33, 1969.
87. Delehay, P., New Instrumental Methods in Electrochemistry, Interscience (New York), 1954.
88. Gould, R.F., ed., Fuel Cell Systems, American Chemical Society (Washington, D.C.), 1965.
89. Beltzer, M., "Low Temperature Intermediate pH Fuel Cell Electrolyte," J. Electrochem. Soc., 114(12):1200-06, 1967.
90. Linke, W., Solubilities, 4th ed., Vol. II, American Chemical Society (Washington, D.C.), 1965.
91. Cooper, J.B., unpublished data.



## LIST OF SYMBOLS

a	constant in Tafel relationship
b	Tafel slope
$C_b$	bulk concentration
$C_o$	surface concentration
D	diffusion coefficient
$e^-$	electron
f	proportionality factor in Temkin isotherm
F	Faraday constant
$\Delta G_f^*$	activation energy for forward reaction
h	Planck constant
i	current density
$i_l$	limiting current density
$i_o$	exchange current density
k	Boltzmann constant
$k'$	rate constant
$k_j$	rate constant for jth step
K	equilibrium constant
l	Langmuir constant
$l_o$	Langmuir constant at zero coverage
L	electrode height
n	number of electrons in overall reaction
P	partial pressure
$P_{O_2}$	oxygen partial pressure
R	gas constant or resistance
S	site on catalyst

## LIST OF SYMBOLS (continued)

T	temperature
V	voltage
z	number of electrons transferred in a single step
$z_i$	valence

Greek

$\beta$	symmetry factor
$\delta$	boundary layer thickness
$\eta$	overpotential
$\theta$	fractional coverage
$\kappa$	specific conductance
$\tau$	transmission coefficient
$\phi$	potential
$\phi_m$	potential at electrode surface
$\phi_{R,m}$	rational potential at reversible conditions
$\psi$	potential at outer Helmholtz plane

## APPENDIX A

## List of Equipment and Materials

## I. Electronics for Potentiostatic and Galvanostatic Test

## 1. Potentiostats

a). Tacussel type PRT-30.1 -  $\pm 30$  volt putput voltage;  $\pm 100$  ma output current; includes phase correction network. (Ryaby Assoc., Passaic, N.J.).

b). Wenking model 6250 TR -  $\pm 15$  volt output;  $\pm 300$  ma output current; (Brinkmann Instr., Inc., Des Plaines, Ill.).

2. Digital Electrometer - Keithley model 615 -  $10^{-12}$  to  $10^{-1}$  amps. full scale (as ammeter),  $\pm 0.5\% \pm 1$  digit accuracy ( $10^{-1}$  to  $10^{-7}$  ranges). (Keithley Instr., Inc., Cleveland, Ohio).

3. Digital Multimeter - Non-Linear Systems model MX-3 - 19.99mv to 1000 V DC ranges;  $10^8$  ohm input impedance (min) on mv ranges (as voltmeter). (Non-linear Systems, Inc., Del Mar. California).

4. Strip Chart Recorder - Texas Instr. model FS02W6D - 2 channel, 9.75 inch grid, 10 mv to 10 volt full scale,  $10^5$  ohm input impedance (min). (Texas Instr., Houston, Tex.).

5. Oxygen and pH measuring system - Radiometer BMS3 Blood Micro System with PHM 72 Digital Acid - Base Analyser - pH,  $PO_2$ ,  $PCO_2$  capabilities, 0-12 oH units  $\pm .002$  unit reproducibility.  $PO_2$  measurements to one decimal  $\pm 0.5$  mm Hg reproducibility. (London Co., Cleveland, Ohio).

## II. Gas System

1. Nitrogen - Prepurified grade (General Stores, Univ. of Mo., Columbia).
2. Oxygen - Extra dry grade, 99.6% min. purity (Matheson Gas Products, Joliet, Ill.).
3. Gas Proportioner - Matheson Model 665 with #600 and #601 tubes (Matheson Gas Products, Joliet, Ill.).
4. Gas Washing Bottle - Fisher Scientific #3-040C, 500 ml capacity (Fisher Scientific Co., St. Louis, Mo.).
5. Compressed Air Filter - Beckett Harcum #3F8-7 (Aiken Eng. Co., Lenexa, Kan.).
6. Regulators
  - a) Oxygen - IL320 Single Stage (Matheson Gas Products, Joliet, Ill.).
  - b) Nitrogen - PIL Double Stage (Meco Sales, Columbia, Mo.)

## III. Reagents

1. Chemicals - All chemicals of reagents grade (includes NaCl,  $\text{Na}_2\text{HPO}_4$ ,  $\text{NaH}_2\text{PO}_4$ , KCl, Hg, etc.) (Fisher Chemical Co., St. Louis, Mo.)
2. Culture Media - #152 H BME (10X) with Hank's salts without L-Glutamine and sodium bicarbonate (Grand Island Biological Co., Grand Island, New York).
3. Albumin - Bovine serum albumin, Cohn Fraction V, 96-99% (Sigma Chemical Co., St. Louis, Mo.).

#### IV. Automated Load Switching System -

1. Electrometer - Keithley model 619C - 0.001 to 100 volts full scale,  $\pm 1\%$  of full scale accuracy (all ranges), greater than  $10^{-14}$  ohms input impedance (Keithley Instr., Cleveland, Ohio).
2. Switches
  - a). Cell switching - 18 position, 3 deck, #RS30-2528 (Chicago Dynamics, Ind., Chicago, Ill.).
  - b). Resistor switching - 24 position, 16 deck, #RS-2536 (Chicago Dynamics Ind., Inc., Chicago, Ill.).
3. Computer - Basic Linc 8, with 8K core (Digital Equipment Corp., Maynard, Mass.).
4. Water bath circulating pump - Jabsco B3M6 (ITT Fluid Handling Div., Costa Mesa, Calif.).
5. Water Bath Temperature Regulator - Porta Temp, Thomas #9936-P15 (Arthur H. Thomas, Phila., Pa.)
6. Timer - Made by Space Sciences Research Center Electronics Shop.

#### V. Miscellaneous

1. Calomel electrodes - Thomas #4857-F15 (Arthur H. Thomas, Phila., Pa.)
2. H-Cells - Pyrex glass; made by Univ. of Mo. Glassblowing shop.
3. Platinum foil - 0.002 inch thick, Fisher #13-755B (Fisher Scientific Co., St. Louis, Mo.)
4. Platinum wire - 22 gauge (0.025 inch dia.), Fisher #13-765E (Fisher Scientific Co., St. Louis, Mo.).
5. Millipore Filters and Holder - Millipore Corporation (Bedford, Mass.)

## APPENDIX B

## Culture Media Composition

(from Grand Island Biological Co. Cat., 1969-70, p. 75)

## BME, Basal Medium (Hanks')

Component	mg/L	Component	mg/L
NaCl	8000	L-Methionine	7.5
KCl	400	L-Phenylalanine	16.5
$\text{Na}_2\text{HPO}_4 \cdot 2\text{H}_2\text{O}$	60	L-Threonine	24
$\text{MgSO}_4 \cdot 7\text{H}_2\text{O}$	100	L-Tryptophan	4
$\text{MgCl}_2 \cdot 6\text{H}_2\text{O}$	100	L-Valine	23.5
$\text{KH}_2\text{PO}_4$	60	Biotin	1
$\text{CaCl}_2$ (anhyd.)	140	Folic acid	1
Glucose	1000	Choline Cl	1
L-Arginine HCl	21	Nicotinamide	1
L-Cystine	12	D-Ca pantothenate	1
L-Tyrosine	18	Pyridoxal HCl	1
L-Histidine	8	Thiamine HCl	1
L-Isoleucine	26	Riboflavin	0.1
L-Leucine	26	i-Inositol	1.8
L-Lysine	29	Phenol red	10.0

## APPENDIX C

Computations for Limiting Current Density from  
Diffusion Layer Theory

The magnitude of the diffusion limiting current density can be estimated from the equation:

$$i_L = \frac{nFD C_b}{\delta}$$

The value for  $n$  for the overall oxygen reduction reaction is equal to 4 and  $F$  is the Faraday ( $9.65 \times 10^4$  coulomb/equivalent). The value of  $D$ , the diffusion co-efficient, for oxygen in water at  $25^\circ$  has been given as  $2.6 \times 10^{-5}$   $\text{cm}^2/\text{sec}$  (44), and would not vary significantly from this value for the purpose of a rough approximation of  $i_L$ . The thickness of the boundary layer,  $\delta$ , in a well stirred solution on a vertical electrode is of the order of  $5 \times 10^{-3}$   $\text{cm}$  (45). The oxygen concentration in saline at 0.202 atm  $\text{PO}_2$  can be interpolated from data given for the Ostwald co-efficient at  $25^\circ\text{C}$  (90). Thus,  $C_b = 0.0296 \times 0.202 = 5.98 \text{ cm}^3 \text{ O}_2/\text{L saline}$ . The diffusion limiting current is then calculated as:

$$i_L = \frac{4 \times 9.65 \times 10^4 \times 2.6 \times 10^{-5} \times 5.98 \times 10^{-3}}{24.4 \times 5 \times 10^{-3}}$$

$$= 0.491 \text{ ma/cm}^2$$

## VITA

Jeffrey Bruce Cooper was born in Philadelphia, Pennsylvania on May 28, 1946. He attended public schools in Philadelphia and entered Drexel Institute of Technology in January, 1964, receiving a B.S. in Chemical Engineering in June, 1968. During his undergraduate schooling he spent fifteen months as a cooperative student at the E. I. Dupont DeNemours Coating Division Plant in Philadelphia.

In 1968, Mr. Cooper began graduate training as a predoctoral fellow of the National Institutes of Health. He received the Degree of Master of Science in Biomedical Engineering from Drexel University in June, 1970. He began work at the Space Sciences Research Center, University of Missouri in September, 1969, as a student in the Chemical Engineering department. He was awarded a Shell Companies Fellowship for the summer of 1971.

Mr. Cooper is a member of Sigma Xi, Phi Kappa Phi, Phi Lambda Upsilon, and Tau Beta Pi honorary Societies. He is also a student member of the American Institute for Chemical Engineers and the Electrochemical Society.

In December, 1967 he married the former Madelaine Claire Weiss. They have one child, Marilyn, born in 1969.



Digitization Information Page

Local identifier Cooper1972

Source information

Format Book  
Content type Text  
Source ID Gift copy from department; not added to MU Libraries collection.  
Notes original text is very light

Capture information

Date captured June 2023  
Scanner manufacturer Fujitsu  
Scanner model fi-7460  
Scanning system software ScandAll Pro v. 2.1.5 Premium  
Optical resolution 600 dpi  
Color settings 8 bit grayscale  
File types tiff  
Notes

Derivatives - Access copy

Compression Tiff: LZW compression  
Editing software Adobe Photoshop  
Resolution 600 dpi  
Color grayscale  
File types pdf created from tiffs  
Notes Images cropped, straightened, brightened